Aalto University

Commissioning of MRI-only simulation for radiotherapy planning in pelvis

Reko Kemppainen

Licentiate thesis

Doctoral Programme in Science

11-Dec-2019

Supervisor: Professor Risto Ilmoniemi

Advisor: Jani Keyriläinen, Timo Kiljunen, Marko Pesola

Aalto University
Name of School
Name of Department
Research group

Aalto University

Aalto University, P.O. BOX 11000, 00076 AALTO
www.aalto.fi

Abstract of licentiate thesis

Author Reko Kemppainen

Title of thesis Commissioning of MRI-only simulation for radiotherapy planning in pelvis

Department Department of Neuroscience and Biomedical Engineering

Field of research Neuroscience and biomedical engineering

Supervising professor Risto Ilmoniemi

Thesis advisor(s) Jani Keyriläinen, Timo Kiljunen, Marko Pesola

Thesis examiner(s) Juha Nikkinen

Number of pages 41 **Language** English

Date of submission for examination 23.10.2019

Abstract

Modern radiation therapy delivery techniques enable ever conformal delivery of the radiation increasing the likelihood for successful treatment and reducing complications in nearby healthy tissue. In order to improve the treatment outcomes, in addition to advanced radiation delivery techniques, more accurate knowledge about the location and spread of both disease and organs at risk (OAR) is needed. Thus, the use of magnetic resonance imaging (MRI) has increased substantially during recent years. In MRI, the contrast resolution for soft tissue is superior compared to other imaging modalities enabling precise target definition and contouring of the OARs.

Currently, the use of MRI in radiation therapy is based on co-registration of the images facilitating the use of the information provided by MRI while computed tomography (CT) is used for dose computation and as a reference image for patient positioning. Unfortunately, the dual modality workflow is laborious and cost inefficient. In addition, the co-registration uncertainty propagates to treatment uncertainty causing systematic error. During recent years several research groups have published methods enabling the generation of so-called synthetic CT (sCT). It can be used like traditional CT for density information in dose computation and as positioning reference images. The use of sCT enables external beam radiation therapy workflow using only MR imaging.

In this work we studied the commissioning and accuracy of MRI-only workflow for external beam radiation therapy (EBRT) of pelvic malignancies. The commissioning test shall cover all steps in the radiation therapy workflow where geometric or dosimetric accuracy is affected by the substitution of the CT by the sCT.

In publications I and III, we assessed the dosimetric accuracy of sCT images in pelvis by comparing to dose distributions computed using CT images. In publications II and III, we studied the patient positioning accuracy when sCT images are used as reference images. In addition, in publications I and III we evaluated the impact of geometric distortions to the total accuracy of MRI-only workflow.

According to our results, the use of studied sCT method is sufficiently accurate for clinical use for pelvic indications. In addition, image-guided radiation therapy based on MR images is accurate enough so that the total geometric accuracy improves compared to current CT based workflow.

Keywords Radiation therapy, MRI, Commissioning

Aalto-yliopisto

Aalto-yliopisto, PL 11000, 00076 AALTO
www.aalto.fi

Lisensiaatin tutkimuksen tiivistelmä

Tekijä Reko Kemppainen

Työn nimi Magneettikuvaukseen perustuvan sädehoidon suunnittelun käyttöönotto lantion alueella

Laitos Neurotieteen ja lääketieteellisen tekniikan laitos

Tutkimusala Neurotiede ja lääketieteellinen tekniikka

Vastuuprofessori Risto Ilmoniemi

Työn ohjaajat Jani Keyriläinen, Timo Kiljunen, Marko Pesola

Työn tarkastajat Juha Nikkinen

Jätetty tarkastettavaksi 23.10.2019 **Sivumäärä** 41 **Kieli** englanti

Tiivistelmä

Modernit sädehoitotekniikat mahdollistavat yhä tarkemman kohteenmukaisen sädehoidon antamisen, mikä lisää hoidon onnistumisen todennäköisyyttä ja vähentää komplikaatioita ympäröivissä terveissä kudoksissa. Parempiin hoitotuloksiin pääsemiseksi sädehoidossa tarvitaan kuitenkin, kehittyneiden hoitotekniikoiden lisäksi, yhä tarkempaa tietoa hoitokohteen ja riskielinten sijainnista. Tämän takia ionisoimattoman säteilyn käyttöön perustuvan magneettikuvauksen (MK) käyttö on lisääntynyt voimakkaasti sädehoidossa viime vuosina. MK:ssa pehmytkudosten välinen kontrasti on muita kuvausmodaliteetteja parempi, mikä mahdollistaa tarkemman kohteen määrittelyn ja riskielinten rajauksen.

Nykyinen käytäntö MK-kuvien osalta sädehoidossa perustuu tietokonetomografia- (TT) ja MK-kuvien rekisteröintiin, jolloin MK-kuvien antama lisäinformaatio voidaan hyödyntää, vaikka itse hoitokenttien annoslaskenta ja potilaan kohdistus on TT-kuviin perustuvaa. Kahden kuvausmodaliteetin käytöstä aiheutuu ylimääräistä työtä ja kustannuksia. Lisäksi kuvien rekisteröintiin liittyvä virhe lisää epävarmuutta hoidon tarkkuudessa. Viime aikoina useat tutkimusryhmät ovat julkaisseet menetelmiä, joiden avulla on mahdollista muodostaa sädehoidon annoslaskennassa tarvittava tiheyskartta (laskennallinen TT-kuva) suoraan magneettikuvausta käyttäen. Näin sädehoito on mahdollista toteuttaa pelkän magneettikuvan perusteella, jolloin yllä mainitut kahden kuvausmodaliteetin käytöstä aiheutuvat ongelmat voidaan välttää.

Tässä työssä tutkittiin MK-kuviin perustuvan laskennallisen TT-kuvan käyttöönottoa ja tarkkuutta lantion alueen ulkoisessa sädehoidossa. Käyttöönotto-testien tulee kattaa kaikki sellaiset vaiheet, jossa MK-pohjainen suunnittelu vaikuttaa joko geometriseen tai dosimetriseen tarkkuuteen.

Ensimmäisessä ja kolmannessa osatyössä tutkittiin mahdollisuutta käyttää MK:ta sädehoitopotilaiden lantion alueen annoslaskennassa säteilyn vaimennuskorjaukseen. Toisessa ja kolmannessa osatyössä määritettiin potilasasemoinnin epätarkkuus käytettäessä MK-pohjaista menetelmää vertaamalla perinteiseen TT-kuvaan pohjautuvaan menetelmään. Lisäksi ensimmäisessä ja kolmannessa osatyössä arvioitiin MK:n geometrisen vääristymän vaikutuksia kokonaistarkkuuteen.

Tutkimuksen perusteella menetelmän käyttö lantion alueella on riittävän tarkka kliiniseen käyttöön. Lisäksi kuvantaohjattu sädehoito magneettikuvien pohjalta on riittävän tarkkaa, jotta potilaan asemointitarkkuus ei huonone suhteessa nykyiseen TT-pohjaiseen suunnitteluun.

Avainsanat Sädehoito, MRI, Käyttöönotto

Preface

The work for this thesis was conducted in collaboration between Turku University Hospital (Tyks) Department of Oncology and Radiotherapy, Docrates Cancer Center and Philips MR Therapy Oy. The collaboration aimed at assessment and feasibility evaluation of the new products developed by Philips MR Therapy, Finland.

First and foremost, I would like to thank Prof. Risto Ilmoniemi for supervision and guidance during the process and my former bosses Dr. Teuvo Vaara and Dr. Antti Honkanen for the flexibility to allow me to pursue my interest at work and facilitating the collaboration with the hospitals.

I'm grateful to all three instructors of the thesis for invaluable support: Dos. Jani Keyriläinen, Dos. Timo Kiljunen and Dr. Marko Pesola. I have been lucky to have around me such a group of highly skilled hospital physicists oriented in research.

I want to express my gratitude to the colleagues at Philips. Especially, Dr. Panu Vesanen, Dr. Aleksi Halkola, M.Sc. Matti Lindström and M.Sc. Pavel Tomas for interesting discussions and support.

The persons involved in the collaboration at both Docrates and Tyks have been very helpful while conducting their duties in busy clinics. Especially, I want to thank medical physicist Sami Suilamo for discussion and insights during my visits at Tyks.

Thanks to my parents, Seija and Yrjö, and my mother and father in law, Raija and Juha, for supporting our family in our efforts in finishing our studies by taking care of Anton and Aada — two lovely but energetic children.

Finally, I would like to thank my wife, Sanna, for taking care of our family while I have needed time to conduct the research.

Helsinki, 9 October 2019
Reko Antti Kemppainen

Contents

List of Abbreviations and Symbols

AP	anteroposterior
BW	bandwidth (receiver)
CC	craniocaudal
CT	computed tomography
CTV	clinical target volume
DRR	digitally reconstructed radiograph
EBRT	external beam radiation therapy
FOV	field-of-view
GTV	gross tumor volume
HU	Hounsfield unit
IGRT	image-guided radiation therapy
LR	left-right (direction)
MRI	magnetic resonance imaging
MRCAT	magnetic resonance for calculating attenuation
OAR	organ at risk
QA	quality assurance
RT	radiation therapy or radiotherapy
pCT	pseudo CT (a.k.a. synthetic CT, sCT)
PTV	planning target volume
sCT	synthetic CT (a.k.a. pseudo-CT, pCT)
sCTb	synthetic CT with bulk HU values
sCTc	synthetic CT with continuous HU values
SD	standard deviation

List of Publications

This licentiate dissertation consists of a summary and of the following publications which are referred to in the text by their numerals

I. Kemppainen R, Suilamo S, Tuokkola T, Lindholm P, Deppe MH, Keyriläinen J. Magnetic resonance-only simulation and dose calculation in external beam radiation therapy: a feasibility study for pelvic cancers. Acta Oncol. Taylor 8 Francis; 2017;56:792–8. DOI:10.1080/0284186X.2017.1293290.

II. Kemppainen R, Vaara T, Joensuu T, Kiljunen T. Accuracy and precision of patient positioning for pelvic MR-only radiation therapy using digitally reconstructed radiographs. Phys. Med. Biol. IOP Publishing; 2018;63:aaad21. DOI:10.1088/1361-6560/aaad21.

III. Kemppainen R, Suilamo S, Ranta I, Pesola M, Halkola A, Eufemio A, Minn H., Keyriläinen J. Assessment of dosimetric and positioning accuracy of a magnetic resonance imaging-only solution for external beam radiotherapy of pelvic anatomy. Phys. Imaging Radiat. Oncol. Elsevier; 2019;11:1–8. DOI: 10.1016/j.phro.2019.06.001.

Author's Contribution

Publication I: *"Magnetic resonance-only simulation and dose calculation in external beam radiation therapy: a feasibility study for pelvic cancers"*

The author participated in planning the study, performing the analysis and wrote the manuscript as the corresponding author.

Publication II: *"Accuracy and precision of patient positioning for pelvic MR-only radiation therapy using digitally reconstructed radiographs"*

The author participated in planning the study, performing the analysis and wrote the manuscript as the corresponding author.

Publication III: *"Assessment of dosimetric and positioning accuracy of a magnetic resonance imaging-only solution for external beam radiotherapy of pelvic anatomy"*

The author participated in planning the study, performing the analysis and wrote the manuscript as the corresponding author.

1. Introduction

1.1 Background and research environment

1.1.1 Radiotherapy workflow

The use ionizing radiation as part of cancer treatment to control or kill malignant cells and typically delivered by a linear accelerator, is called radiation therapy (RT). Most commonly, RT is planned individually using computed tomography (CT) image of the patient. The initial CT-scanning performed in the treatment position with fixation devices is called RT simulation. The RT simulation forms the basis for treatment geometry and for both target and organ at risk (OAR) contouring. Contouring is preceded by dose planning. In the dose planning beam geometry and radiation delivery are planned and expected dose map is computed using the radiation attenuation information provided by the CT image (see Figure 1 for illustration of the complete RT workflow).

RT is delivered in fractionated manner – the total prescribed dose is fractioned and delivered sequentially during several days or weeks. During each treatment fraction, the patient is first positioned and then the patient position is verified by imaging. In image-guided radiation therapy (IGRT), X-ray images of the patient, taken in the treatment position, are compared to reference images derived from the planning CT. Patient position verification ensures that the fractionated dose is delivered to the planned target for each fraction.

1.1.2 Radiotherapy planning using MRI

Computed tomography (CT) is currently the primary imaging modality for providing anatomical and tissue density information in the external beam radiation therapy (EBRT) planning of pelvic cancers. Magnetic resonance imaging (MRI) is widely used as a supplement to the CT imaging [1–3]. The most significant advantage of MRI over CT is its better soft-tissue contrast, which results in a more accurate gross tumor volume (GTV) and OAR delineation [4–7]. Additional benefits include the usage of non-ionizing radiation and the versatility of acquisition sequences allowing the cancer- or organ-specific imaging methods [5].

A major drawback of multi-modality imaging in EBRT is the residual registration error remaining when the images from two or more modalities are registered with each other [8]. Recent advances in the use of MRI promise to eliminate the registration error by using only the MR images for planning and dose

calculation in the EBRT of prostate and brain cancer (see the recent reviews [9–11]). In an MRI-only workflow, so-called synthetic CT (sCT) images are generated from the magnetic resonance (MR) images, providing the tissue density information for dose calculation and reference images for patient position verification.

The sCT replaces CT image completely in the radiotherapy workflow called MRI-only (see Figure 1) workflow. Consequently, the parts in the CT-based workflow relying properties of the CT will be affected. Sites considering commissioning of MRI-only workflow into clinical use need to assure that the complete chain of RT remains within acceptable tolerances.

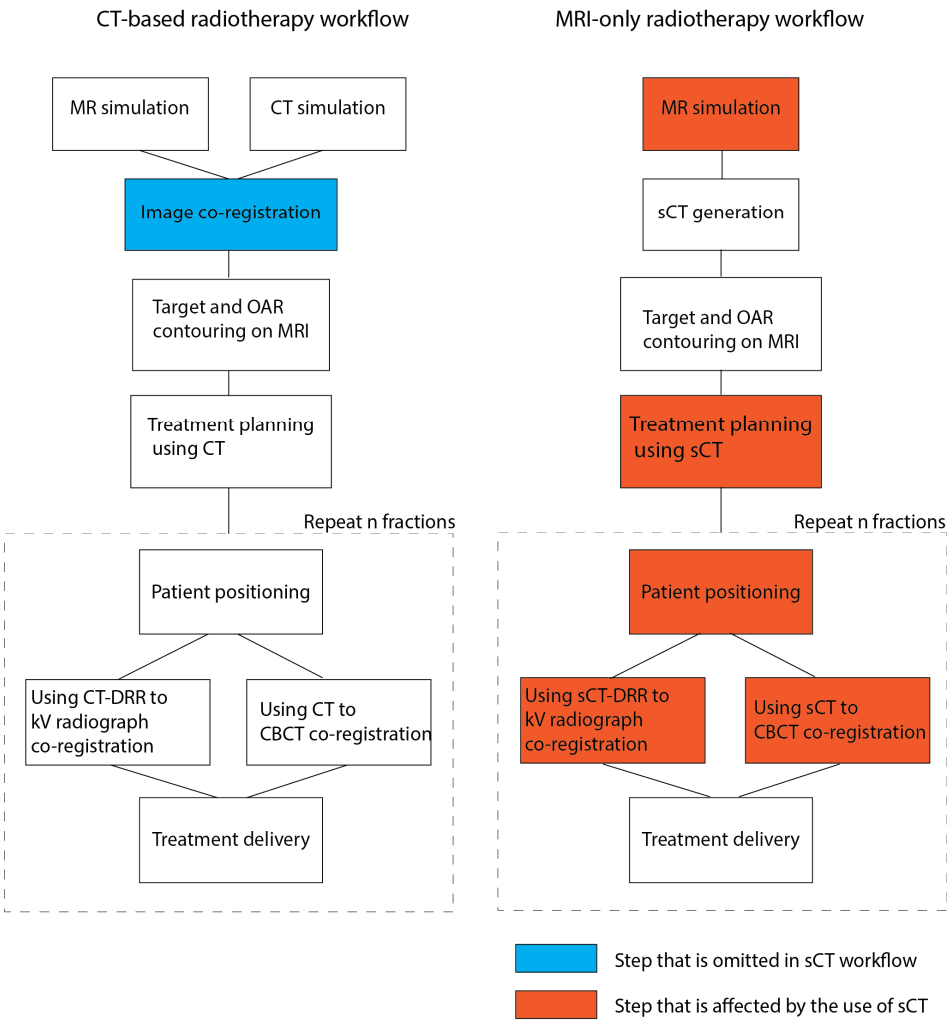

Figure 1: CT-based (left) and synthetic CT (sCT)-based radiotherapy workflow. In CT-based workflow image co-registration may be omitted when using only MR images for the whole process (MRI-only). However, use of sCT in an MRI-only workflow affects geometric accuracy requirements for the MR-imaging, treatment planning, dose computation and patient position verification (red).

1.1.3 Synthetic CT used in this work

A commercially available solution for the sCT generation was used in this work (MRCAT, Philips Oy, Vantaa, Finland). It has been shown that the solution can be used for an accurate dose calculation and patient positioning for prostate

cancer patients [1–3]. In addition, its feasibility for other indications in the pelvic anatomy was demonstrated in our study [4].

During recent years, several sites have performed commissioning of commercial MRI-only solutions, and results have been published in peer-reviewed publications [1–8]. In addition some hospitals have reported the clinical use of an inhouse solution (see e.g. [9]).

Prior to clinical use of an MRI-only method, all aspects affecting the total accuracy of the treatment must be evaluated, a process called commissioning. In particular, dosimetric and geometric accuracy must be quantitatively evaluated so that the impact to total treatment accuracy can be evaluated and accepted for clinical use.

1.2 Objectives and scope

In external radiation therapy (EBRT), the aim is to deliver prescribed dose to defined target with very high accuracy requirements. The high requirements are a consequence of a close physical proximity and radiobiological sensitivity of OARs and clinical target volume (CTV). Consequently, dosimetric and geometric accuracy is directly related to treatment outcomes in EBRT.

The workflow of radiation therapy can be considered as a chain. From each link of the chain, accumulation of uncertainties occurs, and high accuracy is needed in all steps of the treatment process to ensure acceptable total uncertainty. The total uncertainty of the RT workflow is a sum of the uncertainties from each step in the workflow [10]. The MRI-only workflow affects three items in the chain: geometric accuracy from imaging, treatment planning and patient position verification (see

Figure 2).

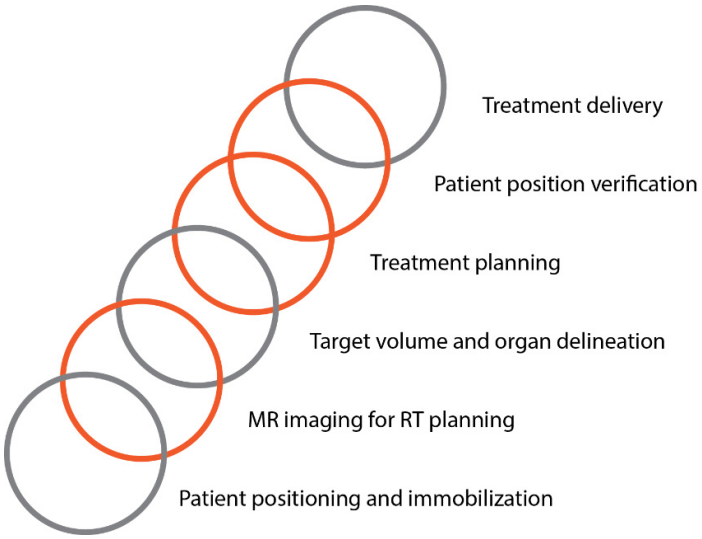

Figure 2: Components of the RT chain contributing to the total accuracy and uncertainties of the RT workflow. The components of the total uncertainty affected using sCT are illustrated as red.

Geometric accuracy of the planning sCT image introduces systematic uncertainties to both geometric and dosimetric accuracy. Thus, the geometric accuracy of sCT plays a critical role in MRI-only workflow. MRI images are inherently distorted due to gradient field nonlinearity and both system and patient related inhomogeneities in the main magnetic field [11–15]. Since the distortion in the MR images will be propagated to the sCT, it is important to quantitatively assess the magnitude of distortion and its impact to dosimetric computation.

In a sCT image, the HU values need to be derived from MRI. Since there is no direct association between MR image intensity on electron density of the tissue, estimated HU-values contain uncertainties. The introduced uncertainties will compromise the dose calculation accuracy achievable when using the sCT. Thus, prior to clinical use, the dosimetric differences need to be analyzed.

In addition to uncertainties in HU unit of the sCT, also the appearance of the image will differ from CT. Depending on the sCT generation method the appearance can be bulky, when small amount of differing HU values are used, or it can have a continuum of HU values like a real CT. However, the differences between sCT and CT may impact the image registration process occurring in the patient position verification. Thus, the impact to positioning accuracy needs to be assessed in a realistic use scenario.

Overall, the purpose of the commissioning is to ensure that the chain of RT is acceptable.

2. Aims of the thesis

The primary focus of the work presented in this thesis was the commissioning and the quantitative assessment of a commercial MRI-only method for pelvic external beam radiation therapy. The specific aims were:

- To perform an evaluation of the dosimetric accuracy of use of a commercially available MRI-only for radiation therapy of pelvic malignancies (Paper I and III).
- To evaluate the accuracy and precision of patient positioning using a commercially available sCT generation method for pelvic radiotherapy (Paper II and III).
- To evaluate the impact of geometric distortion in MRI-only based radiation therapy of pelvic malignancies (Papers I and III).

3. Materials and methods

3.1 Generation of synthetic CTs

Two different versions of synthetic CT (sCT) were used in the study. Both versions have been released as commercial MRI-only solutions (Magnetic resonance for Calculating Attenuation, MRCAT, Philips Oy, Vantaa, Finland). The first version used a bulk assignment of HU values, which is referred to as sCTb in this study. The second version was an improved version of the MRCAT providing continuous HU values called sCTc hereafter.

Generation of the sCT is based on mDIXON MR image [16]. Bone structures in the sCT are automatically segmented inside the body using the multiple contrasts provided by the mDIXON scan. Both the bone and outline segmentation employ a model-based segmentation approach trained on patient and volunteer mDIXON image datasets. The model contains information of average bone shape and how the shape varies in the training population. The model is adapted to an actual patient image using features (such as gray value edges) found within the image, while at the same time, a constraint for the shape of the segmented structure prevents the segmentation from being attracted to a wrong position [17].

Voxels inside the bone segmentation are assumed to contain either compact or spongy bone. An intensity threshold is used; lower intensities are considered to consist of compact bone, while voxels with higher intensity are assumed to contain spongy bone. The choice of the threshold value has been selected so that average bone density match with CT on population level. Figure 3 shows the flowchart for the prostate (bulk HU value) sCTb algorithm.

The same flowchart applies also to the sCTc algorithm. In particular, the sCTc algorithm also relies on the availability of a *body mask* and a *bone mask*. Like for sCTb, classification between fat tissue and water tissue is based on the fat and water intensities in the respective sCT source images. The key difference between the sCTb and sCTc algorithms is in the assignment of the HU values—in sCTc, the classification between fat and water is continuous. The HU values are interpolated linearly between the respective limit values for soft tissue.

In sCTb, bone voxels are classified as either compact bone or bone marrow. In sCTc, the compactness is described with a continuous-valued bone index. The bone index is converted into a HU value through a piecewise-linear mapping.

The outmost body layer, representing skin, can also be classified as partially air. This models the partial volume effect.

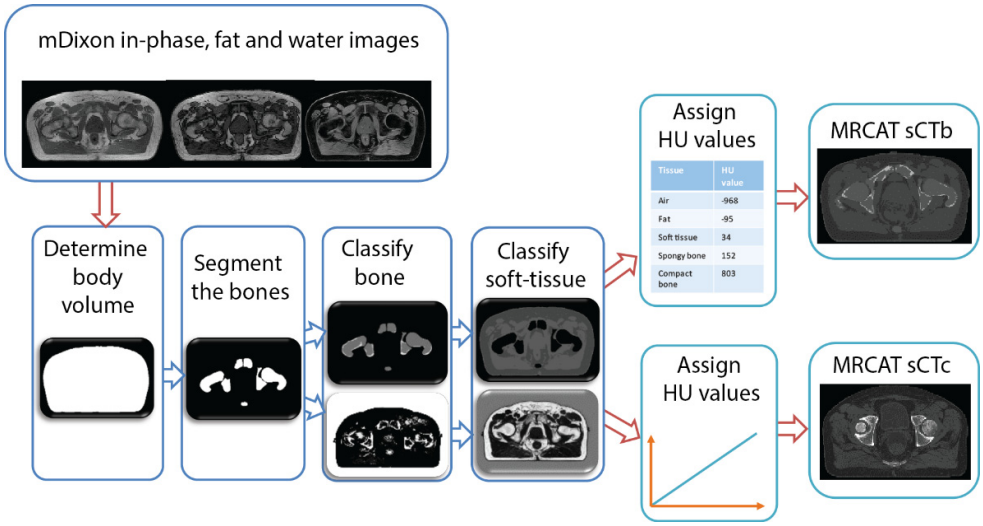

Figure 3: Flowchart for the bulk and continuous HU value sCT algorithm. The continuous-value sCT algorithm is otherwise similar, but the soft tissue classification and the bone tissue classification are continuous-valued instead of discrete. The HU values are respectively interpolated continuously.

The assignment of continuous HU value starts by estimating the centers of fat-rich and water-rich voxel clusters. The soft tissue voxels are mapped continuously between water and fat clusters. The voxel intensities in the water-fat-plane are projected to a line, which connects the cluster centers. *Fat fraction* x_{fat} is defined such that $x_{\text{fat}}=0$ at the water center and $x_{\text{fat}}=1$ at the fat center. The complement of the fat fraction is water fraction $x_{\text{water}}=1-x_{\text{fat}}$. In the outmost body layer, the relation between fat and water fractions is modified by the presence of air fraction. The air fraction in the outermost voxel layer of the body mask is quantified using normalized voxel intensity.

Dense bone manifests on the mDixon images as voxels with low signal intensity. Hence, the voxels within the bone mask are classified according to their "darkness", i.e. the distance of the voxels from the water-fat classification line.

Fat and water fractions and bone index are mapped to HU values using a linear fitting. A single linear fit is used for soft tissue, while for bone tissue, a two-staged polyline is used to distinguish between spongy bone and compact bone.

3.2 Performance evaluations of MRI-only methods

To ascertain that sCT can meet high demands for dosimetric and geometric accuracy, medical physicists perform commissioning of MRI-only simulation prior to clinical use. In commissioning, all aspects related to the performance of the method need to be assessed including dosimetric agreement, geometric and patient positioning accuracy.

3.2.1 Dosimetric accuracy

When computed tomography (CT) is used for homogeneity correction of external beam dose calculation, one can always verify the correctness of calculations by measuring the absorbed dose in a phantom. The mapping between HUs and electron or mass density can be regarded correct if the delivered dose inside

a phantom is within acceptable dose accuracy tolerance. A fundamental property of MRI-only methods is that the dosimetric accuracy can't be measured directly as sCT methods don't provide meaningful images of phantoms. Consequently, performance must be evaluated by comparing to current gold standard, i.e., CT-based dose computation.

Table 1: Patient demographics in dosimetric agreement studies (Publications I and III).

	Pelvic lymph node	Rectal cancer	Gynecological cancer	Prostate post-operative	Prostate definitive
Publication I					
Average age (years)	65.7 (6.2)	68.2 (10.6)	67.3 (14.0)	68.7 (6.8)	70.3 (8.0)
Sex (males/females)	15/0	10/5	0/15	15/0	15/0
Publication III					
Average age (years)	-	69.2 (12.8)	72.8 (8.3)	-	74.3 (4.8)
Sex (males/females)	-	3/2	0/5	-	5/0

For dose agreement assessment, CT and sCT images were first registered and then resampled to the same image grid. The clinical radiotherapy plan, originally optimized using the planning CT, was then copied to sCT and recomputed to the same dose grid (see Figure 4 for illustration of the workflow).

The dose distributions were computed with Eclipse 13.6 (Varian Medical Systems Finland Oy, Helsinki, Finland) treatment planning system (TPS) using an anisotropic analytical algorithm (AAA) (publication III) or Pinnacle3 (version 9.10, Philips Medical Systems Inc., Fitchburg, WI, USA) TPS with collapsed cone algorithm (publication I). Computed doses were used to compute both DVH and gamma comparisons.

The DVH evaluation was based on the structures that were copied from the planning CT to sCT based on rigid registration. Minimum, median and maximum ($D_{2\%}$, $D_{50\%}$, $D_{98\%}$) dose points were evaluated for the PTVs while volumes of $V_{95\%}$ and $V_{70\%}$ were assessed for the OARs. The results were computed as a relative difference respect to prescribed dose for dose points ($\frac{\boldsymbol{D(sCT)-D(CT)}}{\boldsymbol{D_{presc.}}}$) or structure volume ($\frac{\boldsymbol{V(pCT)-V(CT)}}{\boldsymbol{V_{struct.}}}$) for volume points.

In addition, the dose distributions between sCT and planning CT were compared by means of 3D gamma analysis using the Plastimatch 1.7.3 (http://plastimatch.org/index.html), an open source software for image processing, (publication III).

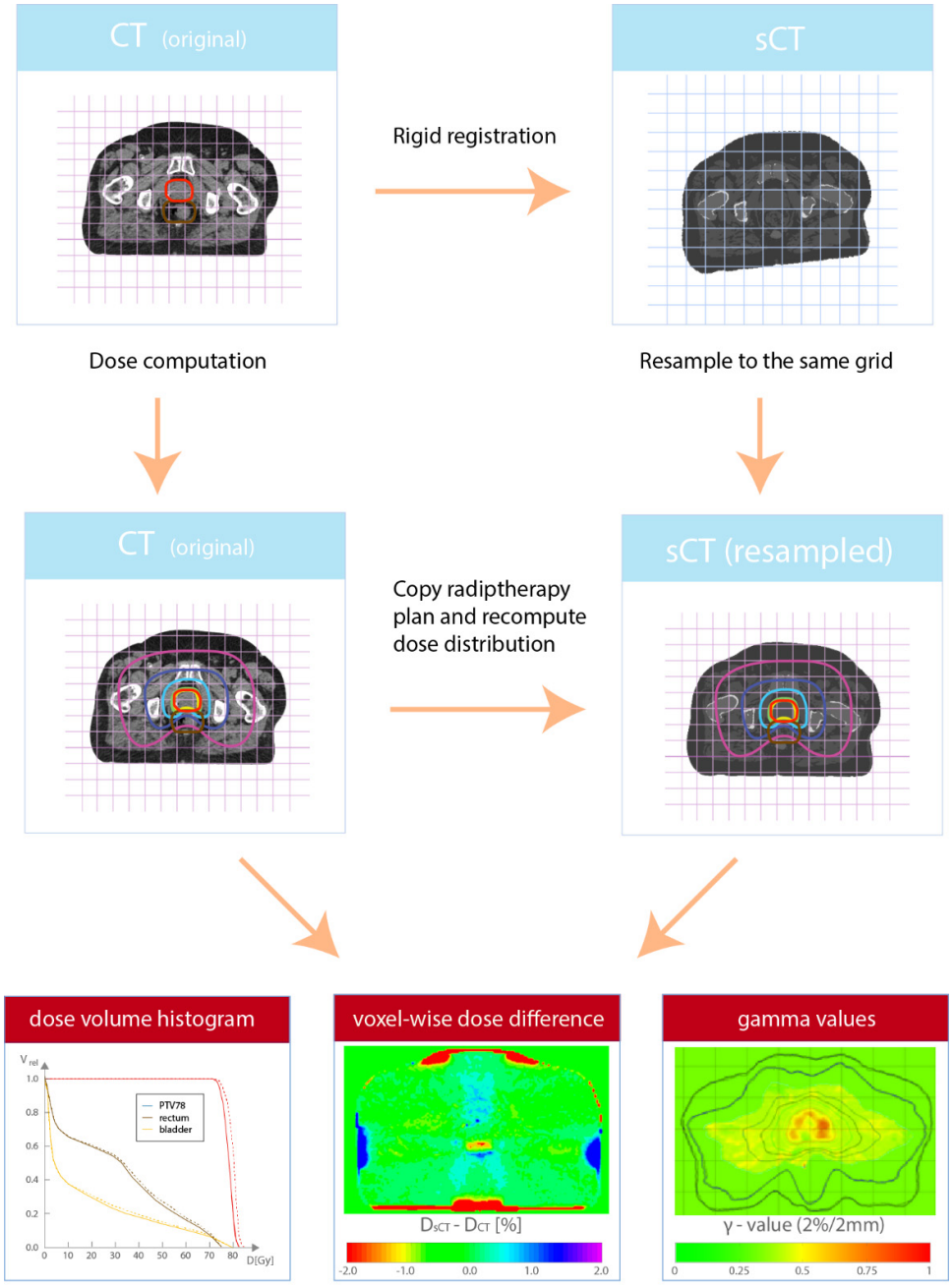

Figure 4: The workflow for dosimetric agreement evaluation. First, CT and sCT were rigidly registered and resampled to the same image grid (image rotation exaggerated for the sCT). Resampling ensures identical dose computation grid for further analysis when the radiotherapy plan is copied from CT to sCT. The differences between the two dose distributions were analyzed by means of dose volume histogram (DVH) differences, voxel-wise dose differences and using 3D gamma analysis.

3.2.2 Patient positioning accuracy

Patient position verification is a procedure during a radiotherapy treatment fraction where the position and orientation of the patient is compared to planned positioning. Patient position verification enables accurate delivery of the fractionated dose to the target.

Modern external beam radiotherapy devices are equipped with planar and/or volumetric X-ray imaging capabilities. Typically, a flat panel detector and X-ray generator are attached to the treatment machine allowing rotation of the beam around the patient. Alternatively, mega voltage (MV)-treatment beam with a flat panel detector can be used.

To evaluate patient positioning accuracy, the use of sCT-based workflow is compared to standard CT-based positioning including both planar (publications I and III) and volumetric (publication III) registrations.

Planar evaluation

In the Digitally reconstructed radiograph (DRR) studies, 20 consecutive patients were included in both publication I and III. Manual registrations between CT-DRR and planar kV-radiograph were compared with the manual registrations between sCT-DRR to planar kV-radiograph (see Figure 5 for visualization of performed registration workflow). The manual registrations were performed using a Matlab-based tool simulating the paired registration of planar kV- and DRR-images in two orthogonal directions simultaneously. The observers were asked to perform manual registrations of the paired projections shown to them in random order.

Five observers registered the CT- and sCT-based DRRs to daily localization radiographs (kV-setup images) in both studies. Each image pair was evaluated three times by the same observer to obtain repeated measurements enabling the assessment of measurement quality in terms of inter- and intra-observer variability (publication II). In total, 300 (5 observers, 20 patients, 3 repetition) registration were performed per method in both publications. The assessment of positioning accuracy was performed by computing the mean and standard deviation (SD) of the difference of registrations obtained by CT-DRR and sCT-DRR.

Volumetric evaluation

The cone beam computed tomography (CBCT) based verification of patient position was studied by comparing the registrations between CT to CBCT and sCT to CBCT relying on either bony structures or soft tissue contrast. In both registration methods, ten consecutive patients with a randomly chosen fraction were selected and the registration between the images were performed in the Offline Review module of Eclipse TPS (Varian Medical Systems Finland Oy, Helsinki, Finland). The performance of the bone-based registration was assessed as a difference between CT and sCT positioning. The observer was instructed to position the patient using automatic registration tools prior to the treatment. Both PTV and OAR structures were visible during the registration.

In the evaluation of soft-tissue-based position verification, two datasets were prepared using patients with radical prostate cancer. The first set contained original CT, sCT and CBCT images, where the fiducial markers were visible in the images directly or as contours. In the second set, the markers were removed from CT, sCT and CBCT images using the Photoshop 6 (Adobe Inc., City of San José, CA, USA) image processing tool. Three evaluators performed registrations for both image sets (see Figure 5) and the difference between marker-based and soft tissue-based registration was used as the goodness metric of registration for both modalities independently.

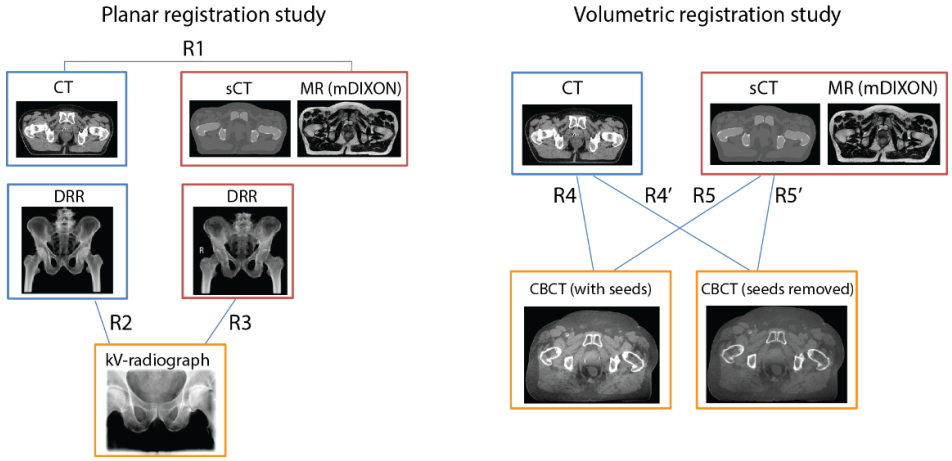

Figure 5: Performed registrations in the patient positioning accuracy study for planar (left) and volumetric (right) registrations. In the planar registration study, the sCT images were rigidly registered to the planning CT using bones, making the reference registration (R1). Both CT- and sCT-based DRRs were registered to an orthogonal planar kV-radiographs pair facilitating comparison between the registrations R2 and R3. In the volumetric registration study, bone-based registration accuracy is evaluated by comparing R4 to R5 whereas, for the soft-tissue based registration the difference R5-R5' and R4-R4' are compared.

3.3 Geometric accuracy of magnetic resonance imaging

In MRI, geometric distortions can arise from various sources. The most significant sources of distortion result from the MR system itself and the patient being imaged [15,18] (see Table 2). In addition, MR-imaging related aspects, such as patient motion, can cause distortions.

The inhomogeneity of the static magnetic field, B_0, creates a spatial displacement of the MR signal along the frequency encoding direction in the image plane, and along the slice selection direction in 2D imaging. The amplitudes of these distortions are related to the strength of the gradient fields along the frequency and slice encoding directions, respectively [18].

In addition, non-linearities in the gradient fields, B_{grad}, translate into spatial displacements in all spatial directions. It has been shown that geometric distortions related to the magnetic field B0 decrease with increasing gradient strength, while gradient-related distortions are virtually independent of the gradient strength [18].

Patient induced field distortions result from large changes of magnetic susceptibility (such as air-tissue interfaces) within the patient [13,19]. These local

field distortions contribute to the total distortion like system induced Bo-distortions. Unlike system related distortions, patient induced distortions vary from patient to patient making their correction more challenging.

In this thesis, the most probable sources of geometric distortion were evaluated using the workflows illustrated in Figure 6.

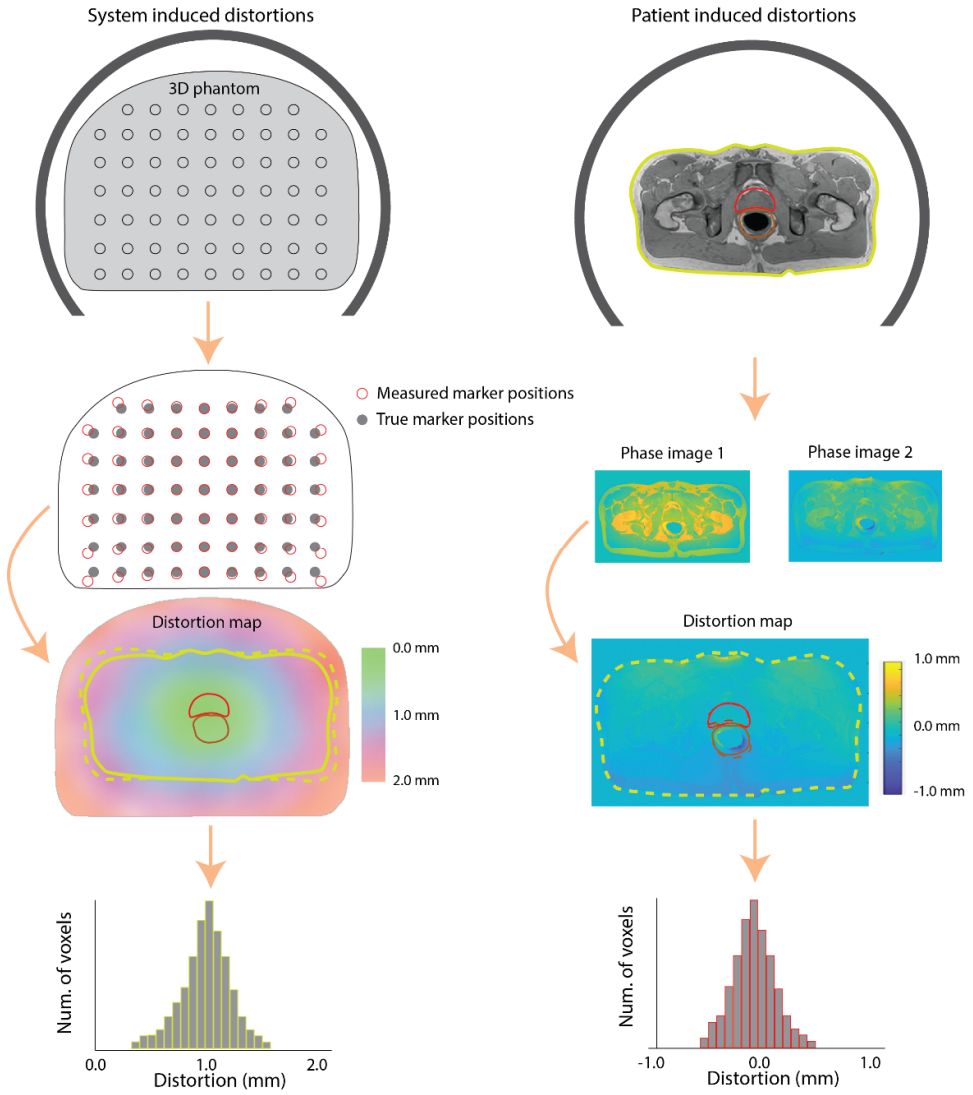

Figure 6: Workflow for analyzing both system (left) and patient (right) induced geometric distortions in MR-images. System induce distortions were measured using a rigid 3D phantom containing MR-positive markers. A distortion map is computed from discrepancies between known and measured marker positions and the map is interpolated to the patient image grid to quantitate the patients contour distortions. Patient induced distortions were analyzed by obtaining an estimate of magnetic field distortion within the patient by mean of dual echo gradient echo image.

3.3.1 MR-system induced geometric distortions

Spatial displacement of the MR signal that originates from static field inhomogeneity and gradient non-linearity can, with 2D Fourier transformation imaging techniques be expressed as [18,20]:

$$\Delta z(x,y,z) = \frac{\Delta B_{grad,z}(x,y,z)}{G_{slice}} + \frac{\Delta B_0(x,y,z)}{G_{slice}} \quad (1)$$

$$\Delta y(x,y,z) = \frac{\Delta B_{grad,y}(x,y,z)}{G_{phase}} \quad (2)$$

$$\Delta x(x,y,z) = \frac{\Delta x(x,y,z)}{G_{read}} + \frac{\Delta B_0(x,y,z)}{G_{read}} \quad (3)$$

with z = slice selection direction, y = phase encoding direction, and x = frequency encode (readout) direction.

Usually geometric accuracy of MRI-devices is tested using existing tools such as ACR (American College of Radiology) phantom. Unfortunately, the diameter of existing phantoms is not sufficient to cover the used FOV in radiotherapy use of MRI. Instead larger, more appropriate phantoms will be needed in MRI-only commissioning.

In publications I and III, a large 3D phantom was used to measure the system-induced geometric distortions arising from gradient field non-linearity and static magnetic field (B0) inhomogeneity. The 3D phantom consists of seven acrylic plates with inter-plate distances of 65 mm. Each plate contains 240 fiducial markers placed in a regular grid with inter-fiducial distances of 25 mm. The phantom was scanned with a T1-weighted fast field echo (FFE) sequence [21] using the same MR scanner type that was used for the generation of the sCT images.

The error as a function of the location inside the MR scanner was determined by comparing the fiducial locations to the known phantom grid. In order to assess the impact of geometric distortions to RT, the 3D distortion map was interpolated to the individual patient's sCT image grid. Using the obtained distortion map, the distortion of the patients PTV and OAR contours were analyzed (see Figure 6 illustration of the workflow). The analysis constituted of measuring the impact of geometric distortions to patient dose calculations.

3.3.2 Patient induced geometric distortions

Patient induced distortion was assessed in publication I by obtaining a ΔB_0 field map for each patient using a dual echo gradient echo MR-image as suggested by Baldwin et al. [22] and Stanescu et al. [23]. The phase images were unwrapped using an algorithm developed by Jenkinson *et al.* [24].

The phase difference between the two images is used to compute a pixel-per-pixel distortion map ΔB_0 in units of millimeters as follows:

$$\Delta B_0 = \frac{\Delta\phi}{2\pi\,\Delta TE}\frac{\Delta x}{BM_x}, \quad (4)$$

where $\Delta\phi$ (radians) is the phase difference between two echoes acquired with phase difference of ΔTE (s), Δx is the pixel size (mm) and BM_x is the receiver

bandwidth (Hz per pixel) of the sequence being studied (see Figure 6 for illustration of the workflow).

Impact of patient induced distortions were analyzed by computing the histogram voxel-by-voxel distortions.

Table 2: Summary of main contributing factors to geometric distortions in MRI.

Distortion	Direction of distortion	Where occurs?	Mitigation	Sequence dependent?	Main field dependency
Static B_0-field inhomogeneity	-Frequency encoding - Slice selection (only in 2D imaging)	Distortions increase with increasing distance from isocenter	-Increase receiver bandwidth -Use of thin slices in 2D imaging	Yes	Distortion scales linearly with field strength
Patient induced static field inhomogeneity	-Frequency encoding - Slice selection	Near large susceptibility differences	Increase receiver bandwidth	Yes	Distortion scales linearly with field strength
Gradient nonlinearity	All directions	Distortions increase with increasing distance from isocenter	use 3D geometry correction	No	Independent of static field strength
Eddy Currents	All directions	Usually very small, observable with DWI-EPI (causes time varying inhomogeneity during signal readout)	Increase receiver bandwidth	Yes, depends on gradient amplitude and slew rate (and receiver BW)	Independent of static field strength

3.3.3 Body outline differences between sCT/MRI and CT

In addition to geometric distortion related to system and patient induced magnetic field distortions, the body outline can differ between CT and sCT because of other reasons. These include, for example, patient breathing motion and scan duration, being substantially longer in MRI compared to CT.

The differences between body outlines in CT and sCT were evaluated as a function of angle from the treatment isocenter in publication III (for illustration of the analysis see Figure 7).

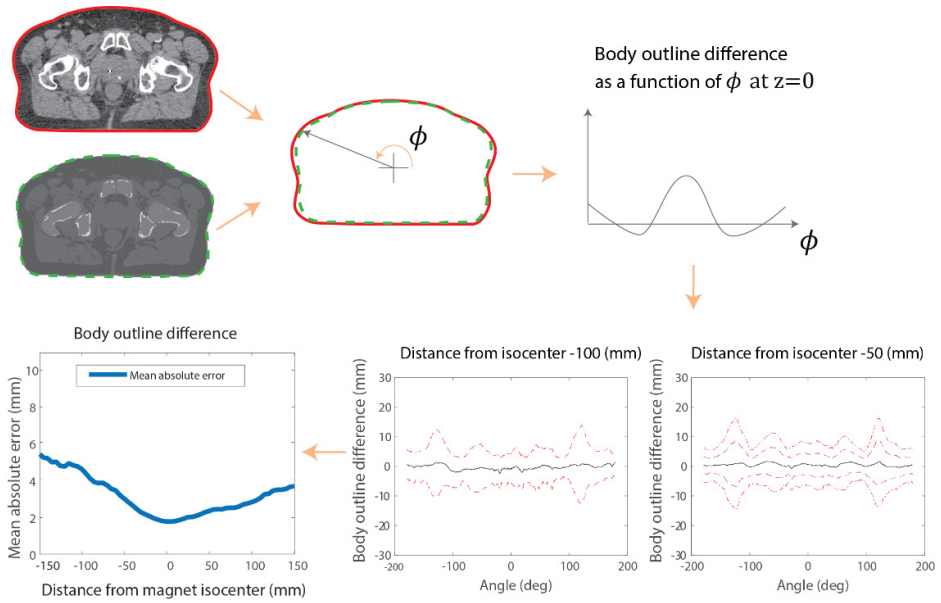

Figure 7: Workflow for body outline difference evaluation. First the body outlines from CT and sCT are overlaid. Then the difference between the outlines are computed along a radial line originating from the treatment isocenter. Thus, the difference also reflects the body outline difference along the treatment beam path. The body outline differences from all patients are averaged at various craniocaudal distances from the isocenter for more condensed information.

3.4 Acceptability of MRI-only workflow

Use of sCT may potentially introduce both dosimetric and geometric inaccuracies. In addition, both sources of inaccuracies may contribute systematically and/or randomly to total treatment accuracy (see Table 3).

When performing dosimetric or position verification evaluations for a sCT discrepancies will be expected. For example, CT and sCT are taken during a separate imaging session and, consequently, it is expected that similar dose or positioning accuracy variations apply that are present inter-fractionally. Thus, the introduced differences must not exceed the average difference that is observed between two fractions. In addition, the use of sCT should not introduce any observable systematic differences to dosimetric or geometric accuracy.

Possible degradations of geometric accuracy in MRI-only workflow compared to the combined workflow of using CT with registered MR should be assessed by comparing to the reduction of systematic uncertainty of up to 2 mm [25] for not having to register CT and MR modalities [26].

Table 3: Contribution of differences between CT and sCT to random and systematic dosimetric and geometric accuracy and precision of MRI-only treatments.

Target of evaluation		Acceptance criteria	Affects
Dosimetric agreement	systematic	Total dosimetric accuracy should not exceed acceptance limit	Under or over dosage of CTV and/or OARs.
	random	Keep below inter-fraction variation	Under or over dosage of CTV and/or OARs.
Positioning	systematic	Total geometric accuracy should not exceed acceptance limit	Strongly affects likelihood for geometric miss
	random	Keep below inter-fraction variation for used IGRT strategy	Contributes to likelihood of geometric miss
MR geometric accuracy	systematic	Total geometric accuracy should not exceed acceptance limit	- Strongly affects likelihood for geometric miss - Body outline distortion affects dose computation accuracy

3.4.1 Achievable dosimetric accuracy

Different tolerance levels for total accuracy requirement of RT have been proposed in the literature in order to ensure adequate tumor control, converging towards a tolerance of 3.0-3.5% [27]. When eradication of the tumor is desirable, an accuracy of 5% in delivered absorbed dose to the target volume has been recommended by ICRU [28].

A way of quantifying the total uncertainty is to analyze the uncertainty in the different links in the radiotherapy treatment chain. In Table 4 up-to-date estimates of uncertainties in modern RT process are presented. The figures are based on AAPM estimates [29] and more up-to-date estimates presented by IAEA [30].

Table 4: Estimates of uncertainty in modern RT (in terms of one standard deviation) in absolute dose in the patient for the complete treatment procedure using megavoltage photons. Uncertainty expressed as one standard deviation (SD).

Sources of Uncertainties	Uncertainty (%)
Dose at the calibration point in water	1.5
Additional uncertainty for other points	0.6
Beam Monitor stability	1.0
Beam flatness	1.5
Patient data	1.5
Patient set up and organ motion	2.5
Dose calculation	2
TOTAL	4.2

3.4.2 Achievable geometric accuracy

The geometric uncertainty cumulates from practically all steps required for the complete external beam workflow [10,31]. In Table 5 the sources of geometric uncertainties are presented and divided into uncertainties causing systematic and random error in the workflow of external beam radiation therapy. The registration uncertainty for a CT-to-MR registration for a prostate case was estimated to be 2 mm based on current reports in scientific literature [25].

Table 5: Achievable geometric accuracy in external beam radiation therapy of pelvis using combined workflow utilizing CT for dose computation and MRI for target and OAR contouring. Uncertainty expressed as one standard deviation (SD). The Planning target volume (PTV) margin is calculated as 2.5*SE+0.7*RE, where SE is systematic error and RE is random error.

	Systematic error (mm)			Random error (mm)		
Contributing factor	**RL**	**AP**	**CC**	**RL**	**AP**	**CC**
Target delineation	1.8	1.8	2.8	0	0	0
Target MR geometrical distortion	0.2	0.2	0.2	0	0	0
MR to CT registration	2	2	2	0	0	0
Total treatment planning uncertainty	**2.7**	**2.7**	**3.4**	**0**	**0**	**0**
Intra-fraction uncertainty	0	0	0	0.4	1.4	1.4
DRR to X-ray registration	0	0	0	0.5	0.5	0.1
X-ray imaging uncertainty	1	1	1	0	0	0
Bone segmentation inaccuracy	0	0	0	0	0	0
Total set-up uncertainty	1	1	1	0.6	1.5	1.4
Total	**2.9**	**2.9**	**3.6**	**0.6**	**1.5**	**1.4**
Total systematic and random error	3.9	3.9	5.0	0.6	1.5	1.4
PTV margin (mm)	**7.6**	**8.2**	**10.0**			

4. Summary of results

4.1 Dosimetric agreement

Dosimetric accuracy of used sCT generation method was evaluated in publications I and III.

The mean (SD) dose differences of the PTV mean dose computed over cancer groups, each with 15 patients, were less than 0.2 (0.4) % between sCTc and CT. The mean relative dose differences for studied volumes were less than 0.3 (0.6)% for OARs (see the Table 6).

Table 6: Mean (SD) dosimetric differences between sCT and CT-based dose computations. Results from publication III.

	Pelvic lymph nodes (n=15)	Rectal cancer (n=15)	Gynecological cancer (n=15)	Prostate cancer, post-operative (n=15)	Prostate cancer, definitive (continuous HU, n=15)	Prostate cancer, definitive (bulk HU, n=15)
DVH comparison						
PTV						
Mean	0.0 (0.4)	0.1 (0.3)	-0.2 (0.4)	0.1 (0.3)	0.1 (0.2)	0.1 (0.2)
$D_{2\%}$	0.1 (0.5	0.5 (0.6)	0.1 (0.4)	0.2 (0.6)	0.1 (0.2)	0.1 (0.2)
$D_{50\%}$	0.0 (0.4)	0.1 (0.3)	-0.2 (0.4)	0.0 (0.3)	0.1 (0.2)	0.1 (0.2)
$D_{98\%}$	-0.1 (0.3)	0.0 (0.4)	-0.2 (0.5)	0.0 (0.3)	0.1 (0.3)	0.1 (0.2)
Rectum						
$V_{95\%}$	0.1 (0.3)	-	-0.2 (1.8)	0.1 (0.4)	0.1 (0.1)	0.1 (0.1)
$V_{75\%}$	0.0 (0.1)	-	-0.3 (0.6)	0.0 (0.2)	0.0 (0.1)	0.0 (0.1)
Bladder						
$V_{95\%}$	-0.1 (0.3)	0.1 (0.5)	-0.1 (0.9)	-0.1 (0.2)	0.0 (0.2)	0.0 (0.2)
$V_{75\%}$	0.0 (0.2)	0.1 (0.2)	0.0 (0.2)	0.0 (0.1)	0.0 (0.1)	0.0 (0.1)
Gamma statistics ($V_{10\%}$)						
2%/2mm	97.7 (0.7)	96.2 (2.0)	97.0 (1.5)	98.0 (0.6)	99.1 (0.5)	98.9 (0.4)
Dose statistics per volume						
$V_{10\%}$	0.0 (0.2)	0.1 (0.3)	-0.1 (0.3)	-0.1 (0.2)	-0.1 (0.2)	-0.3 (0.2)

The mean gamma-index pass-rate evaluation was highest for the prostate cancer patients and lowest for the gynecological and rectal cancer patients. Among all groups, the average pass-rates within volumes of V10% were higher than 95% with 2%/2mm gamma-criteria, respectively. The lowest pass-rate was for the

rectum cancer group being 96.2 (2.0) %. The mean relative dose differences were less than 0.3 (0.3) % for all studied cancer groups and volumes of interest.

4.1.1 Acceptable dosimetric deviation

In Table 7 the total uncertainty is estimated when the error from MRI-only based dose calculation is taken into account (see Table 4). Assuming a 2% uncertainty in the calculation algorithm when used on CT data, an additional uncertainty of 2.6% due to the MRI-only dose planning step fulfils the 5% dose accuracy criterion today.

Table 7: Determination of the total uncertainty (in units of 1 SD) when MRI dose planning is introduced to the radiotherapy treatment chain. Based on the estimates in Table 4.

Additional uncertainty inherent from MRI-based dose planning (mm)	Total Uncertainty (%)
1	4.4
2	4.7
3	5.2

4.2 Positioning accuracy

Positioning accuracy and precision were evaluated in publications II and III.

4.2.1 Positioning based on planar images

Using the bulk sCT method (sCTb) in publication I, mean (SD) differences between DRR-to-kV radiograph registrations were -0.5 (1.4), -0.1 (1.3) and 0.1 (0.8) mm in AP, CC and LR directions, respectively. Whereas, with the sCT with continuous HU values (sCTc) in publication III, the differences were -0.1 (1.4), 0.3 (1.2) and -0.1 (0.8) mm. Boxplot of the differences with both methods is illustrated in Figure 9.

Typical digitally reconstructed radiographs from CT, sCTc and sCTb are illustrated in Figure 8.

4.2.2 CBCT-based positioning

For the bone-based positioning studied with ten patients, the mean (SD) observer differences were 0.1 (1.1) mm, 0.1 (0.6) mm and -0.0 (0.2) mm in AP, CC and LR directions, respectively (see Figure 10).

For the soft-tissue-based positioning in the AP direction, the mean (SD) differences between fiducial markers- and soft-tissue-based registrations were 0.5 (1.8) mm, 0.5 (1.8) mm and 1.1 (1.8) mm for CT, sCTc and sCTb, respectively. In the CC direction, the mean (SD) differences were -0.2 (1.1) mm, -0.6 (1.3) mm and -0.8 (2.3) mm, respectively. Furthermore, the smallest registration differences were seen in the LR direction, being 0.1 (0.7) mm, -0.4 (0.7) mm and -0.2 (0.6) mm for CT, sCTc and sCTb, respectively.

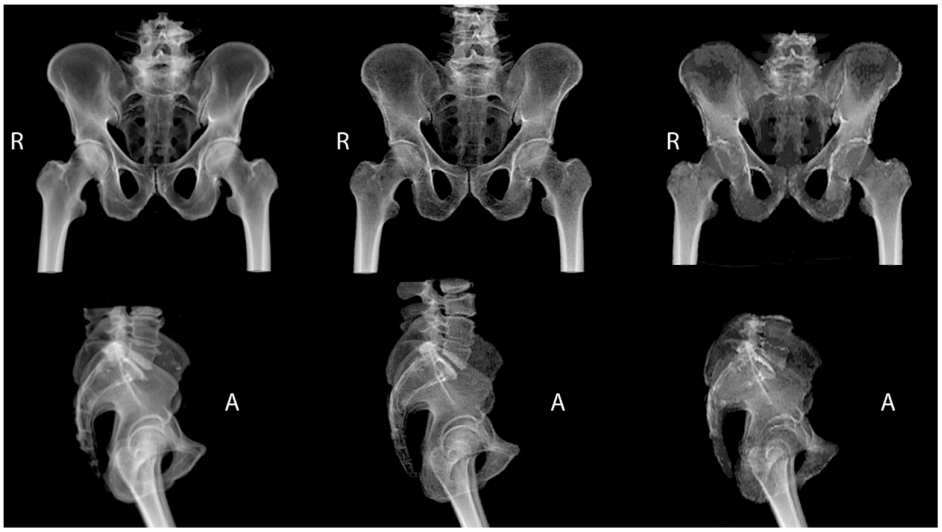

Figure 8: Example DRR images from Eclipse treatment planning system using bone rendering (HU values less than 100 and above 1000 omitted). CT (left), sCTc with continuous HU values (middle), and sCTb with discrete HU values, (right).

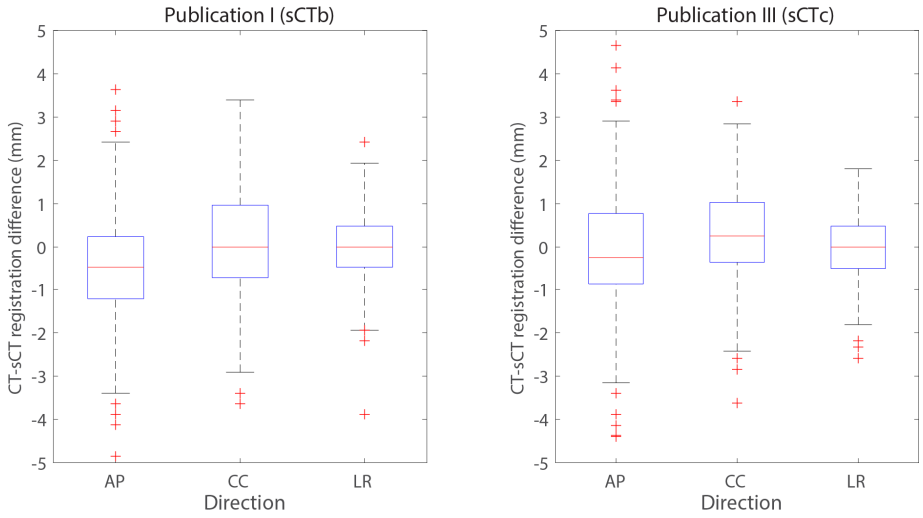

Figure 9: Boxplot of difference between CT-DRR to planar kV-image in anteroposterior (AP), cranio-caudal (CC) and left-right (LR) directions in publication I (left) and III (right).

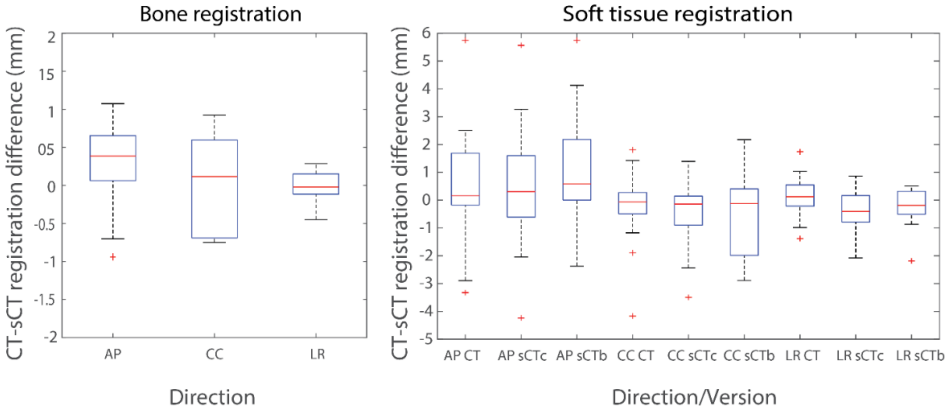

Figure 10: Left: Box-plot of registration difference between CT-to-CBCT and sCTb-to-CBCT using bone-based registration in left-right (LR), anterior-posterior (AP) and cranio-caudal (CC) direction. Right: Box-plot of registration differences between CT to CBCT and sCT to CBCT using soft-tissue contrast with respect to marker-based registration in AP, CC and LR directions.

4.2.3 Total spatial uncertainty between workflows

Comparison of Table 5 and Table 8 shows that omission of the CT to MR co-registration in the MRI-only workflow reduces the systematic uncertainty in the EBRT workflow of pelvis. In turn, according to our results, use of sCT for patient positioning may add both systematic and random geometric uncertainty resulting from increased DRR to X-ray image registration uncertainty. However, the analysis showed that smaller margin of 6.9 vs. 7.6, 6.8 vs. 8.8 and 8.6 vs. 10 mm in right-left, anteroposterior and craniocaudal directions can be used in MRI-only workflow vs. MR-fusion based workflow. Furthermore, in Publication II we showed that when registration errors are larger than 1.7 mm, 1.5 mm, and 1.1 mm in AP, CC and LR directions, statistically significantly smaller CTV to PTV margin was needed in MRI-only workflow.

Table 8: Achievable geometric accuracy in external beam radiation therapy of pelvis using MRI-only workflow. Uncertainty expressed as one standard deviation (SD). The PTV margin is calculated as 2.5*SE+0.7*RE, where SE is systematic error and RE is random error.

	sCT systematic error (mm)			sCT random error (mm)		
Contributing factor	**RL**	**AP**	**CC**	**RL**	**AP**	**CC**
Target delineation	1.8	1.8	2.8	0	0	0
MR geometrical distortion	0.2	0.2	0.2	0	0	0
MR to CT registration	0	0	0	0	0	0
Total treatment planning uncertainty	1.8	1.8	2.8	0	0	0
Intra-fraction movement	0	0	0	0.4	1.4	1.4
DRR to X-ray registration [1]	1	1	0.6	0.5	0.5	0.1
X-ray imaging uncertainty	1	1	1	0	0	0
Total set-up uncertainty	1.4	1.4	1.2	0.6	1.5	1.4
Total	**2.3**	**2.3**	**3.0**	**0.6**	**1.5**	**1.4**
Total systematic and random error	2.9	2.9	4.1	0.6	1.5	1.4
PTV margin (mm)	**6.2**	**6.8**	**8.6**			

4.3 Geometric accuracy

Geometric accuracy of used sCT generation method was evaluated regarding system induced geometric distortions (publications I and III) and the contribution of patient induces distortion was assessed in publication I.

4.3.1 System's geometric accuracy

Geometric fidelity of the MR images was assessed for all patients and PTVs in the ROIs consisting of the clinical RT planning structures.

For all OAR structures, the distortion was measured to be less than 1 mm for all patients and PTVs (see illustration of the organ and disease specific figures

[1] Based on results from publication II, Figure 6

in Figure 11). Furthermore, the maximum distortion in the body outline at which the radiation beam enters the body was less than 2 mm for all prostate and rectal cancer patients. For one gynecological patient, the body outline distortion was greater than 2 mm in the cranial end of the PTV. However, it can be seen in the standard deviation of the body outline distortion that the distortion was less than 2 mm for most of the outline.

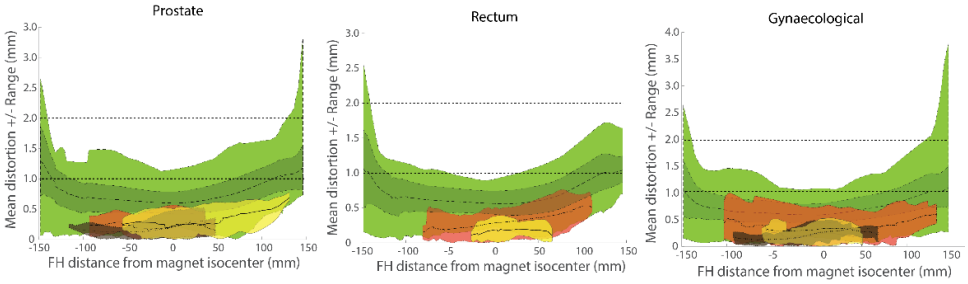

Figure 11: Population mean (range) distortion per structure as a function of distance from the isocenter of the device along craniocaudal direction

4.3.2 Patient-induced geometric distortions

Patient-induced geometric distortions were studied in the pelvis anatomy for four patients. In Figure 12, an example of the magnitude of patient-induced distortion is given in axial plan near the isocenter of the MR device. Largest distortions were found near tissue-air interfaces (around rectum and near body outline). The distortions were found to be less than the pixel size of 1 mm for all studied patients.

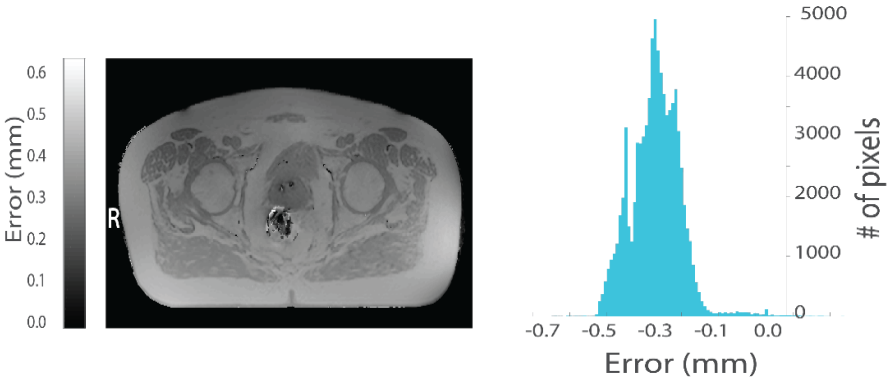

Figure 12: Evaluation of patient induced geometric distortion was based on phase map.

4.3.3 Body outline distortions

The body outline differences, and the MRI-system-induced geometric distortion were the smallest close to the isocenter of MRI device. Nearby the isocenter, the difference of body outline between CT and sCTc was 2 mm on average, but it increased farther away from the isocenter and reaches the average difference of 6 mm at 150 mm (see Figure 13). The contribution of geometric distortion to the skin outline difference was less than 2 mm within the investigated volumes.

The systematic difference between CT and sCTc body outlines was observed for various CC distances from the isocenter of MRI device (see Figure 14). The largest systematic differences were present toward the cranial end of the studied FOV at angles corresponding patient's anterior direction (angle 0°). Towards the caudal end, systematic differences were not found, but the random uncertainty increased.

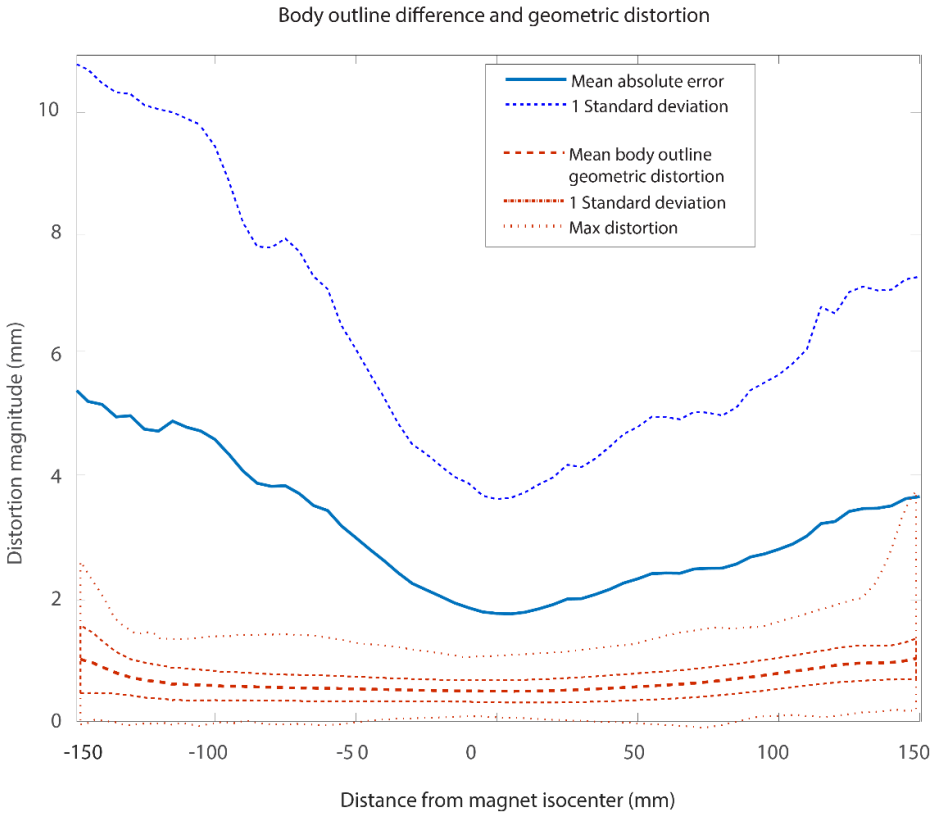

Figure 13: Mean absolute body outline difference (solid blue line) and mean+1SD (dash-dotted line) between CT and sCT images. Mean body outline geometric distortion (dashed red line), mean +1SD (red dashed-dotted) and max distortion (red dashed line) of the body outline due to geometric distortions of MR images as a function of (cranio-caudal) distance from the isocenter of MRI device.

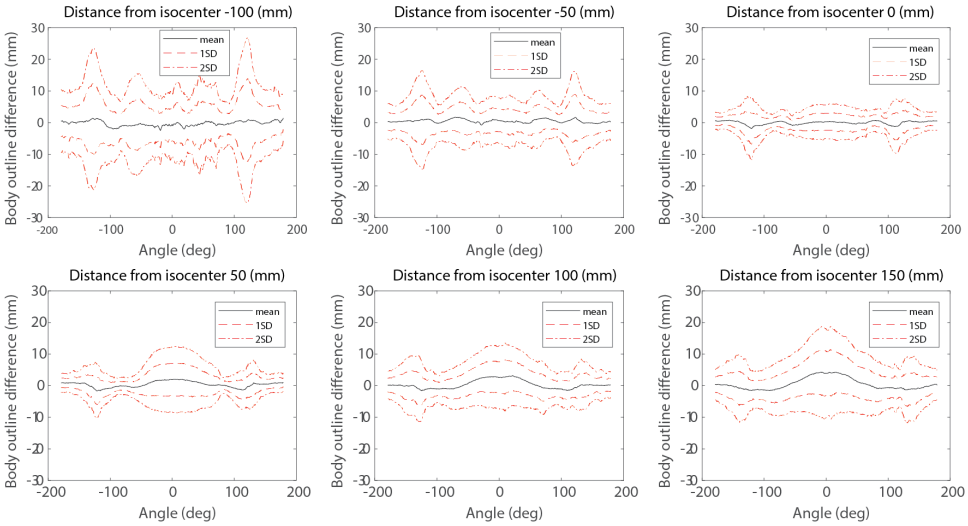

Figure 14: Body outline difference between CT and sCT images (CT - sCT) for various cranio-caudal positions (at the distances from -100 (caudal-end) to 150 mm (cranial-end) from the isocenter of MRI device) averaged over all 75 patients included in the study.

5. Discussion

5.1 MRI-only for EBRT of pelvic malignancies

MRI-only radiotherapy will eliminate the systematic registration errors introduced when transferring MRI information to the CT. However, challenges concerning the deficient information about electron or mass density, necessary for dose calculation and patient setup are introduced [26,32,33]. Thus, prior to clinical use of MRI-only, all impacted aspects of the workflow need to be assessed thoroughly—a procedure called commissioning.

The results described in this thesis has paved the way for the implementation of a clinical MRI-only radiotherapy workflow for pelvic malignancies. Specifically, the work was focused on:

- Dosimetric accuracy of a commercial sCT method
- Geometric accuracy of patient positioning in the MRI-only workflow
- Geometric accuracy of MR images used for sCT generation

5.1.1 Dosimetric agreement

The dosimetric accuracy was assessed by comparing sCT- to CT-based dose computation. In publication III, the dosimetric differences between CT and sCTc were found to be small among all cancer groups. Considering mean (SD) gamma-index pass-rates of 98.0 (0.6)%, 96.2 (2.0)% and 96.5 (2.3)% using 2%/2mm gamma-criteria and mean (SD) dose differences of -0.1 (0.2)%, 0.1 (0.3)% and -0.1 (0.3)% for the prostate base, rectum and gynecological cancer patients, the dosimetric agreement was found to meet the clinical acceptance criteria. Maspero *et al.* [34] used a deep learning-based sCT approach and evaluated its applicability for pelvic cancer patients and obtained pass-rates that were in line with this study. In addition, Maspero et al. [4] evaluated the feasibility of the same method used in this study (sCTb) for rectal cancer patients obtaining the mean gamma-index pass-rate of 95.2 (4.0)% and mean dose deviation of -0.3 (0.2)% of prescription dose.

Our results from publications I and III and those by Maspero *et al.* [34] showed that the dosimetric agreement was decreased for rectum and gynecological cancer patients in comparison to prostate cancer patients. According to the body outline comparison between CT and sCT, the difference increases farther away from the imaging isocenter along CC axis. However, this was unlikely

due to geometric distortion, which increases with growing distance from the isocenter, but rather due to breathing and positioning differences between CT and MRI modalities. Thus, higher dosimetric disagreement for patients with longer PTVs in cranio-caudal (CC) direction might arise from these differences. It has been suggested by Persson *et al.* that systematic differences between body outlines on CT and MRI could be attributable muscle relaxation during longer scan time [8].

Acceptability of dosimetric agreement
According to our results, the mean dosimetric uncertainty resulting from the use of the sCT remained below 1% for all tumor groups and all patients (Table 2 in Publication III). Thus, the impact to the total dosimetric uncertainty of the EBRT workflow remains on acceptable level (see Table 7).

5.1.2 Patient positioning

Positioning based on planar images

In this study, we measured the accuracy of sCT DRR to planar kV-image registration for IGRT of pelvic EBRT by comparing to a CT DRR to kV-image registration. According to the results, average positioning differences were smaller than 0.5 mm in all directions, respectively. These figures are similar to what has been reported for DRR to kV registrations for sCTs based on manually contoured bone segmentations in a similar measurement setup [35].

Based on the results, given that there is an uncertainty associated with CT-to-MR registration larger than 1.7 mm, 1.5 mm, and 1.1 mm in vertical, longitudinal and lateral direction, it's likely that use of MRI-only has a positive effect to the total geometric accuracy. In the literature uncertainties of 2 mm have been reported for prostate RT (Roberson et al [25]). Thus, we conclude that in terms of total geometric accuracy benefits of using sCT likely outweigh the small increase in sCT DRR-based positioning uncertainty.

CBCT-based positioning

The mean difference between bone-based positioning between CT to CBCT and sCT to CBCT was less than 0.2 mm in all directions. The result was in agreement with earlier studies reporting sub-millimeter accuracy for the bulk HU version of the used sCT method [1,5].

Here, for the first time the soft-tissue prostate positioning of a sCT method was evaluated by comparing it to the fiducial marker-based reference. No differences in the performance between CT and sCTc were observed. However, for sCTb, the differences were slightly larger in the CC and AP directions but not in LR direction. Thus, no major difference in positioning performance was found between the methods.

Like the planar evaluation, we conclude that the benefits of the use of sCT in term of total spatial uncertainty will out weight the small positioning error introduced when sCT images are used for patient position verification.

5.1.3 Geometric accuracy

According to the literature, the geometric accuracy of 2 mm in ROI and 1 mm in PTV is desired for MR-guided RT [15]. In addition, MR systems dedicated to radiotherapy would require geometric accuracy within 2 mm [36]. We found that for all the patients the system-induced geometrical distortion was less than 1 mm for PTV and OAR volumes. In addition, the deformation of body contour was less than 2 mm for all except one gynecological patient, when considering only the area at which the radiation beam enters the body. In Figure 11, however, one can see that the geometric distortion of body outline increases rapidly in the periphery of analyzed volumes. This indicates that 30 cm FOV in the CC direction cannot be increased for larger PTVs without compromising the geometric accuracy.

Patient-induced distortions in transversal plane were assessed in the vicinity of MR device's isocenter for avoiding the contribution of system induced B0 inhomogeneity. The largest distortions were found in air-tissue interfaces. The acceptable distortions were less than ± 0.5 mm for all studied patients being smaller than system related distortions. When optimizing MR-sequences to be used in RT planning, the receiver bandwidth must be set high enough to avoid distortions of up to several millimeters [23]. In agreement with our results, Adjeiwaah *et al.* [13] found that the magnitude of patient-induced susceptibility distortions to be larger compared with residual system distortions at all delineated structures except the external contour.

The overall geometric accuracy of the MR images was found to be acceptable for EBRT of the pelvic area radiotherapy.

5.2 Uncertainties and limitations in this study

A fundamental property of MRI-only strategies is that the dosimetric accuracy can't be measured without comparing to CT-based dose computations. This results into laborious dose comparison in both commissioning of a new method and when a MRI-only solution or the MR-imaging is updated.

It is common that evaluations of sCT methods are performed with a relatively small sample sizes and as a single center studies [32,33]. The sample sizes are limited as manual comparison is very laborious. The small sample size limits also the reliability of generalizability of our results. Unfortunately, inclusion of sample sizes required for covering the clinical variation of patients is not feasible with manual and laborious comparative analysis performed in this study. From the hospitals point of few the benefits of using MRI-only may be out weighted by the burden of performing the comparisons. Thus, more automated and standardized methods to establish and maintain dosimetric and geometric accuracy of MRI-only methods needs to be developed.

Each sCT method is different in terms of segmentation of soft-tissue and bones. Thus, it is mandatory that all methods are commissioned using the clinical workflow and local patient cohort at the site. Consequently, the results presented in this thesis may not apply for other sites and, especially, for other sCT generation methods. However, the results shall be interpreted as a reference for

the performance evaluations at other hospitals performing their own evaluations of the method.

Our evaluation of the MR-related distortion was limited to the MR image that was used for sCT generation. In addition, other MR-images are taken within the same imaging session and used for target and OAR contouring. The geometric accuracy may vary from sequence to sequence and the results obtained in this work will not cover other sequence types and acquisition parameters. For example, echo planar imaging (EPI), used for, e.g. diffusion weighted imaging, produces order of magnitude larger distortions [22]. The current practice of characterizing MR geometric distortions utilizing spatial accuracy phantoms alone may not be enough for an MRI-only radiotherapy workflow. Therefore, measures to mitigate patient induced susceptibility effects in clinical practice such as patient-specific correction algorithms are needed to complement existing distortion reduction methods, especially for EPI based imaging [13].

5.3 Challenges and outlook of MRI in RT

A few hospitals have reported about clinical use of MRI-only [1,6,9]. Interest toward MRI-only is growing but there remain some important challenges that need to be addressed prior to wider clinical acceptance of MRI-only.

Quality assurance (QA) plays an important role in radiation therapy by ensuring the high accuracy requirements in delivery of treatments. When the role of MR imaging changes from auxiliary to primary, also the demands for the QA will become stricter. Even though there are some publications related to QA in MRI-only [37], it remains an area requiring further development and investigation. Especially, quality assurance of dosimetric accuracy for individual patients remains a challenge. Possible solutions for patient dosimetric QA is the use of the electronic portal imaging dosimetry (EPID) [38,39] or patient bulk anatomical density maps [40].

The typical scan duration of MRI-only simulation is around 20 minutes Tyks. It is evident that substantial organ motion may take place within the scanning session. The movement of soft-tissue between sequences, for example prostate or difference in bladder volume, could be mitigated by MR-positive markers [41] so that position of the prostate could be verified to be the same between images.

5.4 Conclusions

Pelvic cancer patients would benefit from the usage of sCT in terms of decreased total uncertainties in EBRT [34,42,43]. This study demonstrated dosimetric, positioning, and geometric accuracy of an sCT for the EBRT of pelvic cancers. This study covered several possible positioning workflows that have not been assessed previously. The results were relevant when aiming to extend the use of sCT method to pelvic cancer patients in general.

We showed that the dosimetric, geometric and positioning accuracy is enough for clinical use of the method investigated.

References

1. Tyagi N, Fontenla S, Zhang J, Cloutier M, Kadbi M, Mechalakos J, et al. Dosimetric and workflow evaluation of first commercial synthetic CT software for clinical use in pelvis. Phys Med Biol. 2017;62:2961–75.
2. Christiansen RL, Jensen HR, Brink C. Magnetic resonance only workflow and validation of dose calculations for radiotherapy of prostate cancer. Acta Oncol (Madr). 2017;56:787–91.
3. Bratova I, Paluska P, Grepl J, Sykorova P, Jansa J, Hodek M, et al. Validation of dose distribution computation on sCT images generated from MRI scans by Philips MRCAT. Reports Pract Oncol Radiother. 2019;24:245–50.
4. Kemppainen R, Suilamo S, Tuokkola T, Lindholm P, Deppe MH, Keyriläinen J. Magnetic resonance-only simulation and dose calculation in external beam radiation therapy: a feasibility study for pelvic cancers. Acta Oncol (Madr). 2017;56:792–8.
5. Maspero M, Tyyger MD, Tijssen RHN, Seevinck PR, Intven MPW, van den Berg CAT. Feasibility of magnetic resonance imaging-only rectum radiotherapy with a commercial synthetic computed tomography generation solution. Phys Imag Radiat Oncol. 2018;7:58–64.
6. Kemppainen R, Suilamo S, Ranta I, Pesola M, Halkola A, Eufemio A, et al. Assessment of dosimetric and positioning accuracy of a magnetic resonance imaging-only solution for external beam radiotherapy of pelvic anatomy. Phys Imag Radiat Oncol. 2019;11:1–8.
7. Maspero M, Seevinck PR, Schubert G, Hoesl MAU, Asselen B van, Viergever MA, et al. Quantification of confounding factors in MRI-based dose calculations as applied to prostate IMRT. Phys Med Biol. 2017;62:010.
8. Persson E, Gustafsson C, Nordström F, Sohlin M, Gunnlaugsson A, Petruson K, et al. MR-OPERA: A Multicenter/Multivendor Validation of Magnetic Resonance Imaging–Only Prostate Treatment Planning Using Synthetic Computed Tomography Images. Int J Radiat Oncol Biol Phys. 2017;99:692–700.
9. Tenhunen M, Korhonen J, Kapanen M, Seppälä T, Koivula L, Collan J, et al. MRI-only based radiation therapy of prostate cancer: workflow and early clinical experience. Acta Oncol (Madr). 2018;0:1–6.
10. Van Herk M. Errors and Margins in Radiotherapy. Semin Radiat Oncol. 2004;14:52–64.
11. Walker A, Liney G, Metcalfe P, Holloway L. MRI distortion: Considerations for MRI based radiotherapy treatment planning. Australas Phys Eng Sci Med. 2014;37:103–13.
12. Moerlandt MA, Beersmat R, Bhagwandient R, Wijrdemant HK, Bakkerl G. Analysis and correction of geometric distortions in 1.5 T magnetic resonance images for use in radiotherapy treatment planning. Phys Med Biol Phys Med Biol. 1995;40:1651–64.
13. Adjeiwaah M, Bylund M, Lundman JA, Thellenberg Karlsson C, Jonsson JH, Nyholm T. Quantifying the effect of 3T MRI residual system and patient-induced susceptibility distortions on radiotherapy treatment planning for prostate cancer. Int J Radiat Oncol. 2017;100:317–24.
14. Chen Z, Ma C-M, Paskalev K, Li J, Yang J, Richardson T, et al. Investigation of MR image distortion for radiotherapy treatment planning of prostate cancer. Phys Med Biol. 2006 Mar 21;51:1393–403.
15. Weygand J, Fuller CD, Ibbott GS, Mohamed ASR, Ding Y, Yang J, et al. Spatial

Precision in Magnetic Resonance Imaging-Guided Radiotherapy: The Role of Geometric Distortion. Int J Radiat Oncol. 2016;95:1304–16.
16. Eggers H, Brendel B, Duijndam A, Herigault G. Dual-echo Dixon imaging with flexible choice of echo times. Magn Reson Med. 2011;65:96–107.
17. Ecabert O, Peters J, Schramm H, Lorenz C, Von Berg J, Walker MJ, et al. Automatic model-based segmentation of the heart in CT images. IEEE Trans Med Imaging. 2008;27:1189–202.
18. Fransson A, Andreo P, Pötter R. Aspects of MR Image Distortions in Radiotherapy Treatment Planning. Strahlenther Onkol. 2001;177:59–73.
19. Glide-Hurst C, Nejad-Davarani S, Weiss S, Zheng W, Chetty IJ, Renisch S. Per-organ assessment of subject-induced susceptibility distortion for MR-only male pelvis treatment planning. Radiat Oncol. 2018;13:1–9.
20. Bakker CJG, Moerland MA, Bhawandien R, Beersma R. Analysis of machine-dependent and object-induced geometric distortion in 2DFT MR imaging. Magn Reson Imaging. 1992;10:597–608.
21. van der Meulen P, Groen JP, Tinus AMC, Bruntink G. Fast Field Echo imaging: An overview and contrast calculations. Magn Reson Imaging. 1988;6:355–68.
22. Baldwin LLN, Wachowicz K, Fallone BG. A two-step scheme for distortion rectification of magnetic resonance images. Med Phys. 2009;36:3917.
23. Stanescu T, Wachowicz K, Jaffray D. Characterization of tissue magnetic susceptibility-induced distortions for MRIgRT. Med Phys. 2012;39:7185–93.
24. Jenkinson M. Fast, automated, N-dimensional phase-unwrapping algorithm. Magn Reson Med. 2003;49:193–7.
25. Roberson PL, McLaughlin PW, Narayana V, Troyer S, Hixson G V., Kessler ML. Use and uncertainties of mutual information for computed tomography/magnetic resonance (CT/MR) registration post permanent implant of the prostate. Med Phys. 2005;32:473–82.
26. Owrangi AM, Greer PB, Glide-Hurst CK. MRI-only treatment planning: Benefits and challenges. Phys Med Biol. 2018;63.
27. Thwaites D. Accuracy required and achievable in radiotherapy dosimetry: have modern technology and techniques changed our views? J Phys Conf Ser. 2013;444:012006.
28. Determination of Absorbed Dose in a Patient Irradiated by Beams of X or Gamma Rays in Radiotherapy Procedures. ICRU Report 24. ICRU; 1976.
29. Papanikolaou N, Battista J, Boyer A. AAPM Report No. 85 Tissue inhomogeneity corrections for megavoltage photon beams. AAPM Task Gr 65. 2004;
30. Andreo P, Radiation M, Section P. IAEA TRS-398: Absorbed Dose Determination in External Beam Radiotherapy based on Standards of Absorbed Dose to Water. 2006;2006.
31. Nyholm T, Nyberg M, Karlsson MG, Karlsson M. Systematisation of spatial uncertainties for comparison between a MR and a CT-based radiotherapy workflow for prostate treatments. Radiat Oncol. 2009;4:54.
32. Johnstone E, Wyatt JJ, Henry AM, Short SC, Sebag-Montefiore D, Murray L, et al. Systematic Review of Synthetic Computed Tomography Generation Methodologies for Use in Magnetic Resonance Imaging–Only Radiation Therapy. Int J Radiat Oncol Biol Phys. 2018;100:199–217.
33. Edmund JM, Nyholm T. A review of substitute CT generation for MRI-only radiation therapy. Radiat Oncol. 2017;12:28.
34. Maspero M, Savenije MHF, Dinkla AM, Seevinck PR, Intven MPW, Jurgenliemk-Schulz IM, et al. Dose evaluation of fast synthetic-CT generation using a generative adversarial network for general pelvis MR-only radiotherapy. Phys Med Biol. 2018;63:1–14.
35. Korhonen J, Kapanen M, Sonke J-J, Wee L, Salli E, Keyriläinen J, et al. Feasibility of MRI-based reference images for image-guided radiotherapy of the pelvis with either cone-beam computed tomography or planar localization images. Acta Oncol (Madr). 2015 Sep 18;54:889–95.
36. No. 46 AR. COMPREHENSIVE QA FOR RADIATION ONCOLOGY Published for the by the American Institute of Physics COMPREHENSIVE QA FOR. Medicine (Baltimore).

37. Sun J, Dowling J, Pichler P, Menk F, Rivest-Henault D, Lambert J, et al. MRI simulation: End-to-end testing for prostate radiation therapy using geometric pelvic MRI phantoms. Phys Med Biol. 2015;60:3097–109.
38. Torres-Xirau I, Olaciregui-Ruiz I, van der Heide UA, Mans A. Two-dimensional EPID dosimetry for an MR-linac: Proof of concept. Med Phys. 2019;
39. Torres-Xirau I, Olaciregui-Ruiz I, Baldvinsson G, Mijnheer BJ, Van Der Heide UA, Mans A. Characterization of the a-Si EPID in the unity MR-linac for dosimetric applications. Phys Med Biol. 2018;63.
40. Choi JH, Lee D, Connor LO, Chalup S, Welsh JS, Dowling J, et al. Bulk Anatomical Density Based Dose Calculation for Patient-Specific Quality Assurance of MRI-Only Prostate Radiotherapy. 2019;9:1–10.
41. Lim TY, Kudchadker RJ, Wang J, Bathala T, Szklaruk J, Pugh TJ, et al. Development of a magnetic resonance imaging protocol to visualize encapsulated contrast agent markers in prostate brachytherapy recipients: initial patient experience. J Contemp Brachytherapy. 2016;8:235–42.
42. Liu L, Jolly S, Cao Y, Vineberg K, Fessler JA, Balter JM. Female pelvic synthetic CT generation based on joint intensity and shape analysis. Phys Med Biol. 2017;62:2935–49.
43. Katz LM, Wang H, Duckworth T, Kim D, Das IJ, Lymberis SC. Use of Synthetic CT for Magnetic Resonance–Only Based External Beam Pelvic Radiation Therapy of Cervical Cancer. Int J Radiat Oncol. 2017;99:E676–7.

Publication 1

Kemppainen R, Suilamo S, Tuokkola T, Lindholm P, Deppe MH, Keyriläinen J. Magnetic resonance-only simulation and dose calculation in external beam radiation therapy: a feasibility study for pelvic cancers. Acta Oncol., 2017;56:792–8.

ACTA ONCOLOGICA, 2017
http://dx.doi.org/10.1080/0284186X.2017.1293290

Taylor & Francis
Taylor & Francis Group

ORIGINAL ARTICLE

Magnetic resonance-only simulation and dose calculation in external beam radiation therapy: a feasibility study for pelvic cancers

Reko Kemppainen[a,b], Sami Suilamo[c,d], Terhi Tuokkola[e], Paula Lindholm[d], Martin H. Deppe[a] and Jani Keyriläinen[c,d]

[a]Philips MR Therapy, Vantaa, Finland; [b]Department of Neuroscience and Biomedical Engineering, Aalto University School of Science, Espoo, Finland; [c]Department of Medical Physics, Turku University Hospital, Turku, Finland; [d]Department of Oncology and Radiotherapy, Turku University Hospital, Turku, Finland; [e]Turku PET-Centre, Turku University Hospital, Finland and University of Turku, Turku, Finland

ABSTRACT

Background: The clinical feasibility of using pseudo-computed tomography (pCT) images derived from magnetic resonance (MR) images for external bean radiation therapy (EBRT) planning for prostate cancer patients has been well demonstrated. This paper investigates the feasibility of applying an MR-derived, pCT planning approach to additional types of cancer in the pelvis.

Material and methods: Fifteen patients (five prostate cancer patients, five rectal cancer patients, and five gynecological cancer patients) receiving EBRT at Turku University Hospital (Turku, Finland) were included in the study. Images from an MRCAT (Magnetic Resonance for Calculating ATtenuation, Philips, Vantaa, Finland) pCT method were generated as a part of a clinical MR-simulation procedure. Dose calculation accuracy was assessed by comparing the pCT-based calculation with a CT-based calculation. In addition, the degree of geometric accuracy was studied.

Results: The median relative difference of PTV mean dose between CT and pCT images was within 0.8% for all tumor types. When assessing the tumor site-specific accuracy, the median [range] relative dose differences to the PTV mean were 0.7 [−0.11;1.05]% for the prostate cases, 0.3 [−0.25;0.57]% for the rectal cases, and 0.09 [−0.69;0.25]% for the gynecological cancer cases. System-induced geometric distortion was measured to be less than 1 mm for all PTV volumes and the effect on the PTV median dose was less than 0.1%.

Conclusions: According to the comparison, using pCT for clinical EBRT planning and dose calculation in the three investigated types of pelvic cancers is feasible. Further studies are required to demonstrate the applicability to a larger cohort of patients.

ARTICLE HISTORY
Received 4 January 2017
Accepted 2 February 2017

Introduction

Computed tomography (CT) is currently the primary imaging modality for providing anatomical and tissue density information for external beam radiation therapy (EBRT) planning of prostate, rectal, and gynecological cancers. Magnetic resonance imaging (MRI) is widely used as a supplement to CT imaging in the planning of EBRT for pelvic cancers. The major advantages of MRI over CT are primarily better soft tissue contrast, which results in more accurate gross tumor volume (GTV) and organ at risk (OAR) delineation, lower inter-observer variability, better organ at risk (OAR) visibility, and better regional lymph node characterization [1]. Additional benefits include the usage of non-ionizing radiation and the versatility of existing imaging methods for cancer type or organ specific imaging methods [1].

A major drawback of multi-modality imaging in radiation therapy (RT) is the registration errors introduced when images from two or more imaging modalities are registered and fused [2]. Recent advances in the use of MRI in RT promise to eliminate this registration error by using only MR images for planning and dose calculation in EBRT of prostate [3–7] and brain [8,9]. In an MR-only workflow, the so-called pseudo-CT images are generated from the MR images, providing tissue density information for dose calculation and reference images for patient position verification at the linear accelerator. However, despite the benefits of MR-based RT planning, it has not been investigated if it is possible to use existing pseudo-CT methods for other cancer types in the pelvic anatomy [1,10,11]. The pseudo-CT methods suitable for prostate may not be directly applicable to other pelvic targets due to the larger treatment volumes that are characteristic of pelvic tumors in general.

The geometric accuracy of images used in RT directly affects the required treatment margins and treatment outcomes of EBRT [12]. Consequently, geometric accuracy of MRI has been studied in several publications and also reviewed recently [12]. However, a major limitation of previous studies has been that they only consider volumes relevant for a dual-modality workflow, whereby MR-images are registered to a planning CT. The accuracy of the full body contour is relevant in the context of an MR-only workflow due to its direct impact on dose calculation accuracy. Thus, we find it

CONTACT Reko Kemppainen reko.kemppainen@gmail.com Philips MR Therapy, 01510 Vantaa, Finland
Supplemental data for this article can be accessed here.

important to study the effect of geometric distortions on dose calculation accuracy, especially for the large PTV volumes typically treated in pelvic cancers.

The aim of this study was to evaluate the feasibility of an existing MR-only method in terms of dose calculation and geometric accuracy in EBRT for the pelvic area in general. The method is singularly used for prostate cancer, presently the only indication included in the labeling of this method. Since large target volumes are typically treated in gynecological and rectal cancer patients, both system-related geometric distortion and patient-induced distortion were evaluated in the pelvic anatomy in order to quantify their impact on the dose planning and calculation accuracy.

Material and methods

Study design and image acquisition

The study cohort consisted of 15 consecutive pelvic cancer patients (five prostate, five rectal, and five gynecological) treated with EBRT at the Department of Oncology and Radiotherapy of Turku University Hospital in Turku, Finland. The mean (±SD) age was 74.3 (±4.8), 69.2 (±12.8), and 72.8 (±8.3) years and mean (±SD) weight was 91.4 (±21.7), 73.8 (±8.6), and 74.4 (±18.3) kg for the prostate, rectal, and gynecological groups, respectively. In the prostate cancer group, the PTV (volume mean (±SD) was 410 (±520) cm^3) included prostate, seminal vesicles and, for two patients, extra capsular tumor extension was detected from the MR-images. For the rectal cancer group, the PTV (volume mean (±SD) was 1530 (±410) cm^3) was contoured according to clinical practice for preoperative EBRT of rectal cancer. For three out of the five gynecological patients, the PTV (volume mean (±SD) was 1910 (±990) cm^3) included the primary tumor, the regional lymph nodes and, when applicable, other likely volumes of spread disease.

In pelvic cancer, GTVs, including both the primary tumor and involved lymph nodes, were delineated in the MR images, and CTV was created by adding 5–15mm to GTVs in order to include subclinical or microscopic extensions of the disease. CTV also included regional lymph nodes at high risk for the spreading of microscopic cancer. PTV was then created by adding 10–15 mm margins to CTV. PTV determinations were performed according to international guidelines on treating prostate, rectal, or gynecological cancer. Two gynecological and one prostate cancer patient received postoperative RT, and for those patients, a postoperative tumor bed was included in the CTV. The time in between the CT and the MR simulations was less than 1 d for all patients. The manufacturer's 3D gradient non-linearity correction algorithm was used in all the MR images.

CT simulation images were acquired using an Aquilion LB (Toshiba Corp., Tokyo, Japan) scanner with 2-mm-thick slices, $1 \times 1\,mm^2$ in-plane resolution, and 120 kV tube voltage. MR images were recorded with the Ingenia 1.5T HP (Philips Medical Systems International B.V., Best, Eindhoven, The Netherlands) scanner. For all patients, a transaxial T1-weighted three-dimensional (3D) mDIXON sequence [13] (a resolution of $1.04 \times 1.04 \times 2.50\,mm^3$) covering the full body contour was acquired and used as a source for MRCAT (Magnetic Resonance for Calculating ATtenuation, Philips, Vantaa, Finland) images. The MR imaging time was less than 200 s for all patients, who were positioned similarly during the imaging for CT and MR simulation. In the MR scan, patients were placed in a supine position on a flat RT couch top and an anterior MR-coil was placed above the imaging volume using a coil holder provided by the manufacturer.

MRCAT pseudo-CT generation

In the pCT generating algorithm, CT-like density maps were computed from the mDIXON MR-images in a two-step approach (see online Supplementary material for more detailed description of pCT generation). In the first step, the content of the MR image was categorized into five classes. In the second step, each voxel was assigned the following HU values: air (−968 HU), fat (−86 HU), water-rich tissue (42 HU), spongy bone (198 HU), and compact bone (949 HU). The densities used for dose calculation were then obtained from tabulated calibration values provided by the manufacturer and were based on the combination of average population values and values cited in the literature [14].

RT treatment planning and image processing

Pinnacle^3 (version 9.10. Philips Medical Systems Inc., Fitchburg, WI, USA) treatment planning system (TPS) was used for generating and calculating the plans for this study. All clinical plans were originally done in Eclipse (version 13.6, Varian Medical Systems Oy, Helsinki, Finland) TPS and exported to Pinnacle^3, where the clinical plans were re-optimized using the original contours and a volumetric modulated arc therapy (VMAT) technique with two arcs. Planning was performed first using pCT images and clinical contours. The plans were then copied to the planning CT-image using identical planning parameters. The copied plan was recalculated based on the CT image in Pinnacle^3 TPS using an adaptive convolution algorithm. The CT-to-density calibration curve was based on a recent calibration with the RMI 465 (Gammex Inc., Middleton, WI) phantom. The pCT-specific calibration curve provided by the manufacturer was used for pCT-based calculations.

In order to avoid confounding factors in dose comparison, the original CT was first deformable registered to the pCT source image (called CT_DIR) using Mirada (Mirada Medical Ltd., Oxford, UK) medical imaging software. The deformable registration was required since differences in the body outline would have otherwise caused dose differences that were not related to the performance of the pCT. Furthermore, it allows compensation of bladder and rectum filling differences and inner organ movement. An example of deformable registration can be seen in Figure S2 in the online Supplementary material.

The deformable image registration may bias the dose comparison results since MRI-related geometric distortions are not taken into account due to the body outline matching between pCT and CT images [12,15]. Furthermore, geometric inaccuracies may take place also in PTVs and OARs further away from the isocentre of the MR. In order to assess the impact of the MR-system's geometric accuracy on RT

planning, another plan (called CT_DIR_C) where all structures were corrected according to measured system's geometric distortion was created (see below for a description of distortion measurement). This allowed the dose calculation discrepancies originating purely from the geometric inaccuracies to be studied independently from other sources, such as density differences.

Evaluation of dose calculation accuracy

Dose volume histogram (DVH) curves and gamma differences were analyzed for any changes between pCT- and CT-based plans. Relevant PTV's DVH-metrics were selected to reflect the near maximum ($D_{2\%}$) and near minimum ($D_{98\%}$) values. For the OARs investigated in this study, i.e., rectum and bladder, the DVH-comparison dose of $D_{35\%}$ was tabulated. In addition, the differences in the median of mean doses to PTVs and OARs were calculated. In order to investigate the impact of tumor type to pCT performance, statistical analysis was performed to assess the significance of the differences between the prostate groups and the other two groups. The rationale for the statistical analysis is that the performance of pCT has been demonstrated for prostate EBRT and if no significant differences are found in the comparison to rectal and gynecological targets, such result would indicate clinical feasibility.

In addition to DVH comparison, the dose distributions between pCT and planning CT were compared by means of 3D gamma analysis using VeriSoft (version 6.1, PTW-Freiburg, Freiburg, Germany) treatment plan verification software. Doses below 30% of the maximum dose in the calculated volume were excluded from the analysis. The statistical tests were performed to determine if there is a significant difference between clinical pCT for prostate and pCT for the other pelvic areas (rectal and gynecological cancers).

All dose differences are given as relative differences between the CT-based and pCT-based plans that can be formulated as (pCT-CT)/CT. Thus, positive values indicate dose deficiency if the treatment and dose calculation were based on pCT.

Assessment of geometric fidelity

Geometric distortions can be caused by both the MR system and the patient [12]. In this study, a large 3D phantom was used to measure the system-induced geometric distortions arising from gradient field non-linearity and static magnetic field (B0) inhomogeneity. In addition, patient-induced geometric distortion was assessed by calculating a B0 inhomogeneity map from two-phase images of a dual-echo fast field-echo (FFE) image as suggested by Baldwin et al. [17] and Stanescu et al. [18]. The imaging parameters were as follows: TE1 of 1 ms, TE2 of 5.6 ms, TR of 6.8 ms, slice thickness of 4 mm, and pixel size of $1 \times 1\,mm^2$. Since the measured distortion originates from both the patient and the system, the patient-induced distortion was assessed in the neighborhood of the MR system's isocentre, where system-related B0 inhomogeneity was the smallest. The phase images were unwrapped using an algorithm developed by Jenkinson et al. [19]. For the patient-induced distortion assessment, the additional dual-echo scan was included to the hospital's clinical MR protocol for a group of four patients.

The large FOV-3D phantom consists of seven acrylic plates with inter-plate distances of 65 mm. Each plate contains 240 fiducial markers placed in a regular grid with inter-fiducial distances of 25 mm. The phantom was scanned with a T1-weighted FFE sequence using the same MR scanner type that was used for the generation of the pCT images. The imaging parameters were as follows: a FOV of $560 \times 560 \times 400\,mm^3$, an acquisition voxel size of $1.5 \times 1.5 \times 2.0\,mm^3$, a TE/TR of 3.4/6.7 ms, and a water–fat shift of 0.5 mm. The error as a function of the location inside the MR scanner was determined by comparing the fiducial locations to the known phantom grid. In order to assess the impact of geometric distortions to RT, the 3D distortion map was interpolated to the CT image grid of the individual patients. The distortion map was then used for the geometric correction of the RT structures. The corrected structures were created as DICOM RT structure sets using MATLAB (version R2016b, The MathWorks Inc., Natick, MA, USA) mathematical computing software and imported to Pinnacle^3 TPS for dose calculation. The original CT_DIR plan was copied (the new plan is called CT_DIR_C) and the structures were replaced with the geometrically corrected structures. Finally, the impact on dose calculation was simulated by using the density override in Pinnacle, so that volume outside the distortion-corrected body outline was assigned as air and the volume inside the corrected outline was assigned as water for voxels for which there was air in the uncorrected image.

Statistical analysis

Statistical analysis was conducted using Minitab (version 17, Minitab Inc., State College, PA, USA) numerical analysis software. The data were analyzed for statistical difference with the non-parametric Mann–Whitney *U* test. This test was chosen due to the fact that the same data were not used for both treatment options and normality could not be guaranteed. For the statistical difference, 95% confidence level was required ($p < 0.05$).

Results

Dose comparison

The mean (± SD) relative dose difference in PTV mean dose computed over all 15 patients was 0.2 (± 0.5)% and the median of relevant PTV DVH-points was less than 0.9% for all studied tumor types, indicating good agreement between pCT and planning CT in terms of dose calculation accuracy. For the studied OARs, the median relative differences were less than 1.2% (see Table 1).

The gamma pass rates were high for all studied PTVs and pass criteria. The median pass rate was the highest for the prostate patients and the lowest for gynecological patients. Although the differences between groups were small, statistically significant differences to the prostate group were found for the gamma criteria of 2%/1 mm in both the rectal and the gynecological groups. In addition, there was a

Table 1. Median (min;max) relative difference (%) between MRCAT and CT_DIR-based plans for relevant dose volume histogram (DVH)-points and mean dose. Statistical tests were performed for equivalent median between prostate and rectal or gynecological group, $p < 0.05$ indicating statistically significant difference.

	Prostate	Rectal	Gynecological
PTV			
Mean	0.73 (−0.11;1.05)	0.30 (−0.25;0.57), $p = 0.09$	0.09 (−0.69;0.25), $p = 0.06$
$D_{2\%}$	0.70 (0.53;0.46)	0.08 (−0.67;0.48), $p > 0.10$	−0.20 (−1.23;0–06), $p = 0.04$
$D_{50\%}$	0.56 (−0.11;1.04)	0.26 (−0.26;0.54), $p > 0.10$	0.10 (−0.65;0.20), $p = 0.06$
$D_{98\%}$	0.87 (−0.11;1.42)	0.57 (0.09;1.02), $p > 0.10$	0.22 (−0.51;0.72), $p > 0.10$
Rectum (OAR)			
Mean	0.23 (−0.19;1.25)	[N/A]	−0.14 (−1.10;0.23), $p > 0.10$
$D_{35\%}$	0.45 (−0.63;1.78)	[N/A]	−0.19 (−1.00;0.62), $p > 0.10$
Bladder (OAR)			
Mean	0.17 (−0.79;0.64)	−0.20 (−0.25;0.43), $p > 0.10$	−0.45 (−0.75;0.13), $p > 0.10$
$D_{35\%}$	−1.19 (−1.41;0.73)	0.24 (−0.42;0.56), $p > 0.10$	−0.24 (−0.65;0.02), $p > 0.10$

PTV: planning target volume; OAR: organ at risk.

Table 2. Results of gamma analysis (median pass rate (min;max). Statistical tests were performed for equivalent median between prostate and rectal or gynecological group, $p < 0.05$ indicating statistically significant difference.

	Prostate	Rectal	Gynecological
Gamma criteria			
1%/1mm	99.2 (93.8;100)	97.4 (96.4;99.0), $p > 0.10$	97.3 (94.3;98.9), $p > 0.10$
2%/1mm	100 (99.5;100)	99.0 (98.7;99.8), $p = 0.03$	98.5 (98.1;99.6), $p = 0.02$
2%/2mm	100 (99.8;100)	99.3 (99.1;100), $p = 0.06$	99.2 (98.9;99.8), $p = 0.01$

significant difference in the gynecological group when 2%/2mm pass criteria were used. The results of the gamma analysis are shown in Table 2.

System's geometric accuracy

Geometric fidelity of the MR images was assessed for all patients and PTVs in the ROIs consisting of the clinical RT planning structures. An example of the analysis is illustrated in Figure 1, which demonstrates the contour distortions and ranges (minimum to maximum) and contours of the distortion map as a function of distance from the isocentre of the MR device for the gynecological cancer patient that had the largest PTV in the cranial–caudal direction.

For all OAR structures, the distortion was measured to be less than 1 mm for all patients and PTVs (see illustration of the organ and disease specific figures in Figure 2). Furthermore, the maximum distortion in the body outline at which the radiation beam enters the body was less than 2 mm for all prostate and rectal cancer patients. For one gynecological patient, the body outline distortion was greater than 2 mm in the cranial end of the PTV. However, it can be seen in the standard deviation of the body outline distortion that the distortion was less than 2 mm for the majority of the outline.

Impact of geometric distortion to dose calculation accuracy

According to the results, the impact on dose calculation accuracy due to geometric distortions of the MR images was small. The changes in the PTV DVHs were negligible, the relative difference being less than 0.2% for all studied DVH points (see Table 3). The gamma analysis was in line with the DVH-based analysis: pass rate was highest for prostate cancer patients and lowest for gynecological cancer patients (see Table S1 in the Supplementary material). The median pass rates were significantly different between prostate and gynecological patients.

Patient-induced geometric distortions

Patient-induced geometric distortions were studied in the pelvis anatomy for four patients. In Figure 3, an example of the magnitude of patient-induced distortion is given in axial plan near the isocentre of the MR device. Largest distortions were found near tissue–air interfaces (around rectum and near body outline). The distortions were found to be less than the pixel size of 1 mm for all studied patients.

Discussion

This work aimed at demonstrating the feasibility of using MRCAT pCT for the RT of pelvic cancers in terms of dosimetric and geometric accuracy. Our results show that the calculation accuracy is similar to reported in the literature. For example, Korhonen et al. [3] have reported $D_{50\%}$ to be 0.3 (± 0.2)% for prostate EBRT, and we obtained 0.6 (± 0.5)%, 0.2 (± 0.4)%, and −0.2 (± 0.5)% for prostate, rectal, and gynecological tumor patients, respectively. Furthermore, Siversson et al. [4] have reported mean relative difference of 0.0 (±0.2)% and Kim et al. [5] 0.5% for PTV for EBRT of prostate. However, they are not fully comparable since in the reported studies the same CT scanner, calibration, and dose calculation are used for both pseudo-CT method's development and its validation, and thus this may provide by far too optimistic results. Although no statistical significance was found between prostate and other cancers, the difference in DVH-points was almost significant and due to low power of the test (small sample size and heterogeneous demographics), the conclusions of similarity cannot be strongly considered.

Gamma analysis comparing the dose distributions of pCT and the reference planning-CT showed clinically acceptable pass rate for all cancer groups. The gamma pass rates (1%/

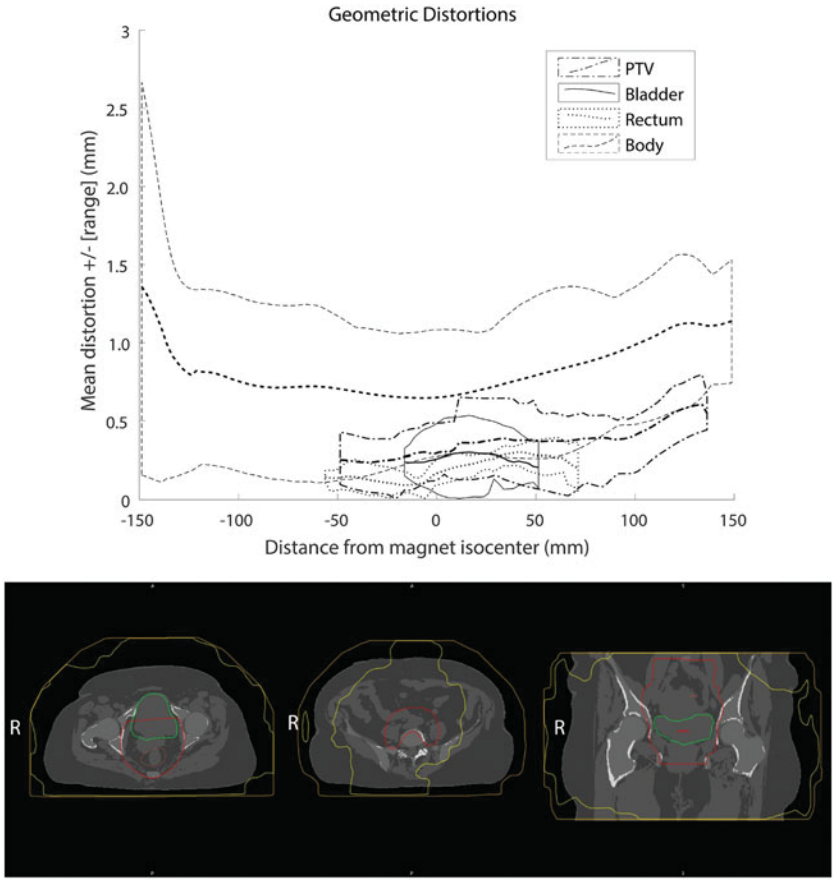

Figure 1. An example of geometric distortion for a patient receiving external beam radiation therapy (EBRT) for cervical cancer. Above: mean and range of distortion for the body (dashed), planning target volume (PTV) (dash-dotted), and organs at risk (OAR) (solid = bladder and dotted = rectum) as a function of distance from the magnet's isocentre along cranial–caudal direction. Below: illustration of the same plan in transversal (left: at the isocentre, middle 132 mm away from the isocentre) and coronal (right) planes with clinical structures and distortion contours of 1 mm (inner) and 2 mm (outer).

1 mm criteria) of 97.9%, 97.5%, and 96.9% for prostate, rectal, and gynecological groups, respectively, were well in line with results reported in the literature. Korhonen et al. [3] have reported a gamma pass rate of 95.7% and Kim et al. [5] 97.2% between pseudo-CT and planning-CT doses evaluated using the criteria of 1%/1 mm for EBRT of prostate cancer.

According to the literature, the geometric accuracy of 2 mm in ROI and 1 mm in PTV is desired for MR-guided RT [12]. We found that for all the patients the system-induced geometrical distortion was less than 1 mm for PTV and OAR volumes. In addition, the deformation of body contour was less than 2 mm for all except one gynecological patient, when considering only the area at which the radiation beam enters the body. The impact of the body outline, PTV, and OAR distortions on dose calculation accuracy was found to be clinically insignificant, the mean relative difference of 0.2% being largest among all studied cancer groups. In Figure 2, however, one can see that the geometric distortion of body outline increases rapidly in the periphery of analyzed volumes. This indicates that 30-cm-FOV in the cranial–caudal direction cannot be increased for larger PTVs without compromising the geometric accuracy.

Patient-induced distortions in transversal plane were assessed in the vicinity of MR device's isocentre for avoiding the contribution of system-induced B0 inhomogeneity. The largest distortions were found in air–tissue interfaces. The acceptable distortions were less than ±0.5 mm for all studied patients being smaller than system-related distortions. When optimizing MR-sequences to be used in RT planning, the receiver bandwidth must be set high enough to avoid distortions of up to several millimeters [17,18]. Patient-induced geometric distortion originating from the susceptibility differences has been studied by Stanescu et al. [18]. For 1.5T system, the maximum distortion was 0.3 mm when a gradient strength of 20 mT/m was used. Since pCT source scan uses gradient strength of approximately 10 mT/m, results are in agreement with the values reported in the literature.

The system-induced geometric distortions are scanner dependent, and thus the results apply only to the scanner type and field strength used in this study. Additionally, the patient-induced distortions are sequence dependent and apply only for the studied sequences. Used 3D phantom for measuring the residual distortions after gradient non-linearity correction was considered as an object of known geometry. Therefore, the measures of geometric distortion may be overestimated due to any deviation from the assumed geometry which is not taken into account in the analysis. Deviations in the phantom geometry could be included into the analysis by using a CT scanner to obtain a geometrically accurate reference image. In our analysis, the measured residual geometric distortion consists of system-

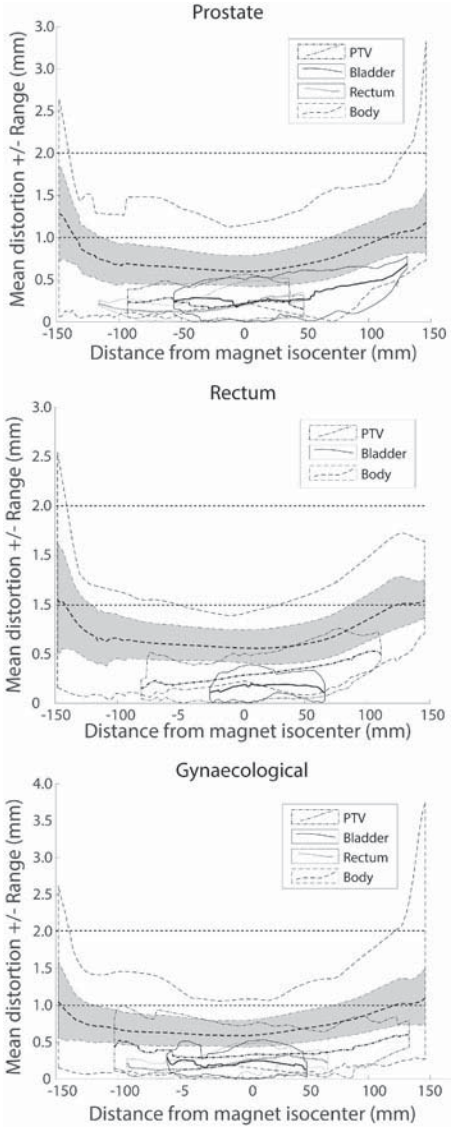

Figure 2. Population mean (± range) distortion per structure as a function of distance from the isocentre of the device along cranial–caudal direction. Dashed = body outline, dash-dotted = planning target volume (PTV), dotted = rectum and solid = bladder. For the body structure, the mean ±1 SD is also given (see the darker area around the mean values). PTV: planning target volume; SD: standard deviation.

related gradient and B0 distortions. In addition, the measured sequence dependent geometric distortion is a measure of both system and patient-induced B0 distortions. Thus, the system-related B0 distortions are measured in both the phantom and the patient experiments and their summation would double the impact of distortions originating from the main magnet. Our method can be considered adequate, since the scope of this study was the assessment of clinical feasibility of using MRCAT pCT for RT of pelvic cancers, rather than providing a quantitative information of geometric distortions.

Currently, the cranial–caudal FOV of pCT image is limited to 300 mm that restricts its application in RT of wider pelvic cancers. Consequently, without increasing the imaging volume, the pCT can be used for RT treatment planning of primary pelvic cancers together with the regional lymph nodes, whereas it is not feasible for PTVs including paraaortic lymph nodes. At Turku University Hospital, around 10% of the PTVs for treating gynecological cancer require larger a FOV than that is possible to calculate by way of the pCT method. Still, it would be feasible to treat the majority of pelvic cancers and overall prostate, rectal and gynecological RT treatments constituted 36%, 10%, and 13% of all EBRT patients. The use of pCT in our clinic would enable MR-only simulation for around 60% of the patients being scanned with MR for RT.

The patient positioning at treatment device is based either on bone registration using orthogonal X-ray images and digitally reconstructed radiographs or on registration of the cone-beam CT and the planning CT. When pCT is used, only two soft-tissue HU-values are used, and thus the registration to the planning image may not be feasible. Robust registration might depend on continuous HU values for soft tissue [18,20]. The verification of pCT-based patient positioning requires further studies before its feasibility can be stated.

Increasing the FOV in the cranio-caudal direction remains a challenge in MRI since the geometric accuracy decreases rapidly farther away from the MR device's isocentre. Furthermore, motion blurring influenced by breathing in the abdomen causes artifacts in the mDIXON image, which may hamper accurate body outline detection. Recent development of MR sequences may address some of the above-mentioned challenges in the near future. Several academic institutions and industry are pursuing the technical advances aimed at in this issue, so it is very probable that over the next few years some solutions will be made commercially available, thus enabling easier utilization of the method on-site [21].

Judging by the results of this work, we conclude that the use of only four tissue classes is adequate to capture individual variance in body composition and to produce clinically acceptable accuracy in dose calculation for prostate, rectal and gynecological cancer patients treated with EBRT. In addition, the geometric accuracy of the MR system used in the study was found to be sufficient for larger PTV, which is a necessity in an MR-only application for the pelvic area in general. Further studies are required to assess the feasibility of soft-tissue or bone-based patient positioning with pCT and to confirm our findings with a larger cohort of patients.

Acknowledgments

The authors thank employees of Philips, Vantaa, Finland, P. Vesanen for assistance with measurements and analysis of geometric distortions, A. Halkola for assistance with reconstruction of MRCAT images, and Kathryn Lessey for proofreading the manuscript. The authors would also like to show our gratitude to radiographers T. Alamäki, S. Kujala, T. Kukko, and M. Saarinen for help in radiological examinations at the Department of Oncology and Radiotherapy of Turku University Hospital.

Disclosure statement

R. Kemppainen and M. Deppe are employed by Philips MR Therapy, Finland.

ORCID

Reko Kemppainen http://orcid.org/0000-0001-9315-2596

Table 3. Median (min;max) relative difference (%) between CT_DIR and geometry-corrected CT plan (CT_DIR_C) plans for relevant dose volume histogram (DVH)-points and mean dose. Statistical tests were performed for equivalent median between prostate and rectal or gynecological group, $p < 0.05$ indicating statistically significant difference.

	Prostate	Rectal	Gynecological
PTV			
Mean	0.10 (0.09;0.11)	0.06 (0.06;0.08), $p = 0.01$	0.08 (0.05;0.10), $p = 0.09$
$D_{2\%}$	0.08 (0.04;0.11)	0.09 (0.07;0.09), $p > 0.10$	0.09 (0.04;0.09), $p = 0.02$
$D_{50\%}$	0.10 (0.07;0.11)	0.07 (0.05;0.08), $p = 0.04$	0.09 (0.05;0.09), $p > 0.10$
$D_{98\%}$	0.12 (0.04;0.22)	0.10 (0.09;0.12), $p > 0.10$	0.09 (−0.14;0.12), $p > 0.10$
Rectum (OAR)			
Mean	−0.51 (−1.02; −0.1)	–	−0.02 (−0.18;0.08), $p > 0.10$
$V_{35\%}$	−0.69 (−1.32;0.06)	–	0.04 (−0.29;0.07), $p > 0.10$
Bladder (OAR)			
Mean	0.01 (−0.12;0.09)	−0.00 (−0.17;0.02), $p > 0.10$	0.01 (−0.04;0.07), $p > 0.10$
$V_{35\%}$	−0.07 (−0.18;0.08)	0.04 (−0.36;0.07), $p > 0.10$	0.07 (0.03;0.09), $p = 0.06$

PTV: planning target volume; OAR: organ at risk.

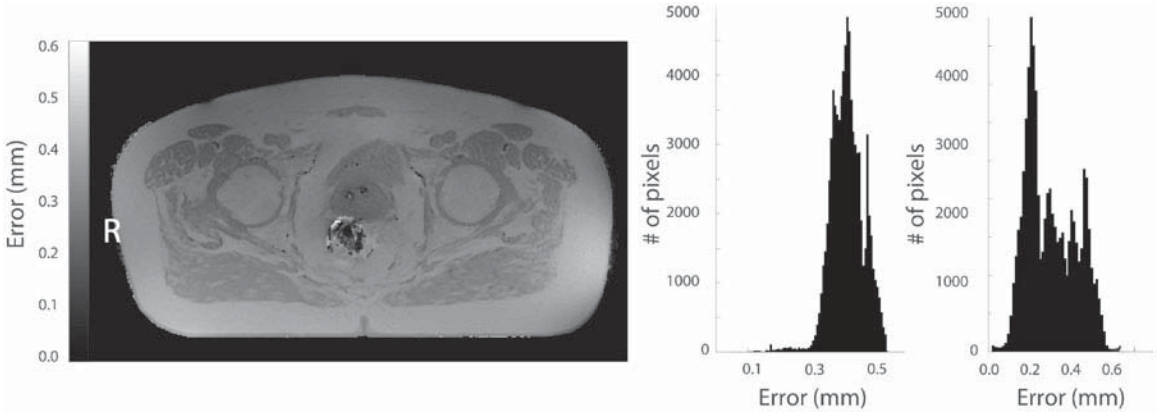

Figure 3. An example of distortion map with color bar showing the amount of distortion (left), histogram of the error around the magnet isocentre (middle) for the example on top and histogram of geometric distortion for all four patients included to the analysis (right).

References

[1] Schmidt MA, Payne GS. Radiotherapy planning using MRI. Phys Med Biol. 2015;60:R323–R361.

[2] Nyholm T, Nyberg M, Karlsson MG, et al. Systematisation of spatial uncertainties for comparison between a MR and a CT-based radiotherapy workflow for prostate treatments. Radiat Oncol. 2009;4:54.

[3] Korhonen J, Kapanen M, Keyriläinen J, et al. A dual model HU conversion from MRI intensity values within and outside of bone segment for MRI-based radiotherapy treatment planning of prostate cancer. Med Phys. 2014;41:11704.

[4] Siversson C, Nordström F, Nilsson T, et al. Technical Note: MRI only prostate radiotherapy planning using the statistical decomposition algorithm. Med Phys. 2015;42:6090–6097.

[5] Kim J, Garbarino K, Schultz L, et al. Dosimetric evaluation of synthetic CT relative to bulk density assignment-based magnetic resonance-only approaches for prostate radiotherapy. Radiat Oncol. 2015;10:239.

[6] Andreasen D, Van Leemput K, Edmund JM. A patch-based pseudo-CT approach for MRI-only radiotherapy in the pelvis. Med Phys. 2016;43:4742–4752.

[7] Dowling JA, Lambert J, Parker J, et al. An atlas-based electron density mapping method for magnetic resonance imaging (MRI)-alone treatment planning and adaptive MRI-based prostate radiation therapy. Int J Radiat Oncol Biol Phys. 2012;83:e5–11.

[8] Andreasen D, Van Leemput K, Hansen RH, et al. Patch-based generation of a pseudo CT from conventional MRI sequences for MRI-only radiotherapy of the brain. Med Phys. 2015;42:1596–1605.

[9] Hsu S-H, Cao Y, Lawrence TS, et al. Quantitative characterizations of ultrashort echo (UTE) images for supporting air-bone separation in the head. Phys Med Biol. 2015;60:2869–2880.

[10] Gwynne S, Mukherjee S, Webster R, et al. Imaging for target volume delineation in rectal cancer radiotherapy – a systematic review. Clin Oncol (R Coll Radiol). 2012;24:52–63.

[11] Dimopoulos J, Schard G, Berger D, et al. Systematic evaluation of MRI findings in different stages of treatment of cervical cancer: potential of MRI on delineation of target, pathoanatomic structures, and organs at risk. Int J Radiat Oncol Biol Phys. 2006;64:1380–1388.

[12] Weygand J, Fuller CD, Ibbott GS, et al. Spatial precision in magnetic resonance imaging-guided radiotherapy: the role of geometric distortion. Int J Radiat Oncol. 2016;95:1304–1316.

[13] Eggers H, Brendel B, Duijndam A, et al. Dual-echo Dixon imaging with flexible choice of echo times. Magn Reson Med. 2011;65:96–107.

[14] Köhler M, Vaara T, Van Grootel M, et al. MR-only simulation for radiotherapy planning. Philips Healthc White Pap. 2015;1–16.

[15] Walker A, Liney G, Metcalfe P, et al. MRI distortion: considerations for MRI based radiotherapy treatment planning. Australas Phys Eng Sci Med. 2014;37:103–113.

[16] Baldwin LLN, Wachowicz K, Fallone BG. A two-step scheme for distortion rectification of magnetic resonance images. Med Phys. 2009;36:3917.

[17] Stanescu T, Wachowicz K, Jaffray DA. Characterization of tissue magnetic susceptibility-induced distortions for MRIgRT. Med Phys. 2012;39:7185–7193.

[18] Jenkinson M. Fast, automated, N-dimensional phase-unwrapping algorithm. Magn Reson Med. 2003;49:193–197.

[19] Korhonen J, Kapanen M, Sonke J-J, et al. Feasibility of MRI-based reference images for image-guided radiotherapy of the pelvis with either cone-beam computed tomography or planar localization images. Acta Oncol. 2015;54:889–895.

[20] Walker A, Liney G, Holloway L, et al. Continuous table acquisition MRI for radiotherapy treatment planning: distortion assessment with a new extended 3D volumetric phantom. Med Phys. 2015;42:1982–1991.

[21] Yang J, Cai J, Wang H, et al. Four-dimensional magnetic resonance imaging using axial body area as respiratory surrogate: initial patient results. Int J Radiat Oncol Biol Phys. 2014;88:907–912.

Publication 2

Kemppainen R, Vaara T, Joensuu T, Kiljunen T. Accuracy and precision of patient positioning for pelvic MR-only radiation therapy using digitally reconstructed radiographs. Phys. Med. Biol. IOP Publishing; 2018;63:aaad21.

IOP Publishing Phys. Med. Biol. 63 (2018) 055009 (10pp) https://doi.org/10.1088/1361-6560/aaad21

Physics in Medicine & Biology

IPEM Institute of Physics and Engineering in Medicine

RECEIVED
10 July 2016

REVISED
1 February 2018

ACCEPTED FOR PUBLICATION
6 February 2018

PUBLISHED
2 March 2018

PAPER

Accuracy and precision of patient positioning for pelvic MR-only radiation therapy using digitally reconstructed radiographs

R Kemppainen[1,3], T Vaara[1], T Joensuu[2] and T Kiljunen[2]

[1] Philips MR Therapy, Äyritie 4, FI-01510, Vantaa, Finland
[2] Docrates Cancer Center, Saukonpaadenranta 2, FI-00180 Helsinki, Finland
[3] Department of Neuroscience and Biomedical Engineering, Aalto University School of Science, Rakentajanaukio 2 C, FI-02150 Espoo, Finland

E-mail: reko.kemppainen@gmail.com

Keywords: radiotherapy, image-guided radiotherapy, MRI-based radiotherapy, digitally reconstructed radioraphs

Supplementary material for this article is available online

Abstract

Background and Purpose. Magnetic resonance imaging (MRI) has in recent years emerged as an imaging modality to drive precise contouring of targets and organs at risk in external beam radiation therapy. Moreover, recent advances in MRI enable treatment of cancer without computed tomography (CT) simulation. A commercially available MR-only solution, MRCAT, offers a single-modality approach that provides density information for dose calculation and generation of positioning reference images. We evaluated the accuracy of patient positioning based on MRCAT digitally reconstructed radiographs (DRRs) by comparing to standard CT based workflow. *Materials and Methods.* Twenty consecutive prostate cancer patients being treated with external beam radiation therapy were included in the study. DRRs were generated for each patient based on the planning CT and MRCAT. The accuracy assessment was performed by manually registering the DRR images to planar kV setup images using bony landmarks. A Bayesian linear mixed effects model was used to separate systematic and random components (inter- and intra-observer variation) in the assessment. In addition, method agreement was assessed using a Bland–Altman analysis. *Results.* The systematic difference between MRCAT and CT based patient positioning, averaged over the study population, were found to be (mean [95% CI]) −0.49 [−0.85 to −0.13] mm, 0.11 [−0.33 to +0.57] mm and −0.05 [−0.23 to +0.36] mm in vertical, longitudinal and lateral directions, respectively. The increases in total random uncertainty were estimated to be below 0.5 mm for all directions, when using MR-only workflow instead of CT. *Conclusions.* The MRCAT pseudo-CT method provides clinically acceptable accuracy and precision for patient positioning for pelvic radiation therapy based on planar DRR images. Furthermore, due to the reduction of geometric uncertainty, compared to dual-modality workflow, the approach is likely to improve the total geometric accuracy of pelvic radiation therapy.

Introduction

In contemporary external beam radiation therapy (EBRT) of prostate cancer, computed tomography (CT) is the primary imaging modality providing anatomical and tissue density information. Magnetic resonance imaging (MRI) is widely used as a supplement to CT in EBRT of prostate cancer. The major advantages of MRI over CT are superior contrast-to-noise ration and better soft tissue differentiation resulting decreased contouring variability for prostate (Debois *et al* 1999) and reduced organs at risk (OAR) dose (Rasch *et al* 1999). Additional benefits include lack of ionizing radiation and versatility of existing MR imaging methods.

Major drawback of multi modal imaging in radiation therapy (RT) is the registration error introduced when images from two or more imaging modalities are registered (Nyholm *et al* 2009). Recent advances in usage of MR in RT promise to eliminate the registration error completely by using only MR images for EBRT planning of prostate cancer (Dowling *et al* 2012, Korhonen *et al* 2014, Kim *et al* 2015, Siversson *et al* 2015). In the MR-only

approach a so called pseudo-CT is obtained based on information available in the MR image. The pseudo-CT is then used to replace the CT image for both dose calculation and generation of digitally reconstructed radiographs (DRRs). Generation of DRRs based on MR images will be required if the patient alignment prior to treatment delivery must be verified by on-board planar x-ray imaging (Karlsson *et al* 2009).

Numerous studies have been published recently that report adequate dose calculation accuracy with different MR-only strategies (Edmund and Nyholm 2017). The focus in MR-only publications has been in dosimetric accuracy and, albeit equally important for total accuracy and treatment outcome, less attention has been paid to complete workflow and geometric accuracy of suggested methods. Prior work has demonstrated that manually delineated pelvic bones can provide sufficient accuracy for patient positioning based on DRR images using bulk assignment of HU values for bones in an MR-only workflow (Chen *et al* 2007, Korhonen *et al* 2015). However, feasibility of positioning methods for image guided radiation therapy (IGRT) may be very sensitive to differing number of density values used for modeling of bones, segmentation accuracy of bones and geometric accuracy of the chosen methods in general. Thus, the published results may not be generalizable to methods that use automated delineation of bones. Feasibility of such pseudo-CT method should be verified independently by realistic use of the images where a human observer registers the DRR images to kV-radiographs.

This study compares MRCAT and CT based DRRs in IGRT for positioning of patients for determining the treatment isocenter locations for daily treatments. The quantitative assessment of suitability of an MRCAT DRR for this purpose is done by simulating the standard clinical workflow of registering DRRs and planar radiographs manually. Planar radiographs (kV-images) taken before the treatment are registered with the MRCAT images and the registration results are compared with those obtained by using the CT-based DRRs. To authors knowledge, a thorough method comparison study has not been conducted to assess the sources of difference between CT and pseudo-CT based DRR patient positioning. For the first time, we analyze the impact to both systematic and random errors. Based on the impact to the required clinical target volume (CTV) margin, we derive an acceptance criterion for the use of pseudo-CT based DRRs.

Methods

Study design and image acquisition

The study cohort consists of 20 prostate cancer patients treated with external beam radiotherapy in the Docrates Cancer Center, Helsinki Finland. Patients were treated according to Docrates' clinical protocol for prostate cancer patients that is based on pelvic CT simulation and additional MR images that are registered with the planning CT for target and OAR contouring. In this study, secondary MR image set was taken that allowed retrospective comparison between CT and MR-based DRRs. Thus, the treatment of the patients was not affected due to the study. The study protocol was approved by the Helsinki University Hospital Coordinating Ethics Committee.

Planning CT images were acquired using Siemens Sensation Open scanner with minimum of 40 cm FH coverage, 2 mm slices, 1 mm × 1 mm in-plane resolution, 120 kV tube voltage, mA modulation (Quality ref. mAs (CareDose) 190 mAs) and B31s reconstruction kernel. MR Images were acquired using Ingenia 1.5 T ($n = 8$) or 3.0 T ($n = 12$) scanners (software version 5.1.7 ($n = 11$), 5.2 (2 cases) or 5.3 ($n = 7$)) (Philips Medical Systems, B.V., Best, Netherlands). For all patients an axial 3D mDIXON sequence (T1-weighted, resolution $1.04 \times 1.04 \times 2.50\,\text{mm}^3$) covering full body contour in axial plane was taken and used for automatic generation of the MRCAT image. The scan protocol for MRCAT was fixed and specified by the manufacturer (Köhler *et al* 2015). Full details of the sequence parameters are given in appendix B (stacks.iop.org/PMB/63/055009/mmedia). MR imaging time was below 200 s for all patients. Patients were immobilized similarly during the CT and MR simulation imaging. In the MR scan, patients were in supine position on a flat table and the anterior MR-coil was placed above the imaging volume using a coil holder provided by the manufacturer.

The kV positioning images were taken with an OBI system (On-Board Imager, Varian Medical Systems, Palo Alto, USA) integrated to a linear accelerator. Two orthogonal projections (AP or PA and LR or RL) were obtained for all patients (pixel-size: $0388 \times 0388\,\text{mm}^2$, FOV: $30 \times 40\,\text{cm}^2$).

MRCAT pseudo-CT generation

For pseudo-CT images, a commercially available MRCAT product, integrated with MR scanner software, was used to generate the images. In the MRCAT generating algorithm, CT-like density maps are generated fully automatically from an mDIXON image (Köhler *et al* 2015).

Bone structures in MRCAT are automatically segmented inside the body using the multiple contrasts provided by the mDIXON scan. Both the bone and outline segmentation employ a model-based segmentation approach trained on patient and volunteer mDIXON image datasets. The model contains information of average bone shape and how the shape varies in the training population. The model is adapted to an actual patient image using features (such as gray value edges) found within the image, while at the same time, a constraint for the

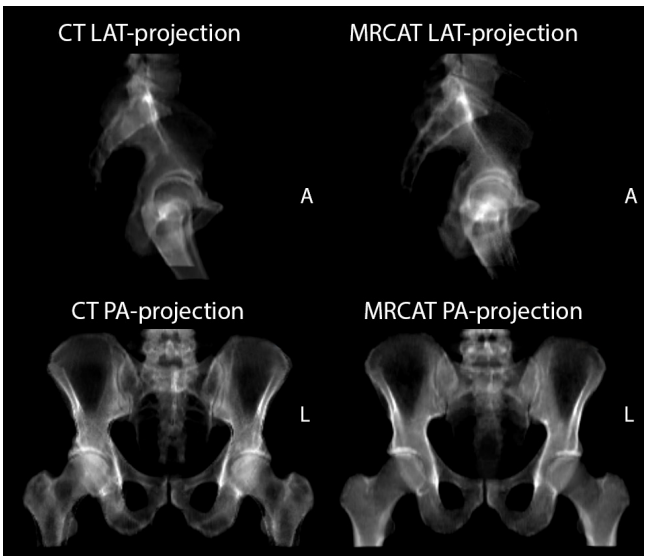

Figure 1. Example of CT (left column) and MRCAT DRR for anterior-posterior (bottom row) and left-right projections calculated in Pinnacle 9.10 TPS. HU density table is modified to filter out soft tissue contribution.

shape of the segmented structure prevents the segmentation from being attracted to a wrong position (Ecabert *et al* 2008).

Voxels inside the bone segmentation are assumed to contain either compact or spongy bone. An intensity threshold is used; lower intensities are considered to consist of compact bone, while voxels with higher intensity are assumed to contain spongy bone. The choice of the threshold value has been selected so that average bone density match with CT on population level.

Treatment planning

RT plans were created based on the simulation CTs according to the Docrates Cancer Center clinical practice. To study the DRRs generated from MRCAT, the structure sets and plans were copied from the original CT to rigidly registered MRCAT image and, thus, the isocenter position was the same, (within accuracy of the registration) in both plans. Pinnacle (Philips Healthcare, version 9.10) treatment planning system (TPS) was used for generating the DRRs (see figure 1 for an example of CT and MRCAT DRRs used in the study).

Evaluation

Five observers (4 radiographers and one physicist) registered the CT- and MRCAT-based DRRs to daily localization radiographs (kV-setup images). Registration was fully manual as is the most common clinical workflow at the site. Each image pair was evaluated three times by the same observer to obtain repeated measurements enabling the assessment of measurement quality in terms of inter- and intra-observer variability. In total, 300 (5 observers, 20 patients, 3 repetition) registration were performed per method.

Dedicated software was used for manual registration that was implemented using a commercial software package (MATLAB® 8.4.0.150421 (R2014b), The MathWorks Inc., Natick, MA, 2014). The registration tool recorded the couch shifts for the longitudinal (SI), lateral (LR) and vertical (AP) directions based on the registration of the images by an expert observer. The images were shown to the observers in a random order without revealing whether the DRR originated from an MRCAT or a CT image. The registration software is available as precompiled Matlab program as supplementary data and the source code to academic users upon email request from the authors.

To obtain a reference for the manual registrations, a registration between CT and MRCAT must be defined. Therefore, the mDIXON source scan was rigidly registered to the planning CT image and this transformation is then used as the MRCAT to CT reference registration. The registration shall eliminate minor orientation and translational difference between scans. See figure 2 for an illustration of the registrations that were performed and evaluated in this study.

Bland Altman plots

Bland Altman plots for repeated measurements were used for visual assessment of method differences. Limits of agreement (LoA) were adjusted for repeated measurements as suggested by Bland and Altman (Bland and Altman 1999). Measurements from multiple observers were not separated in the calculation of LoAs.

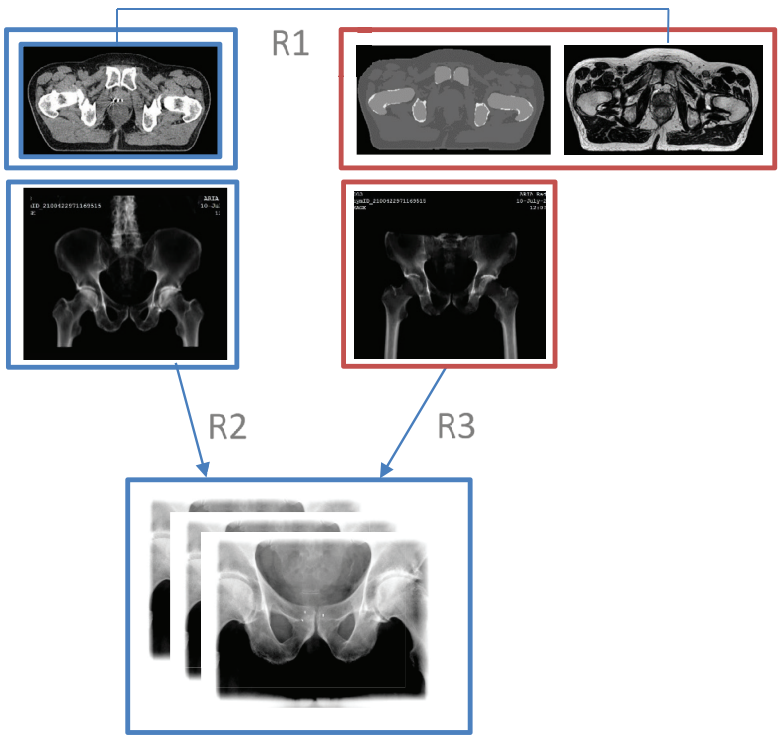

Figure 2. Illustration of registrations used in the study: MRCAT MR-source mDIXON images were rigidly registered to the simulation CT using bones making the reference registration (R1) for the comparison of manual 2D registrations between MRCAT DRRs (R3) and CT DRRs (R2) to the kV radiographs.

Linear mixed effects model (LME)

The following mixed-effects model was used for evaluation of systematic difference and comparison of accuracy and reliability of the two methods:

$$y_{ijk} = \mu + a_i + ab_{ij} + \varepsilon_{ijk}$$

- $i \in \{1, 2, \ldots, 20\}$ is the patient index
- $j \in \{1, 2, \ldots, 5\}$ is the observer index
- $k \in \{1, 2, \ldots, 3\}$ is the kth measurement made by an observer on a certain patient
- y_{ijk} is the observed couch shift for patient i, observer j and measurement k
- μ is the fixed effect population mean for the required couch-shifts
- $a_i \sim N(0, \sigma_a)$ is a patient level random effect that denotes the true deviation from μ for the ith patient
- $ab_{ij} \sim N(0, \sigma_{ab})$ is a random effect describing the bias of the jth reader when measuring the couch-shift for the ith patient. σ_{ab} is the inter-observer repeatability, attributed to the standard deviation of the bias terms amongst all observers
- $\varepsilon_{ijk} \sim N(0, \sigma_\varepsilon)$ is a random error made by the readers when making their kth measurement of the couch-shift for the ith patient. Intra-observer repeatability is identified as the standard deviation parameter σ_ε.

Stan statistical computing language with *R* implementation was used to fit the LME model to the measured data and to estimate the parameters of interest (Carpenter *et al* 2017). Full details of the statistical methods used in this manuscript together with *R* and RStan source code are given in the appendix. Similar LME model has been used for an IGRT method comparison study by Roy *et al* (2015).

Assessment of impact to total geometric deviation

Geometric accuracy of image guidance in RT directly affects required treatment margins and outcomes. Depending on whether a source of error is introduced in the planning phase or randomly during each fraction, the contribution to total uncertainty is either systematic or random (Van Herk 2004). Similarly, introduction of MRCAT reference image in RT can introduce both systematic and random error compared to CT-based workflow (see table 1). Systematic and random errors were analysed separately since their contribution to total uncertainty is different (Van Herk 2004).

To assess the differences in the systematic and random uncertainties between the two methods, the following derived metrics were used:

Table 1. Grouping the method comparison disagreement to systematic and random components.

Difference component	Explanation	Origin of difference	Contribution to MRCAT registration error
$\Delta\mu$	Systematic difference in the population mean over all registrations of the two methods	Systematic difference between MRCAT and CT bone structures for the cohort of patients or systematic error in MR-to-CT reference registration	Systematic difference between MRCAT and CT bone structures results into **systematic** geometric deviation for the whole population in RT workflow
Δa ($\sigma_{\Delta a}$)	Difference in patient mean between CT and MRCAT based registration. SD of Δa is denoted as $\sigma_{\Delta a}$	Difference between MRCAT and CT bone structures varying from patient to patient or random error in MR-to-CT reference registration	Random difference between MRCAT and CT bone structures results to **systematic** geometric error in RT workflow for a patient and random error for a population
$\sigma^2_{ab.\ \mathrm{CT}}$ and $\sigma^2_{ab.\ \mathrm{MRCAT}}$	The inter-observer repeatability (variability) for CT and MRCAT DRR registrations	Difference in the bone representation of CT and MRCAT might cause changes to inter-observer variability reflected by σ_{ab}	Increased inter-observer variability would cause an increase of **random** error in RT workflow
$\sigma^2_{\varepsilon.\ \mathrm{CT}}$ and $\sigma^2_{\varepsilon.\ \mathrm{MRCAT}}$	The repeatability (intra-observer variability) of registration in each method	Difference in the bone representation of CT and MRCAT might cause changes to inter-observer variability reflected by σ_{ε}	Increased intra-observer variability would cause an increase of **random** error in RT workflow

$$\Delta_{\mathrm{sys}} = |\Delta\mu| + \sigma_{\Delta a}$$
$$\Delta\sigma_{\mathrm{rand}} = \sqrt{\sigma^2_{ab.\mathrm{MRCAT}} + \sigma^2_{\varepsilon.\mathrm{MRCAT}}} - \sqrt{\sigma^2_{ab.\mathrm{CT}} + \sigma^2_{\varepsilon.\mathrm{CT}}},$$

where Δ_{sys} is a random variable describing the systematic uncertainty and difference in registrations. It consists of the difference in population mean $\Delta\mu$ and standard deviation of difference in patient registrations, $\Delta a_i = a_i^{\mathrm{CT}} - a_i^{\mathrm{MR}}$, denoted as $\sigma_{\Delta a}$. Furthermore, $\Delta\sigma_{\mathrm{rand}}$ is a random variable describing the difference in random registration error between the two methods consisting of both inter- and intra-observer variability.

To assess that a MR-only solution will improve the total geometric accuracy of RT workflow, the increase in registration uncertainty must be weighed against the reduction of the registration uncertainty present in a dual modality workflow. In RT, uncertainties can be linked directly to the required PTV margins and assessment of method agreement should reflect the impact to total uncertainty of compared workflows.

As proposed by Van Herk (2004) and Roy *et al* (2015), the sufficient CTV to planning target volume (PTV) margin can be expressed as:

$$m_{\mathrm{PTV}} = 2.5\Sigma + 0.7\sigma$$

where Σ (here Δ_{sys}) is the systematic and σ ($\Delta\sigma_{\mathrm{rand}}$ in this study) is the random spatial uncertainty. We use this weighting of the two error components in the assessment of significance of the difference between CT and MRCAT registrations. Consequently, for MRCAT based workflow to be as good as or better than CT based workflow, the following condition must be met for all three directions:

$$\Pr\left(m_{\mathrm{PTV}}^{\mathrm{MRCAT}} - m_{\mathrm{PTV}}^{\mathrm{CT}} < 0\right) \geqslant 0.95.$$

That is, the probability that the required PTV margin in MR-only workflow is smaller than in the dual modality workflow is larger than 95%.

An estimate for registration error of 2 mm from literature was used is our assessment (Roberson *et al* 2005). In addition, we calculate an estimate of registration error for which there is 95% probability that required margin in MR-only workflow is smaller.

Results

Bland Altman plots

The mean difference between the methods [±95% LoA] were −0.5 [−3.2 to +2.3] mm, +0.1 [−2.4 to +2.6] mm and +0.1 [−1.6 to +1.7] for vertical, longitudinal and lateral directions, respectively (see figure 3). The repeatability coefficients were (CT versus MRCAT) 2.1 mm versus 2.6 mm, 1.4 mm versus 2.1 mm and 1.2 mm versus 1.4 mm for vertical, longitudinal and lateral directions.

Systematic differences

No difference in population mean $\Delta\mu$ between CT and MRCAT based positioning were observed in lateral or longitudinal directions (see figure 4, $P(\Delta\mu < 0) = 0.34$). However, for vertical direction a statistically

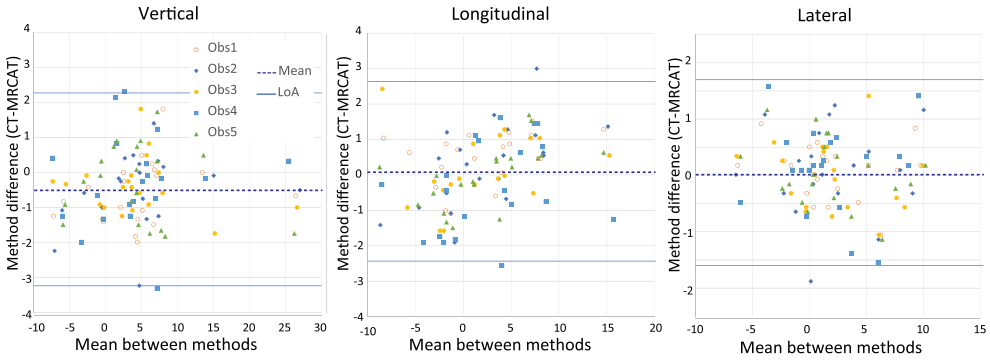

Figure 3. Bland Altman plot for vertical, longitudinal and lateral direction with LoA and mean difference. Obs1-5 show the registration differences between methods per observer.

significant offset of (mean [95% CI]) −0.49 [−0.85 to −0.13] mm was detected ($P(\Delta\mu < 0) > 0.99$). The standard deviation of patient offsets $\sigma_{\Delta a}$ was 0.29 [0.21–0.36] mm, 0.50 [0.40–0.63] mm and 0.63 [0.48–0.76] mm lateral, longitudinal and vertical directions.

Random setup errors

Inter-observer variation was not significantly different between CT and MRCAT based DRR to kV-image registrations in longitudinal ($P(\sigma_{ab,\mathrm{MRCAT}} > \sigma_{ab,\mathrm{CT}}) = 0.58$) or lateral ($P(\sigma_{ab,\mathrm{MRCAT}} > \sigma_{ab,\mathrm{CT}}) = 0.52$) directions. However, the largest difference was observed in vertical direction being statistically significant ($P(\sigma_{ab,\mathrm{MRCAT}} > \sigma_{ab,\mathrm{CT}}) > 0.99$) whereas smaller deviation was measured in longitudinal direction (see figure 5). In lateral direction, inter-observer variability was smallest and almost identical between the two methods.

A statistically significant difference was observed in intra-observer variability between CT and MRCAT based DRR to kV-image registrations in vertical, longitudinal and lateral directions (see figure 5, $P(\sigma_{\varepsilon,\mathrm{MRCAT}} > \sigma_{\varepsilon,\mathrm{CT}}) > 0.99$). The largest difference between methods was observed in longitudinal direction and smallest in lateral direction.

Effect on total uncertainty and on required PTV margin

The estimate of the parameter describing the systematic difference between MRCAT and CT based DRR-to-kV registrations, Δ_{sys}, was (Maximum *a posteriori*, MAP [95% CI]) 1.04 [0.65–1.50] mm, 0.93 [0.65–1.44] mm, and 0.58 [0.44–0.91] mm in vertical, longitudinal and lateral directions (see figure 6). The increases in total random uncertainty were estimated to be below 0.5 mm for all directions being (MAP [95% CI]) 0.31 [0.15–0.48] mm, 0.24 [0.12–0.40] mm and 0.06 [−0.00–0.15] mm for vertical, longitudinal and lateral directions.

When registration errors were larger than 1.7 mm, 1.5 mm, and 1.1 mm in vertical, longitudinal and lateral directions, statistically significantly smaller CTV to PTV margin was needed in MR-only workflow.

Discussion

New pseudo-CT methods are increasingly introduced in the field (Edmund and Nyholm 2017). It is essential to note that assessment of the impact of using such methods to total geometric accuracy is as important as dosimetric accuracy. Currently, assessments of dosimetric accuracy outnumbers assessments of impact to other areas of uncertainty in RT. Thus, studies and methods assessing overall impact of pseudo-CTs beyond dose accuracy are needed.

In this study, we measured both accuracy and precision of MRCAT DRR to planar kV-image registration for IGRT of pelvic EBRT. According to the results, average positioning differences were −0.5 mm, 0.1 mm and −0.1 mm in vertical, longitudinal and lateral directions, respectively. These figures are similar to what has been reported for DRR to kV registrations for pseudo-CTs based on manually contoured bone segmentations in a similar measurement setup (Korhonen *et al* 2015). Namely, the authors reported average positioning differences (±SD) of -0.3 ± 1.0 mm, 0.2 ± 0.9 mm and 0.1 ± 0.5 mm for vertical, longitudinal, and lateral, directions. Prior MRCAT DRR evaluation by Tyagi studied the quality of DRRs using a non-clinical workflow of automatically registering CT and MRCAT DRRs with an algorithm. The average match for all the patients was 0.3 ± 0.4 mm, 0.03 ± 0.6 and 0.5 ± 0.8 mm in lateral, vertical and longitudinal direction respectively. Unfortunately, their results cannot be compared to our manual DRR to kV-image registration study since the figures by Tyagi *et al* do not contain the uncertainty resulting from DRR to kV-image registration nor observer variation and, consequently, is not estimate of clinical performance of the method.

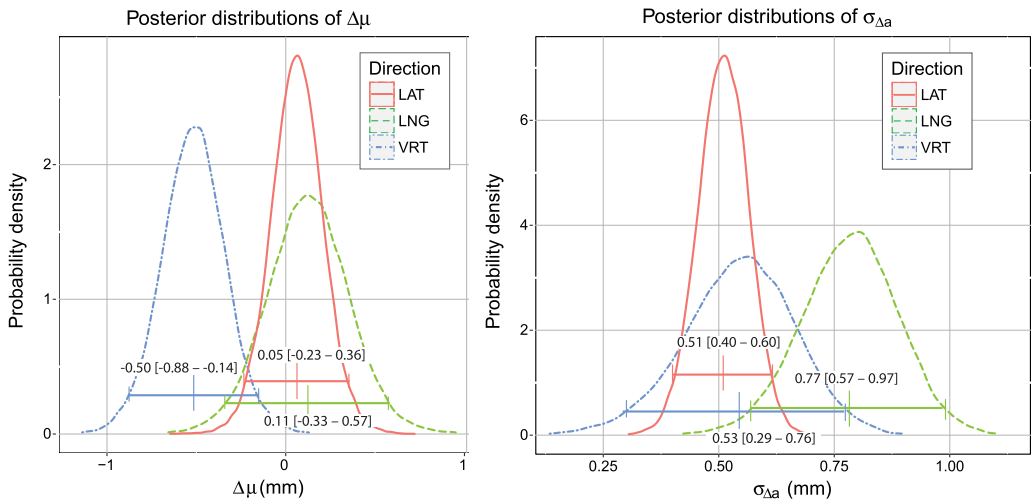

Figure 4. Systematic difference between CT and MRCAT-based DRR registrations to kV-images for VRT (dash-dotted), LAT (solid) and LNG (dashed) directions with mean (vertical bar) and 95% credible interval (horizontal bar). Left: difference of population means $\Delta\mu$. Right: standard deviation of patient offset $\sigma_{\Delta a}$.

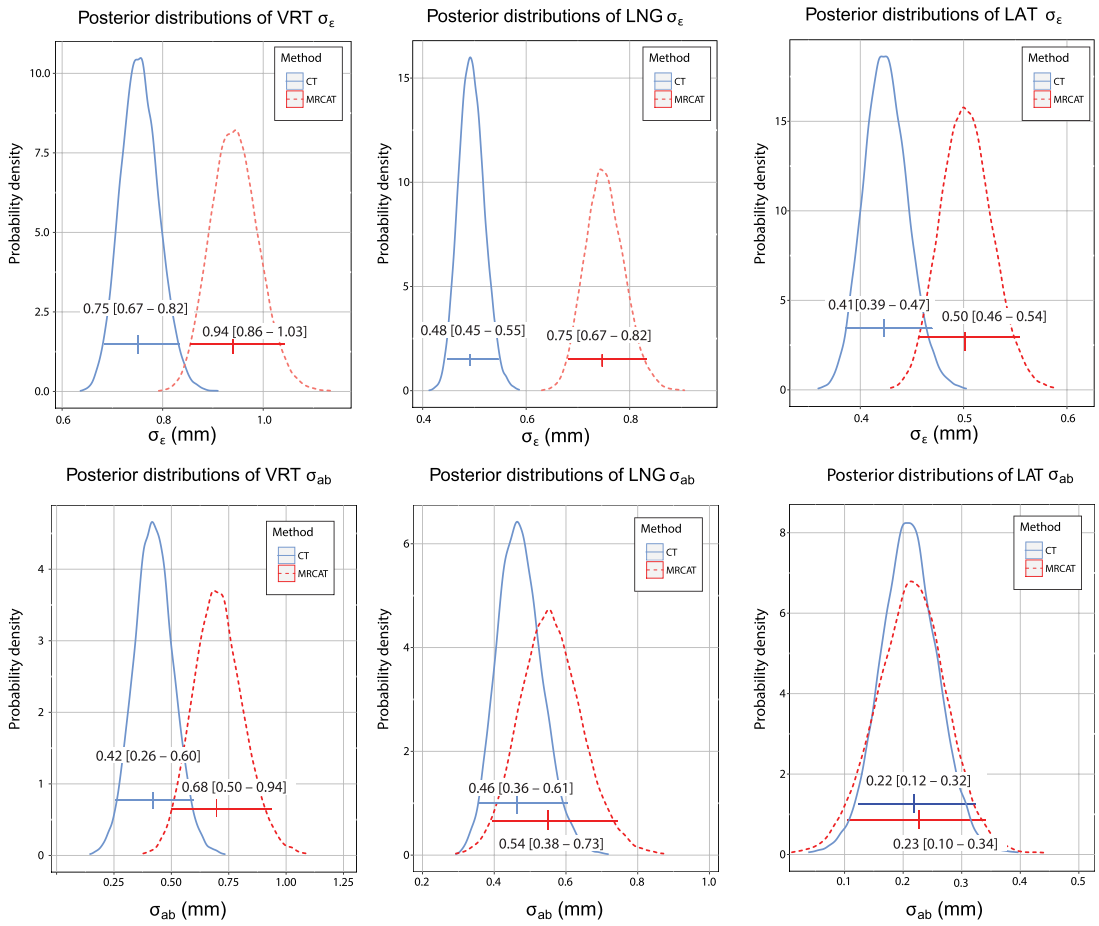

Figure 5. Posterior distribution of intra- (to row) and inter-observer (bottom row) variability in vertical (left), longitudinal (middle) and lateral (right) directions for CT (solid) and MRCAT (dashed) DRR to kV-radiograph registrations. Horizontal bars indicate 95% credible intervals [95% CI] and vertical bars show the maximum *a posteriori* (MAP) point of the distribution.

Alternative methods for assessment of DRR feasibility have also been reported. Unlike in our study, Kim *et al* (2015) used a bounding box width difference for assessment of geometric accuracy of their pseudo-CT method giving 0.4 ± 1.7 mm and -0.6 ± 1.0 mm AP and RL DRRs, respectively. Furthermore, Chen *et al* used a set of eight measurement points defined in both CT and manually segmented pseudo-CT to assess the feasibility of calculated DRRs for IMRT treatment of prostate carcinoma. The maximum difference for a point location between pseudo-CT and CT was 1.3 ± 1.6 mm when averaged over the study population. However, either Kim or Chen

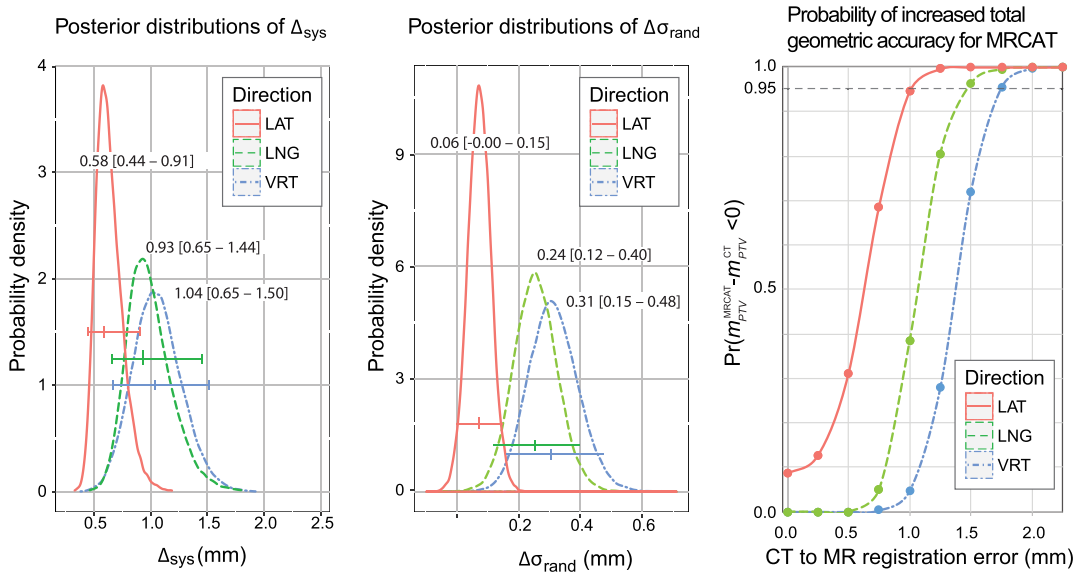

Figure 6. Effect on total systematic (left) and random (middle) geometric uncertainty and probability of reduced required CTV to PTV margin for MRCAT compared to CT workflow (right) for VRT (dash-dotted), LAT (solid) and LNG (dashed) directions with MAP (vertical bar) with 95% credible interval (horizontal bar). On the right, above points where probability is larger than 95%, required margin for MRCAT is statistically significantly lower. Circular marks indicate the points where probability was evaluated.

et al do not report performance metrics measured based on image registrations. In addition, several authors (Kim *et al* 2015, Korhonen *et al* 2015) have reported image similarity scores between pseudo-CT and planning CT DRR. Unfortunately, the similarity metrics have a disadvantage of not measuring positioning accuracy or precision achievable with the investigated method. Furthermore, when using similarity scores, it's difficult to assess the impact to total geometric accuracy and acceptance criteria may not be defined.

Measured difference between registrations in CT and MRCAT based workflow include both true difference and measurement noise. The measurement noise stems mainly from two sources. First, registrations between CT and kV-radiographs are affected by uncertainties stemming from the ~1 mm-pixel sizes and the ~2 mm-slice thickness in the reference images contributing to errors in calculated DRRs (Hurkmans *et al* 2001). Second, the residual errors from planning CT to mDixon source image registrations are contributing to the systematic offsets for each patient. In this study patient positioning uncertainties with MRI-based reference images were analyzed by assuming that the registrations between MRCAT and CT can be regarded as an error free reference for correct patient position. Since such baseline assignment is not truly error free and CT based registration is affected by uncertainties, it is likely that the actual registration uncertainty with MRI- based DRR is smaller than reported in this study. Particularly, when considering the significance of the observed small systematic differences one needs to acknowledge that due to chosen study design these differences can result from MRCAT properties or from the registration uncertainties in the MR to CT reference registration (R1). To our knowledge, there is no simple direct method to measure the performance of MRCAT DRRs for patient position verification purposes using human observers. Thus, our method was to compare to the 'gold standard' CT-based workflow.

Unlike the systematic differences, inter- and intra-observer variability are not affected by the uncertainties of the reference registration. Thus, they can be used for measuring the random positioning error independently for both MRCAT and CT-based DRRs. More importantly, in any method comparison study, simultaneous estimation of repeatability, through repeated measurements of identical conditions, and agreement are necessary in order to analyze the origin of discrepancies between methods (Myles and Cui 2007). No prior studies assess intra-observer variation in image guided patient positioning workflow for prostate cancer patients.

Based on obtained registrations, the inter-observer variability was not significantly different in longitudinal or lateral directions but was slightly increased compared to CT in vertical direction. The increase might be due to degraded visibility of the anterior outline of the pubic bone in the MRCAT DRRs. Intra-observer variability was significantly larger for MRCAT DRRs than CT DRRs in vertical and longitudinal directions. However, the total increase in random registration error was below 0.5 mm for all directions and can be considered insignificant in the context of total geometric uncertainties for pelvic RT.

Based on the results, given that there is an uncertainty associated with CT-to-MR registration larger than 1.7 mm, 1.5 mm, and 1.1 mm in vertical, longitudinal and lateral direction, it's likely that use of MR-only has a positive effect to the total geometric accuracy. In the literature uncertainties of 2 mm have been reported for

prostate RT (Roberson *et al* 2005). Thus, we conclude that in terms of total geometric accuracy benefits of using MRCAT likely outweigh the small increase in MRCAT DRR-based positioning uncertainty. However, as registration errors were not quantitated in this cohort of patients, further research is needed to confirm our findings.

An important patient positioning workflow for EBRT of prostate cancer is based on implantable fiducials (Parker and Damyanovich 2003). The workflow is also feasible with MRCAT (Tyagi *et al* 2017) since most of the fiducials are accurately localized in MR images (Parker and Damyanovich 2003, Jonsson *et al* 2012, Kapanen *et al* 2013) and their contours on DRR images can be used for target position verification and the clinical workflow is feasible (Kapanen *et al* 2013, Tyagi *et al* 2017). However, automatic and robust detection of fiducial markers from MR-images remains a challenge and is a subject of active research (Ghose *et al* 2016, Dinis Fernandes *et al* 2017, Gustafsson *et al* 2017, Maspero *et al* 2017).

The study population consisted of only prostate cancer patients. For other indications in the pelvis, including also female patients, we have demonstrated the feasibility of MRCAT generation, geometric accuracy and dose accuracy, in an earlier study (Kemppainen *et al* 2017). Thus, the results obtained in this study are considered applicable for pelvic anatomy in general. However, further studies are needed to verify the findings and assess robustness of MRCAT for female population.

Currently, contraindications for the use of MRCAT are metal in the imaging volume, such as a metal prosthesis in the hip region, bone anomalies or bone disease in the pelvic area and body diameter in the pelvic area exceeding 50 cm in AP direction. The risk of using contraindicated MRCAT images for RT is mitigated by implementing a safety check in the MRCAT algorithm that prevents the reconstruction of the pseudo-CT in case of atypical bony anatomy or presence of hip implants, for example. Use of MRCAT DRRs for contraindicated patients is beyond the scope of this article and requires further studies.

Use of volumetric positioning image (kV CBCT) is becoming more common due to improved visualization of the daily variation in the anatomy (Moseley *et al* 2007). For prostate, MRCAT could be used also with CBCT-based position verification utilizing implantable fiducial's for registration to daily CBCT (Tyagi *et al* 2017). In general, however, soft-tissue based registration between daily CBCT and MRCAT for position verification needs to be investigated in subsequent studies since MRCAT, with only two soft-tissue density values, might not be robustly registered to a CBCT image.

This study advances research and supports future clinical implementation of MRI-only IGRT by presenting a Bayesian linear mixed effects model (LME) method comparison approach for assessing accuracy and precision of patient positioning. Our analysis method is available, uses widely used open source software and could be easily utilized for assessment of other anatomies or methods. Particularly, we used the LME to compare MRCAT pseudo-CT method to a CT-based workflow and demonstrated the feasibility of the method for kV planar imaging IGRT for pelvic anatomy.

Conclusions

The MRCAT pseudo-CT method provides clinically acceptable accuracy and precision for patient positioning for pelvic RT based on planar DRR images. Use of MRCAT method is associated with a small increase in precision and small systematic difference compared to CT. However, when the slight increase in uncertainty is compared to the uncertainty in CT-to-MR registration in dual modality workflow, MRCAT can be considered more accurate in terms of total accuracy when registration errors are larger than 1.7 mm, 1.5 mm, and 1.1 mm in vertical, longitudinal and lateral directions.

Acknowledgments

The authors thank associate professor Aki Vehtari for comments on Stan model and Bayesian statistics, and Jukka-Pekka Kauppi for suggestions for improving the manuscript text.

The authors would also like to show gratitude to Docrates Cancer Center radiographers for performing the manual registrations required for the study. Especially we would like to thank Aili Aaltonen for her effort on recruitment of the patients.

Disclosure statement

Authors Reko Kemppainen and Teuvo Vaara declare that they were employed by Philips MR Therapy, Finland by the time of conducting the research.

ORCID iDs

R Kemppainen https://orcid.org/0000-0001-9315-2596

References

Bland J M and Altman D G 1999 Measuring agreement in method comparison studies *Stat. Methods Med. Res.* **8** 135–60

Carpenter B *et al* 2017 Stan: a probabilistic programming language *J. Stat. Softw.* **76** 1–32

Chen L *et al* 2007 Magnetic resonance-based treatment planning for prostate intensity-modulated radiotherapy: creation of digitally reconstructed radiographs *Int. J. Radiat. Oncol. Biol. Phys.* **68** 903–11

Debois M *et al* 1999 The contribution of magnetic resonance imaging to the three-dimensional treatment planning of localized prostate cancer *Int. J. Radiat. Oncol. Biol. Phys.* **45** 857–65

Dinis Fernandes C *et al* 2017 Prostate fiducial marker detection with the use of multi-parametric magnetic resonance imaging *Phys. Imaging Radiat. Oncol.* **1** 14–20

Dowling J A *et al* 2012 An atlas-based electron density mapping method for magnetic resonance imaging (MRI)-alone treatment planning and adaptive MRI-based prostate radiation therapy *Int. J. Radiat. Oncol. Biol. Phys.* **83** e5–11

Ecabert O *et al* 2008 Automatic model-based segmentation of the heart in CT images *IEEE Trans. Med. Imaging* **27** 1189–202

Edmund J M and Nyholm T 2017 A review of substitute CT generation for MRI-only radiation therapy *Radiat. Oncol.* **12** 28

Ghose S *et al* 2016 MRI-alone radiation therapy planning for prostate cancer: automatic fiducial marker detection *Med. Phys.* **43** 2218–28

Gustafsson C, Korhonen J, Persson E, Gunnlaugsson A, Nyholm T and Olsson L E 2017 Registration free automatic identification of gold fiducial markers in MRI target delineation images for prostate radiotherapy *Med. Phys.* **44** 5563–74

Hurkmans C W, Remeijer P, Lebesque J V and Mijnheer B J 2001 Set-up verification using portal imaging; review of current clinical practice *Radiother. Oncol.* **58** 105–20

Jonsson J H, Garpebring A, Karlsson M G and Nyholm T 2012 Internal fiducial markers and susceptibility effects in MRI-simulation and measurement of spatial accuracy *Int. J. Radiat. Oncol. Biol. Phys.* **82** 1612–8

Kapanen M, Collan J, Beule A, Seppälä T, Saarilahti K and Tenhunen M 2013 Commissioning of MRI-only based treatment planning procedure for external beam radiotherapy of prostate *Magn. Reson. Med.* **70** 127–35

Karlsson M, Karlsson M G, Nyholm T, Amies C and Zackrisson B 2009 Dedicated magnetic resonance imaging in the radiotherapy clinic *Int. J. Radiat. Oncol. Biol. Phys.* **74** 644–51

Kemppainen R, Suilamo S, Tuokkola T, Lindholm P, Deppe M H and Keyriläinen J 2017 Magnetic resonance-only simulation and dose calculation in external beam radiation therapy: a feasibility study for pelvic cancers *Acta Oncol.* **56** 792–8

Kim J, Glide-Hurst C and Doemer A 2015 Implementation of a novel algorithm for generating synthetic CT images from magnetic resonance imaging data sets for prostate cancer radiation therapy *Int. J. Radiat. Oncol. Biol. Phys.* **91** 39–47

Köhler M, Vaara T, Van Grootel M, Hoogeveen R, Kemppainen R and Renisch S 2015 White paper: MR-only simulation for radiotherapy planning *Philips* pp 1–16

Korhonen J *et al* 2015 Feasibility of MRI-based reference images for image-guided radiotherapy of the pelvis with either cone-beam computed tomography or planar localization images *Acta Oncol.* **54** 889–95

Korhonen J, Kapanen M, Keyriläinen J, Seppälä T and Tenhunen M 2014 A dual model HU conversion from MRI intensity values within and outside of bone segment for MRI-based radiotherapy treatment planning of prostate cancer *Med. Phys.* **41** 11704

Maspero M *et al* 2017 Evaluation of an automatic MR-based gold fiducial marker localisation method for MR-only prostate radiotherapy *Phys. Med. Biol.* **62** 7981–8002

Moseley D J *et al* 2007 Comparison of localization performance with implanted fiducial markers and cone-beam computed tomography for on-line image-guided radiotherapy of the prostate *Int. J. Radiat. Oncol. Biol. Phys.* **67** 942–53

Myles P S and Cui J 2007 I. Using the Bland Altman method to measure agreement with repeated measures *Br. J. Anaesth.* **99** 309–11

Nyholm T, Nyberg M, Karlsson M G and Karlsson M 2009 Systematisation of spatial uncertainties for comparison between a MR and a CT-based radiotherapy workflow for prostate treatments *Radiat. Oncol.* **4** 54

Parker C and Damyanovich A 2003 Magnetic resonance imaging in the radiation treatment planning of localized prostate cancer using intra-prostatic fiducial markers for computed tomography co-registration *Radiother. Oncol.* **66** 217–24

Rasch C, Barillot I and Remeijer P 1999 Definition of the prostate in CT and MRI: a multi-observer study *Int. J. Radiat. Oncol. Biol. Phys.* **43** 57–66

Roberson P L, McLaughlin P W, Narayana V, Troyer S, Hixson G V and Kessler M L 2005 Use and uncertainties of mutual information for computed tomography/magnetic resonance (CT/MR) registration post permanent implant of the prostate *Med. Phys.* **32** 473–82

Roy A, Fuller C D, Rosenthal D I and Thomas C R 2015 Comparison of measurement methods with a mixed effects procedure accounting for replicated evaluations (COM3PARE): method comparison algorithm implementation for head and neck IGRT positional verification *BMC Med. Imaging* **15** 35

Siversson C *et al* 2015 Technical Note: MRI only prostate radiotherapy planning using the statistical decomposition algorithm *Med. Phys.* **42** 6090–7

Tyagi N *et al* 2017 Dosimetric and workflow evaluation of first commercial synthetic CT software for clinical use in pelvis *Phys. Med. Biol.* **62** 2961–75

Van Herk M 2004 Errors and margins in radiotherapy *Semin. Radiat. Oncol.* **14** 52–64

Publication 3

Kemppainen R, Suilamo S, Ranta I, Pesola M, Halkola A, Eufemio A, Minn H., Keyriläinen J. Assessment of dosimetric and positioning accuracy of a magnetic resonance imaging-only solution for external beam radiotherapy of pelvic anatomy. Phys. Imaging Radiat. Oncol. 2019;11:1–8.

Physics and Imaging in Radiation Oncology 11 (2019) 1–8

Contents lists available at ScienceDirect

Physics and Imaging in Radiation Oncology

journal homepage: www.elsevier.com/locate/phro

Original Research Article

Assessment of dosimetric and positioning accuracy of a magnetic resonance imaging-only solution for external beam radiotherapy of pelvic anatomy

Reko Kemppainen [a,b,⊠], Sami Suilamo [c,d], Iiro Ranta [c,d], Marko Pesola [a], Aleksi Halkola [a], Alvin Eufemio [a], Heikki Minn [d], Jani Keyriläinen [c,d]

[a] Philips Oy, Äyritie 4, FI-01510 Vantaa, Finland
[b] Department of Neuroscience and Biomedical Engineering, Aalto University School of Science, Rakentajanaukio 2 C, FI-02150 Espoo, Finland
[c] Department of Medical Physics, Turku University Hospital, Hämeentie 11, P.O. Box 52, FI-20521 Turku, Finland
[d] Department of Oncology and Radiotherapy, Turku University Hospital, Hämeentie 11, P.O. Box 52, FI-20521 Turku, Finland

ARTICLE INFO

Keywords:
Radiotherapy
MRI-only
Image-guided radiotherapy
Position verification

ABSTRACT

Background and purpose: The clinical feasibility of synthetic computed tomography (sCT) images derived from magnetic resonance imaging (MRI) images for external beam radiation therapy (EBRT) planning have been studied and adopted into clinical use recently. This paper evaluates the dosimetric and positioning performance of a sCT approach for different pelvic cancers.
Materials and methods: Seventy-five patients receiving EBRT at Turku University Hospital (Turku, Finland) were enrolled in the study. The sCT images were generated as part of a clinical MRI-simulation procedure. Dose calculation accuracy was assessed by comparing the sCT-based calculation with a CT-based calculation. In addition, we evaluated the patient position verification accuracy for both digitally reconstructed radiograph (DRR) and cone beam computed tomography (CBCT) -based image guidance using a subset of the cohort. Furthermore, the relevance of using continuous Hounsfield unit values was assessed.
Results: The mean (standard deviation) relative dose difference in the planning target volume mean dose computed over various cancer groups was less than 0.2 (0.4)% between sCT and CT. Among all groups, the average minimum gamma-index pass-rates were better than 95% with a 2%/2mm gamma-criteria. The difference between sCT- and CT-DRR-based patient positioning was less than 0.3 (1.4) mm in all directions. The registrations of sCT to CBCT produced similar results as compared with CT to CBCT registrations.
Conclusions: The use of sCT for clinical EBRT dose calculation and patient positioning in the investigated types of pelvic cancers was dosimetrically and geometrically accurate for clinical use.

1. Introduction

Computed tomography (CT) is currently the primary imaging modality for providing anatomical and tissue density information in the external beam radiation therapy (EBRT) planning of pelvic cancers. Magnetic resonance imaging (MRI) is widely used as a supplement to the CT imaging [1–3]. The most significant advantage of MRI over CT is its better soft-tissue contrast, which results in a more accurate gross tumor volume and organ at risk (OAR) delineation [4–7]. Additional benefits include the usage of non-ionizing radiation and the versatility of acquisition sequences allowing the cancer- or organ-specific imaging methods [5].

A major drawback of multi-modality imaging in EBRT is the residual registration error remaining when the images from two or more modalities are registered with each other [8]. Recent advances in the use of MRI promise to eliminate the registration error by using only the MR images for planning and dose calculation in the EBRT of prostate and brain cancer (see the recent reviews [9–11]). In an MRI-only workflow, so-called synthetic CT (sCT) images are generated from the magnetic resonance (MR) images, providing the tissue density information for dose calculation and reference images for patient position verification. Over recent years, commercial solutions for obtaining the sCT for prostate cancer patients have been introduced [12,13].

A commercially available solution for the sCT generation was used in this work. It has been shown that the solution can be used for an accurate dose calculation and patient positioning for prostate cancer patients [13,14]. In addition, its feasibility for other indications in the pelvic anatomy was demonstrated in our earlier study [15]. However,

⊠ Corresponding author at: Philips Oy, Äyritie 4, FI-01510 Vantaa, Finland.
E-mail address: reko.kemppainen@gmail.com (R. Kemppainen).

https://doi.org/10.1016/j.phro.2019.06.001
Received 26 October 2018; Received in revised form 30 May 2019; Accepted 2 June 2019

the bulk assignment of Hounsfield unit (HU) values limits the soft-tissue characterization, and consequently affects the ability to verify treatment position based on a tissue contrast. In addition, the sCT methods suitable for prostate EBRT may not be directly applicable to other pelvic targets due to larger treatment volumes and higher patient demographic variability, both characteristic for the non-prostate pelvic cancer. Thus, additional validation of a sCT solution for general pelvic imaging is required.

The feasibility of sCT methods for general pelvic anatomy including the assessment of both dosimetric and positioning accuracy have not been studied within a single study. Several groups have assessed the dosimetric and positioning for prostate cancer with comparison of continuous HU and bulk HU assignment (see e.g. [16–19]). Two recent studies have evaluated the feasibility of MRI-only workflow for rectal cancers [20,21] . However, to the best of our knowledge, only the dosimetric accuracy has been evaluated for gynecological cancers [22–24] .

The aim of this study was to evaluate the feasibility of an MRI-only method in terms of dose calculation, position verification and geometric accuracy in EBRT for the pelvic anatomy in general. In addition, we have evaluated the necessity of continuous HU values in sCT images for dosimetric and positioning accuracy for prostate cancer patients. This research addressed the use of sCT in pelvis which included the cone beam computed tomography (CBCT)- and digitally reconstructed radiograph (DRR)-based position verification workflows. Furthermore, both bone- and soft-tissue-based registration workflows for CBCT were evaluated.

2. Materials and methods

2.1. Patient cohort and image acquisition

The study cohort consisted of 75 consecutive patients referred to EBRT of pelvic cancers at the Department of Oncology and Radiotherapy of Turku University Hospital in Turku, Finland. The patients were enrolled in between October 2017 and August 2018. The Ethical Committee of the Hospital District of Southwest Finland approved the study, and an informed consent was obtained (reference code: Dnro 116/1801/2017).

There were 20 (27%) female and 55 (73%) male patients divided into five groups each consisting of 15 patients. A total of 45 (60%) patients had a prostate cancer of whom 15 underwent definitive, 15 postoperative, and 15 regional pelvic lymph node EBRT. The remaining two groups consisted of 15 patients with rectal and 15 patients with gynecological cancer, respectively (see the Table 1 for further details).

The CT simulation images were acquired using the Aquilion LB (Toshiba Corp., Tokyo, Japan) scanner with 2-mm-thick slices, 1×1 mm ^{2} in-plane resolution, 120 kV tube voltage, and tube current modulation in cranio-caudal (CC) direction (Toshiba Sure-Exposure 3D SD 12.50). The MR images were recorded with the Ingenia 1.5T HP (sw. version 5.3.1, Philips MR Medical Systems International B.V., Best, Eindhoven, The Netherlands) scanner. For all patients, an axial T1-weighted three-dimensional (3D) mDIXON sequence [13] was acquired covering the full body contour (see the Supplementary Table 1 for MRI parameters). The MR images were used as a source for the sCT generation. Patients were positioned similarly during the imaging for CT and MRI simulation using the same patient positioning devices (including knee support) as during treatment. During the MRI scan, patients were placed in a supine position on a flat EBRT couch top and an anterior MRI-coil was placed above the imaging volume using a coil holder to prevent body outline deformation.

The planar radiograph and CBCT positioning images were acquired with the on-board imager system integrated to a linear accelerator (Varian Medical Systems Inc., Palo Alto, CA, USA). In the DRR study, two orthogonal projections (anterior-posterior (AP) or posterior-anterior (PA); and left–right (LR) or right-left (RL)) were obtained for all patients with a pixel size of 0.388×0.388 mm ^{2}; a field-of-view (FOV) of 30×40 cm ^{2}. For volumetric imaging, the CBCT images were acquired using 125 kV and 80 mAs with a 1×1 mm ^{2} in-plane resolution, 2-mm-thick slices and 160 mm coverage.

2.2. Synthetic CT generation

Two different versions of the sCT generation method (Magnetic Resonance for Calculating Attenuation, MRCAT, Philips Oy, Vantaa, Finland) were used in this study. The first version used a bulk assignment of HU values, which is referred to as sCTb in this study. The second version was an improved version of the MRCAT providing continuous HU values called sCTc hereafter. In the subgroup of patients receiving the radical treatment for prostate cancer (N = 15), both versions were generated for comparison of the methods. For other four cancer groups, only the sCTc was generated to evaluate the new method.

In the sCTb generating algorithm, the CT-like density maps were computed from the mDIXON MR images in a two-step approach [13,25,26] . In the first step, the content of the MR image was categorized into five classes. In the second step, each voxel was assigned the following HU: spongy bone (198 HU), compact bone (949 HU), fat (-86 HU), and water-rich tissue (42 HU).

The sCTc and sCTb used the segmentation of bones and soft-tissue based on mDIXON MR images. However, instead of the bulk assignment, the continuous HU values were used based on fat/water fraction within the voxels. In addition, the voxels on the body outline could partially contain air for modeling the partial volume effect. The sCTc images were obtained from the manufacturer while the sCTb images were generated at the scanner console. See the electronic supplementary material for details of the sCT generation.

2.3. Image processing

The CT images were rigidly registered to the sCTc and resampled to the same pixel grid using B-spline interpolation with the Elastix 4.9.0 [27] program. The registration parameters were the same used by Maspero et al. [28] for the registration between CT and sCT images. In CT images, the air cavities in the bowel and rectum were filled for all patients with 0 HU using the Matlab scripts (MATLAB ® 8.4.0.150421 (R2014b), The MathWorks Inc., Natick, MA, USA). The filling was equivalent to density override by water in the treatment planning

Table 1
Patient demographics and structure details within five different cancer groups (mean (standard deviation)) (PTV: planning target volume).

	Pelvic lymph node	Rectal cancer	Gynecological cancer	Prostate post-operative	Prostate definitive
Patient demographics					
Average age (years)	65.7 (6.2)	68.2 (10.6)	67.3 (14.0)	68.7 (6.8)	70.3 (8.0)
Sex (males/females)	15/0	10/5	0/15	15/0	15/0
Structure details					
PTV volume (cm ^{3})	1233 (4 4 3)	1621 (6 1 1)	1340 (7 1 6)	376 (1 0 2)	130 (43)
Bladder volume (cm ^{3})	231 (1 3 9)	287 (1 8 9)	225 (1 1 8)	239 (1 2 4)	281 (2 2 9)
Rectum volume (cm ^{3})	92 (41)	155 (34)	86 (43)	78.84 (37)	91 (43)

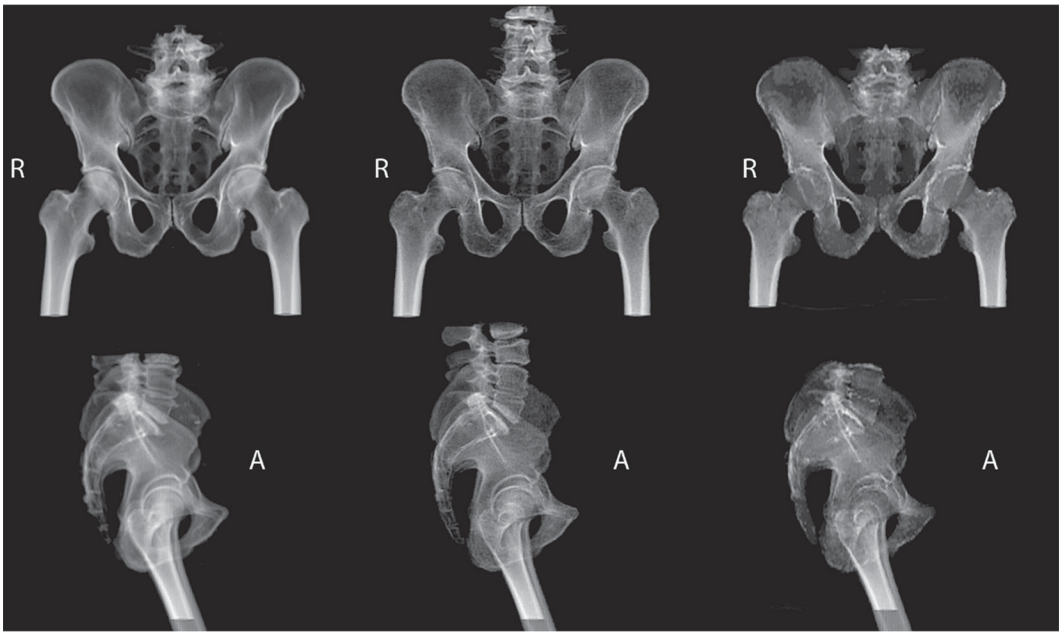

Fig. 1. Example DRR images from Eclipse treatment planning system using bone rendering (HU values less than 100 and above 1000 omitted). CT (left), sCTc with continuous HU values (middle), and sCTb with discrete HU values, (right) (DRR: digitally reconstructed radiograph, HU: Hounsfield unit, CT: computed tomography, sCT: synthetic computed tomography, R: right, A: anterior).

system (TPS) corresponding to a clinical practice used with patients encompassing large air volumes at our institution. The same approach was used [20] or suggested to be used [29] in the dosimetric evaluations of MRI-only methods in order to avoid confounding dosimetric differences not related to the sCT methods.

2.4. Dose calculation accuracy

The dosimetric agreement between planning CT and sCT was evaluated by recalculating the clinical plans in the Eclipse 13.6 (Varian Medical Systems Finland Oy, Helsinki, Finland) TPS using the sCT for inhomogeneity correction, an anisotropic analytical algorithm (AAA) for dose computation and a volumetric modulated arc (VMAT) delivery technique. The voxel grid size for optimization and dose calculation was set to $2.0 \times 2.0 \times 2.0\ \text{mm}^3$. The dosimetric agreement between CT and sCT was evaluated per cancer group for all patients. The evaluation metrics included dose-volume histogram (DVH) comparison for the PTV and OARs, 3D gamma analysis and dose comparison statistics.

The DVH evaluation was based on the structures that were copied from the planning CT to sCT based on rigid registration. Minimum, median and maximum ($D_{2\%}$, $D_{50\%}$, $D_{98\%}$) dose points were evaluated for the PTVs while volumes of $V_{95\%}$ and $V_{70\%}$ were assessed for the OARs. The results were computed as a relative difference with respect to prescribed dose $\left(\frac{D(pCT) - D(CT)}{D_{presc.}}\right)$ for dose points or structure volume $\left(\frac{V(pCT) - V(CT)}{V_{struct.}}\right)$ for volume points.

The 3D gamma analysis was performed using the Plastimatch 1.7.3 (http://plastimatch.org/index.html) open source software for image registration. Various gamma-index pass-rate criteria and dose cut-off values were evaluated using a global gamma-index relative to the maximum dose. The maximum value of gamma-index to compute was set to the default value of two.

2.5. Image similarity and body outline distortion

The differences between CT and sCT images were evaluated by computing a mean absolute error (MAE) and a mean error (ME) between the HU values within the intersection of the body contours of the two images. In addition, to assess the body outline correctness in sCT, the difference between CT and sCT body outline was computed for different CC positions at the distances from −150 to 150 mm from the MRI scanner isocentre. Furthermore, the computed body outline differences were compared with the measured geometric distortion to assess the origin of the differences in body outline.

The assessment ofimage similarity and body outline was performed using a Matlab program. First, the program evaluated the body outline difference at each CC-position for all patients as function of angle. Then the information at each CC-location was condensed by computing the mean absolute difference and standard deviation of the mean absolute difference over all angles and patients.

The MRI-system induced geometric distortions were evaluated by imaging a large 3D phantom containing a regular grid of MRI-positive markers. The parameters of the imaging sequence affecting geometric accuracy (sequence type and receiver bandwidth) were matched with the sCT source image. First, the markers were located, and their positions were compared with the phantom structure in order to compute the geometric distortion at the marker locations. Then, for each included patient, the obtained distortion map was interpolated to the positions defining the body outline structure. Finally, the geometric distortion was evaluated over a study cohort (see a detailed description in [15]).

2.6. Positioning accuracy and precision

A subset of the cohort was selected for the assessment of both the DRR- and CBCT-based position verification before each treatment fraction.

2.6.1. DRR

In the DRR study, 20 consecutive patients were selected consisting of nine females with three rectum and six gynecological cancer patients and eleven males with seven prostate and four rectum cancer patients. The manual registrations between CT-DRR and planar radiograph were compared with the manual registrations between sCT-DRR to planar radiograph (see the Fig. 1 for visualization of DRRs and Supplementary Fig. 1 for visualization of performed registrations). The manual

Table 2
Dose-volume histogram (DVH) comparison for all five pelvic cancer groups and comparison between two synthetic computed tomography (sCT) versions ($\frac{sCT - CT}{CT_{ref}}$, mean relative difference (SD, standard deviation) [range]) including the planning target volume (PTV), rectum and bladder, gamma analysis, dose statistics ($\frac{sCT - CT}{CT}$, mean relative difference (SD)), gamma-index pass-rates (mean (SD) [range]), and Hounsfield unit (HU) similarity evaluation (mean (SD) [range]). $V_{X\%}$ indicates the volume, where the dose is higher than X% of the prescribed dose. For DVH comparison, the CT_{ref} is either prescribed dose (for $D_{X\%}$) or structure volume (for $V_{X\%}$). For dose statistics per volume and PTV mean dose, values are relative to respective value obtained using CT. MAE: mean absolute error, ME: mean error.

	Pelvic lymph nodes (n = 15)	Rectal cancer (n = 15)	Gynecological cancer (n = 15)	Prostate cancer, post-operative (n = 15)	Prostate cancer, definitive (continuous HU, n = 15)	Prostate cancer, definitive (bulk HU, n = 15)
DVH comparison						
PTV						
Mean	0.0 (0.4) [−0.5 – 0.8]	0.1 (0.3) [−0.4 – 0.6]	−0.2 (0.4) [−1.0 – 0.3]	0.1 (0.3) [−0.4 – 0.6]	0.1 (0.2) [−0.2 – 0.4]	0.1 (0.2) [−0.5 – 0.3]
$D_{2\%}$	0.1 (0.5) [−0.6 – 1.2]	0.5 (0.6) [−0.7 – 2.0]	0.1 (0.4) [−0.7 – 0.7]	0.2 (0.6) [−0.4 – 2.0]	0.1 (0.2) [−0.3 – 0.4]	0.1 (0.2) [−0.6 – 0.4]
$D_{50\%}$	0.0 (0.4) [−0.6 – 0.8]	0.1 (0.3) [−0.3 – 0.5]	−0.2 (0.4) [−1.1 – 0.3]	0.0 (0.3) [−0.4 – 0.4]	0.1 (0.2) [−0.3 – 0.4]	0.1 (0.2) [−0.6 – 0.4]
$D_{98\%}$	−0.1 (0.3) [−0.9 – 0.5]	0.0 (0.4) [−1.0 – 0.4]	−0.2 (0.5) [−1.1 – 0.8]	0.0 (0.3) [−0.5 – 0.5]	0.1 (0.3) [−0.3 – 0.5]	0.1 (0.2) [−0.5 – 0.4]
Rectum						
$V_{95\%}$	0.1 (0.3) [−0.3 – 0.5]		−0.2 (1.8) [−4.9 – 3.2]	0.1 (0.4) [−0.4 – 0.8]	0.1 (0.1) [−0.1 – 0.2]	0.1 (0.1) [−0.1 – 0.3]
$V_{75\%}$	0.0 (0.1) [−0.3 – 0.2]		−0.3 (0.6) [−1.7 – 0.5]	0.0 (0.2) [−0.2 – 0.4]	0.0 (0.1) [−0.1 – 0.1]	0.0 (0.1) [−0.1 – 0.1]
Bladder						
$V_{95\%}$	−0.1 (0.3) [−0.6 – 0.7]	0.1 (0.5) [−0.6 – 1.2]	−0.1 (0.9) [−2.8 – 0.9]	−0.1 (0.2) [−0.3 – 0.3]	0.0 (0.2) [−0.7 – 0.3]	0.0 (0.2) [−0.7 – 0.2]
$V_{75\%}$	0.0 (0.2) [−0.2 – 0.5]	0.1 (0.2) [−0.2 – 0.6]	0.0 (0.2) [−0.2 – 0.3]	0.0 (0.1) [−0.1 – 0.1]	0.0 (0.1) [−0.3 – 0.2]	0.0 (0.1) [−0.4 – 0.1]
Gamma statistics (V10)						
2%2mm	97.7 (0.7) [96.0 – 99.3]	96.2 (2.0) [91.3 – 97.8]	97.0 (1.5) [93.0 – 98.7]	98.0 (0.6) [96.7 – 98.8]	99.1 (0.5) [97.7 – 99.7]	98.9 (0.4) [97.8 – 99.6]
Dose statistics per volume						
$V_{10\%}$	0.0 (0.2) [−0.5 – 0.2]	0.1 (0.3) [−0.5 – 0.5]	−0.1 (0.3) [−0.9 – 0.3]	−0.1 (0.2) [−0.4 – 0.2]	−0.1 (0.2) [−0.4 – 0.2]	−0.3 (0.2) [−0.6 – −0.1]
HU-similarity						
MAE	49.1 (4.0) [42.8 – 54.3]	48.6 (2.8) [44.3 – 54.3]	47.7 (7.3) [37.1 – 67.5]	48.9 (3.6) [43.8 – 57.4]	47.4 (3.8) [42.6 – 54.2]	48.0 (5.7) [41.5 – 59.8]
ME	−4.6 (4.1) [−9.7 – 3.6]	−5.3 (4.6) [−14.1 – 2.2]	−6.6 (3.1) [−13.4 – −1.4]	−4.5 (3.4) [−9.9 – 1.1]	−5.7 (4.2) [−14.7 – 3.5]	7.2 (4.1) [−0.9 – 16.1]

registrations were performed using a Matlab-based tool simulating the paired registration of planar kV and DRR images. The observers were asked to perform manual registrations of the paired projections shown to them in random order. The clinical set-up correction protocols per cancer type were not used but all of the cases were registered using the same procedure.

In total, five observers (two medical physicists and three radiographers) performed registrations with three replications of each registration (20 cases × 2 methods × 3 repetitions = 120 number of registrations per observer). In addition, for seven prostate cancer patients both sCTc and sCTb were evaluated to compare the relevance of continuous HU versus bulk HU assignment in the sCT generation (adding 7 cases × 1 method × 3 repetitions = 21 registrations per observer). The fraction used was randomly chosen.

The assessment of positioning accuracy was performed by computing the mean and standard deviation (SD) of the difference of registrations obtained by CT-DRR and sCT-DRR.

2.6.2. CBCT

The CBCT-based verification of patient position was studied by comparing the registrations between CT to CBCT and sCT to CBCT relying on either bony structures or soft-tissue contrast for a subset of ten patients. In each registration methods, ten consecutive patients with a randomly chosen fraction were selected and the registration between the images were performed in the Offline Review module of Eclipse TPS. The registration was restricted to translations corresponding to the treatment couch movements available in the linac.

The performance of the bone-based registration was assessed as a difference between CT and sCT positioning. The observer was instructed to position the patient using automatic registration tools like prior to the treatment. Both PTV and OAR structures were visible during the registration. The bone registration study cohort consisted of four women with gynecological cancer and six men receiving treatment for post-operative prostate cancer.

In the evaluation of soft-tissue-based position verification, two datasets were prepared using the data from the radical prostate cancer group. The first set contained original CT, sCT and CBCT images, where the fiducial markers were visible in the images directly or as contours. In the second set, the markers were removed from CT, sCT and CBCT images using the Photoshop 6 (Adobe Inc., City of San José, CA, USA) image processing tool. First, the DICOM (digital imaging and communications in medicine) images were imported as 16-bit images enabling preservation of the data using the functionality integrated to the Photoshop. Then, the seeds were manually removed using the patch and healing brush tools. After removal, the images were stored as 16-bit TIFF (tagged image file format) images and again as DICOM images using Matlab. Finally, the images were imported back to the TPS for registration. Three evaluators performed registrations for both image sets (see the Supplementary Fig. 2) and the difference between marker-based and soft-tissue-based registration was used as a goodness metric of registration for both modalities independently.

2.7. Statistical analysis

Statistical analysis was conducted using Minitab (version 17, Minitab Inc., State College, PA, USA) numerical analysis software. The data between sCTc and sCTc were tested whether the means of the two dependent groups differ using the two-sample t-test.

3. Results

3.1. Dose difference

The mean (SD) dose differences of the PTV mean dose computed over cancer groups, each with 15 patients, were less than 0.2 (0.4)% between sCTc and CT. The mean dose differences for studied volumes were less than −0.3 (0.6)% (see the Table 2) for OARs. Two outliers for the rectum DVH comparison were identified in the gynecological cancer group. Without including the two outliers, the difference for the rectum V95% was −0.1 (0.8)% [−1.1–1.3] (for visualization of the outlier DVHs see the electronic supplementary material).

The mean gamma-index pass-rate evaluation was highest for the prostate cancer patients and lowest for the gynecological and rectal cancer patients. Among all groups, the average pass-rates within volumes of $V_{10\%}$ were higher than 95% with 2%/2mm gamma-criteria. The lowest pass-rate was for the rectum cancer group being 96.2 (2.0)%. The mean relative dose differences were less than 0.3 (0.3)% for all studied cancer groups and volumes ofinterest. The MAE was less than 50 HU for all studied cancer groups (see the Table 2).

An example of gynecological cancer patient is illustrated in the Supplementary Fig. 4 . More comprehensive set of results are presented in the online supplementary material (see the Supplementary Table 2).

3.2. Bulk to continuous HU comparison

For prostate cancer patients, the mean (SD) dose difference, within a volume receiving more than 10% of the prescribed dose, was −0.1 (0.2)% and −0.3 (0.2)% for sCTb and sCTc, respectively. Statistically significant differences were observed in the mean error (ME, $p < 0.01$) of HU values, mean dose within $V_{10\%}$ ($p < 0.01$) and mean gamma-index pass-rates with 2%/2mm gamma-criteria ($p = 0.04$) (see the Supplementary Table 4).

3.3. Body outline and geometric analysis

The body outline differences and the MRI-system-induced geometric distortion were the smallest close to the isocentre of MRI device. Nearby the isocentre, the absolute difference of body outline between CT and sCTc was 2 mm on average, but it increased farther away from the isocentre and reached the average difference of 6 mm at 150 mm (see the Fig. 2). The contribution of geometric distortion to the body outline difference was less than 2 mm within the investigated volumes.

The systematic difference between CT and sCTc body outlines was observed for various CC distances from the isocentre of MRI device (see

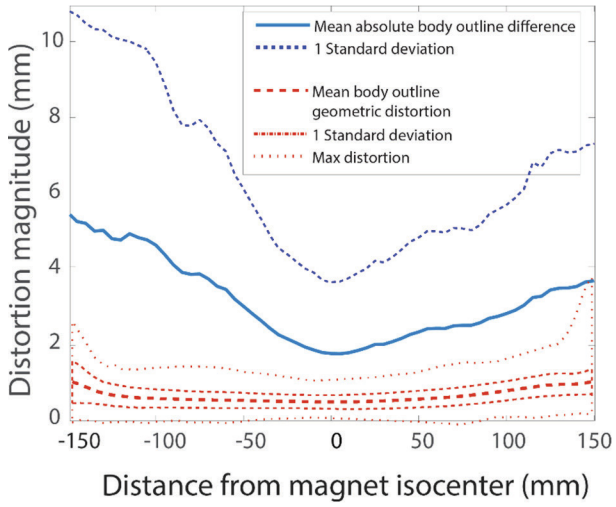

Fig. 2. Mean absolute body outline difference (solid blue line) and mean + 1SD (dash-dotted line) between CT and sCT images. Mean body outline geometric distortion (dashed red line), mean + 1SD (red dashed-dotted) and max distortion (red dashed line) of the body outline due to geometric distortions of MR images as a function of (cranio-caudal) distance from the isocentre of MRI device (SD: standard deviation, CT: computed tomography, sCT: synthetic computed tomography, MRI: magnetic resonance imaging). (For interpretation of the references to colour in this figure legend, the reader is referred to the web version of this article.)

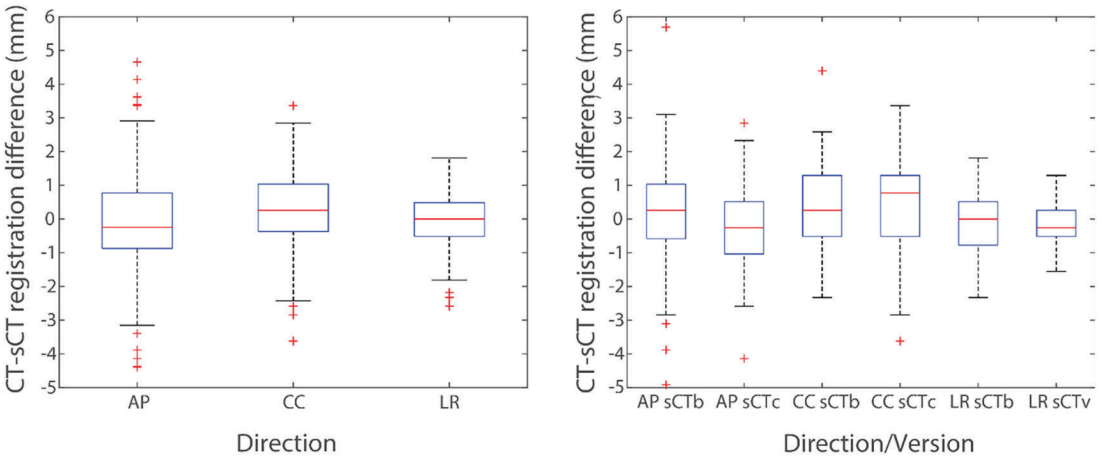

Fig. 3. Left: Box-plot of differences between CT-DRR to planar kV-image and sCTc-DRR to planar kV-image registration for anterior-posterior (AP), cranio-caudal (CC) and left–right (LR) directions evaluated using a group of 20 patients. Right: Box-plot of difference between CT-DRR to planar kV-image and sCT-DRR to planar kV-image registration for AP, CC and LR directions evaluated for bulk HU (sCTb) and continuous HU (sCTc) sCT evaluated using a subset of seven patients. (CT: computed tomography, DRR: digitally reconstructed radiograph, kV: kilovoltage, sCT: synthetic computed tomography, HU: Hounsfield unit).

the Supplementary Fig. 3). The largest systematic differences were present toward the cranial end of the studied FOV at angles corresponding patient's anterior direction (angle 0°). Towards the caudal end, systematic differences were not found, but the random uncertainty increased.

3.4. Positioning

3.4.1. DDR positioning

The mean (SD) difference between CT- and sCTc-based DRR positioning evaluated for 20 patients was −0.1 (1.4) mm, 0.3 (1.1) mm and 0.1 (0.8) mm, in AP, CC and LR direction, respectively (see Fig. 3).

The comparison of sCTb and sCTc was performed using subset of 7 patients. The mean (SD) difference between CT- and sCTc-based DRR positioning was −0.2 (1.2) mm, 0.4 (1.3) mm and −0.1 (0.6) mm, in AP, CC and LR direction, respectively. For sCTb, the difference was 0.2 (1.6) mm, 0.3 (1.2) mm and −0.1 (0.9) mm, respectively.

3.4.2. CBCT positioning

For the bone-based positioning studied with ten patients, the mean (SD) observer differences were 0.1 (1.1) mm, 0.1 (0.6) mm and −0.0 (0.2) mm in AP, CC and LR directions, respectively (see the Fig. 4).

For the soft-tissue-based positioning in the AP direction, the mean (SD) differences between fiducial markers- and soft-tissue-based registrations were 0.5 (1.8) mm, 0.5 (1.8) mm and 1.1 (1.8) mm for CT, sCTc and sCTb, respectively. In the CC direction, the mean (SD) differences were −0.2 (1.1) mm, −0.6 (1.3) mm and −0.8 (2.3) mm, respectively. Furthermore, the smallest registration differences were seen in the LR direction, being 0.1 (0.7) mm, −0.4 (0.7) mm and −0.2 (0.6) mm for CT, sCTc and sCTb, respectively.

4. Discussion

Pelvic cancer patients would benefit from the use of sCT in terms of decreased total uncertainties in EBRT [22–24] . This study aimed at demonstrating dosimetric and positioning accuracy of using MRCAT sCT with continuous HU values for the EBRT of pelvic cancers. This study covered several possible positioning workflows that have not been assessed previously. The results were relevant when aiming to extend the use of sCT method to pelvic cancer patients.

The dosimetric accuracy was assessed by comparing sCT to CT-based dose computation. The dosimetric differences between CT and sCTc were found to be small among all cancer groups. Considering mean (SD) gamma-index pass-rates of 98.0 (0.6)%, 96.2 (2.0)% and

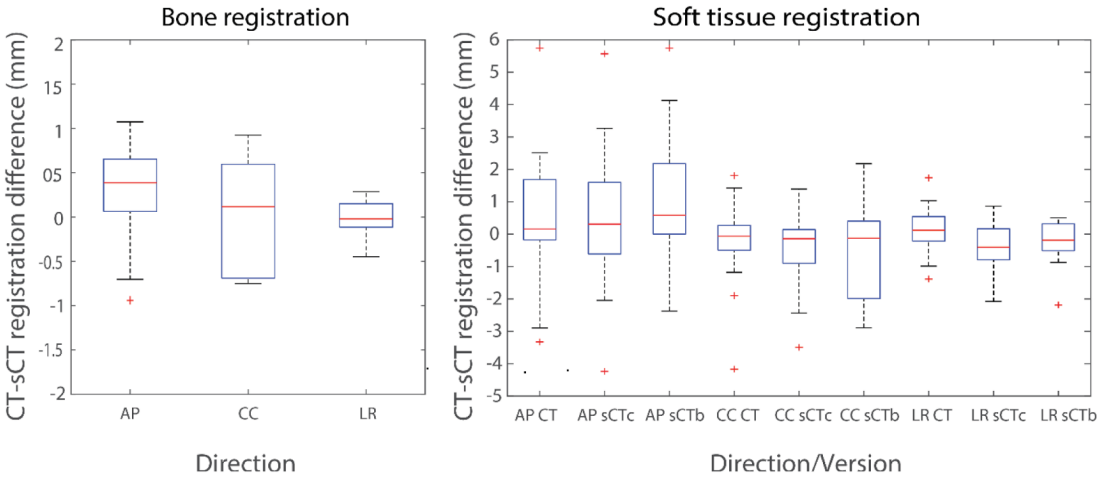

Fig. 4. Left: Box-plot of registration difference between CT-to-CBCT and sCTb-to-CBCT using bone-based registration in left–right (LR), anterior-posterior (AP) and cranio-caudal (CC) direction. Right: Box-plot of registration differences between CT to CBCT and sCT to CBCT using soft-tissue contrast with respect to marker-based registration in AP, CC and LR directions. (CT: computed tomography, CBCT: cone-beam computed tomography, sCT: synthetic computed tomography).

96.5 (2.3)% using 2%/2mm gamma-criteria and mean (SD) dose differences of −0.1 (0.2)%, 0.1 (0.3)% and −0.1 (0.3)% for the prostate base, rectum and gynecological cancer patients, the dosimetric agreement was found to meet the clinical acceptance criteria. Maspero et al. [24] used a deep learning-based sCT approach and evaluated its applicability for pelvic cancer patients. They obtained pass-rates of 95.0 (2.3)%, 91.6 (3.3)% and 92.9 (3.7)% and mean dose difference of −0.1 (0.1), −0.2 (0.2) and −0.1 (0.3) for prostate, rectum and cervix cancer patients using 2%/2mm gamma-criteria, respectively. Although reporting slightly lower agreement, their results were in line with this study.

Wang et al. [21] obtained median gamma-index pass-rate of 99.9% (99.4–100.0%) and medians of the dose difference averages were 0.21 Gy (0.2–0.3 Gy). In addition, Maspero et al. [20] evaluated the feasibility of the same method used in this study (sCTb) for rectal cancer patients obtaining the mean gamma-index pass-rate of 95.2 (4.0)% and mean dose deviation of −0.3 (0.2)% of prescription dose. Liu et al. [22] evaluated the sCT method for gynecological cancer patients obtaining the PTV dose deviation of 0.2 (0.4) Gy for $D_{0.5cc}$ and 0.3 (0.3) Gy for $D_{99\%}$.

Liu et al. [22] and Maspero et al. [24] results showed that the dosimetric agreement was decreased for rectum and gynecological cancer patients in comparison to prostate cancer patients. According to the body outline comparison between CT and sCT, the difference increases farther away from the imaging isocentre along CC axis. However, this was unlikely due to geometric distortion, which also increases with growing distance from the isocentre, but rather due to differences between CT and MRI modalities. Thus, higher dosimetric disagreement for patients with longer PTVs in CC direction might arise from these differences. In addition to random daily variation in body outline due to breathing and positioning, it has been suggested by Persson et al. that systematic differences between body outlines on CT and MRI could be attributable to longer scan time causing body relaxation [30]. Additionally, according to these results the systematic difference in the abdomen could be due to abilities of the two modalities to record the breathing motion.

Interestingly, no major difference in dosimetric performance was found between bulk HU and continuous HU sCT. This implies that already four tissue classes were adequate to capture the individual variance in body composition and to produce clinically acceptable accuracy in the dose calculation for prostate cancer patients treated with EBRT. Larger differences are typically reported between continuous HU and bulk HU sCTs. Kim et al. [18] reported no significant dosimetric difference between continuous HU or bulk-HU sCTs but obtained higher gamma-index passing-rate of 97.2% vs. 94.0% for continuous sCT evaluated with 1%/1 mm gamma-criteria. Largent et al. [17] found that the mean gamma-index pass-rate for continuous HU values (99.5%) was significantly higher than that of bulk density method (96.1%). Both Kim et al. and Largent et al. used only two bulk densities: one for bone and one for soft-tissue that could explain worse dosimetric agreement in comparison to our results. In line with our earlier study, using the sCTb [26], the patient positioning accuracy was found to be at the clinically acceptable level. However, when using continuous HU values for bone, AP positioning precision was improved as compared with the bulk assignment of HU values (sCTb). This could be due to improved visualization of pubis in sCTc, as illustrated in Fig. 1.

The mean difference between bone-based positioning between CT to CBCT and sCT to CBCT was less than 0.2 mm in all directions. The result was in agreement with earlier studies reporting sub-millimeter accuracy for the bulk HU version of the used sCT method [13,20]. Here, for the first time the soft-tissue prostate positioning of a sCT method was evaluated by comparing it to the fiducial marker-based reference. No differences in the performance between CT and sCTc were observed. However, for sCTb, the differences were slightly larger in the CC and AP directions but not in LR direction. Thus, no major difference in positioning performance was found between the methods. In addition, the use of smaller slice width for sCTc could also contribute to the observed difference.

In the DRR and soft-tissue CBCT positioning studies, there were a few outlier registrations as see in Figs. 3 and 4. For the DRR registrations, the differences were greater that is expected for either CT or MRCAT registrations alone as they were affected by the random error related to DRR-to-kV registration uncertainty both for CT and MRCAT. For soft-tissue-based registrations greater than 5 mm differences have also been reported for 28% of the registrations when comparing to seed based truth [31]. Thus, our results are in line with the reported values in the literature. The large difference may result from the poor soft-tissue visibility and artifacts in CBCT images.

Increasing the FOV in the CC direction will remain a challenging task for MRI-only planning since the geometric accuracy decreases rapidly farther away from the isocentre of MRI device. Within the study population, we found that the maximal useful FOV for one station scan was 300 mm in CC direction, while for longer FOV a two-station scan is required. For the longer FOV, the image shutter prevented analysis of geometric accuracy and body outline difference. The patient motion causes artifacts in the mDIXON image that may hamper accurate detection of body outline. Increasing the FOV in the CC direction with an acceptable scan time for preventing the organ motion and more robust motion management in the abdomen region will also remain challenges for general pelvis sCT solutions and they need to be examined further.

In this study, only a subgroup of the cohort was included in the positioning study. Consequently, the number of patients per cancer group was small. However, the positioning protocol for planar kV-image to DRR registration is similar between the groups enabling general conclusions to be drawn from these results. Furthermore, for the bone registration using CBCT images the procedure is similar between various cancer groups. On the contrary, the soft-tissue-based CBCT registration is different between the groups, and thus our conclusions apply only to prostate cancer patients. Further studies are required to assess the feasibility of other cancer types.

The implanted fiducial marker-based workflow was not included in the study although it is the clinical practice for the majority of the patients at our institution and a combination of fiducial marker alignment and soft-tissue analysis is currently the most effective and widely available approach to ensuring the accuracy in image-guided EBRT of prostate [32]. The use of fiducial markers for position verification of prostate has been evaluated for the first MRCAT algorithm (sCTb) by Tyagi et al. [13]. Thus, the re-evaluation was not considered relevant since the use of continuous HU values was not expected to impact seed-based workflow. In addition, the localization of fiducial markers from MR images has been evaluated to be sufficiently accurate and comparable to CT-based fiducial marker localization [33,34].

This study advances research and supports the future clinical implementation of sCT for general pelvic anatomy. It has been shown that continuous HU sCT was required for the accurate position verification of patients, particularly when using the soft-tissue-based registration strategies. However, the method based only on four bulk HU values was dosimetrically adequate. The use of sCT for pelvic cancer patients can be used to obtain the required dosimetric and geometric accuracy.

Acknowledgments

The authors are grateful for the efforts by an application specialist Paula Lindmark (Philips MR Therapy Oy, Vantaa, Finland) and radiographers Tarja Alamäki and Sanna Vehkomäki (Department of Oncology and Radiotherapy, Turku University Hospital, Turku, Finland) for performing the manual registrations required for the positioning study. They would also like to thank Eliisa Löyttyniemi, PhD, (Department of Biostatistics, University of Turku, Turku, Finland) for help in statistical analysis of the manuscript. In addition, we would like to show our gratitude to Lizette Warner, PhD, Head of Clinical Science, MR Oncology, Philips, for overall management of the collaboration.

Disclosure statement

Authors Alvin Eufemio, Aleksi Halkola, Reko Kemppainen and Mark Pesola declare that they were employed by Philips MR Therapy Oy (Vantaa, Finland) by the time of conducting the research. In addition, Turku University Hospital and Philips have a contract for research collaboration.

Appendix A. Supplementary data

Supplementary data to this article can be found online at https://doi.org/10.1016/j.phro.2019.06.001 .

References

[1] Dimopoulos JCA, Schard G, Berger D, Lang S, Goldner G, Helbich T, et al. Systematic evaluation of MRI findings in different stages of treatment of cervical cancer: potential of MRI on delineation of target, pathoanatomic structures, and organs at risk. Int J Radiat Oncol Biol Phys 2006;64:1380–8 .

[2] Gwynne S, Mukherjee S, Webster R, Spezi E, Staffurth J, Coles B, et al. Imaging for target volume delineation in rectal cancer radiotherapy – a systematic review. Clin Oncol (R Coll Radiol) 2012;24:52–63 .

[3] Hoskin P, De Bari B, Bossi A, Villeirs G, Fonteyne V, Pieters BR, et al. ESTRO ACROP consensus guideline on CT- and MRI-based target volume delineation for primary radiation therapy oflocalized prostate cancer. Radiother Oncol 2018;127:49–61 .

[4] Schmidt MA, Payne GS. Radiotherapy planning using MRI. Phys Med Biol 2015;60:R323–61 .

[5] Metcalfe P, Liney GP, Holloway L, Walker A, Barton M, Delaney GP, et al. The potential for an enhanced role for MRI in radiation-therapy treatment planning. Technol Cancer Res Treat 2013;12:429–46 .

[6] Chandarana H, Wang H, Tijssen RHN, Das IJ. Emerging role of MRI in radiation therapy. J Magn Reson Imaging 2018;48:1468–78 .

[7] Dirix P, Haustermans K, Vandecaveye V. The value of magnetic resonance imaging for radiotherapy planning. Semin Radiat Oncol 2014;24:151–9 .

[8] Nyholm T, Nyberg M, Karlsson MG, Karlsson M. Systematisation of spatial uncertainties for comparison between a MR and a CT-based radiotherapy workflow for prostate treatments. Radiat Oncol 2009;4:54 .

[9] Owrangi AM, Greer PB. Glide-Hurst CK. MRI-only treatment planning: benefits and challenges. Phys Med Biol 2018;63 .

[10] Johnstone E, Wyatt JJ, Henry AM, Short SC, Sebag-Montefiore D, Murray L, et al. Systematic review of synthetic computed tomography generation methodologies for use in magnetic resonance imaging-only radiation therapy. Int J Radiat Oncol Biol Phys 2018;100:199–217 .

[11] Edmund JM, Nyholm T. A review of substitute CT generation for MRI-only radiation therapy. Radiat Oncol 2017;12:28 .

[12] Siversson C, Nordström F, Nilsson T, Nyholm T, Jonsson J, Gunnlaugsson A, et al. Technical Note: MRI only prostate radiotherapy planning using the statistical decomposition algorithm. Med Phys 2015;42:6090–7 .

[13] Tyagi N, Fontenla S, Zhang J, Cloutier M, Kadbi M, Mechalakos J, et al. Dosimetric and workflow evaluation of first commercial synthetic CT software for clinical use in pelvis. Phys Med Biol 2017;62:2961–75 .

[14] Christiansen RL, Jensen HR, Brink C. Magnetic resonance only workflow and validation of dose calculations for radiotherapy of prostate cancer. Acta Oncol 2017;56:787–91 .

[15] Kemppainen R, Suilamo S, Tuokkola T, Lindholm P, Deppe MH, Keyriläinen J. Magnetic resonance-only simulation and dose calculation in external beam radiation therapy: a feasibility study for pelvic cancers. Acta Oncol 2017;56:792–8 .

[16] Korhonen J, Kapanen M, Keyriläinen J, Seppälä T, Tenhunen M. A dual model HU conversion from MRI intensity values within and outside of bone segment for MRI-based radiotherapy treatment planning of prostate cancer. Med Phys 2014;41. 011704 .

[17] Largent A, Barateau A, Nunes JC, Lafond C, Greer PB, Dowling JA, et al. Pseudo-CT generation for MRI-only radiation therapy treatment planning: comparison among patch-based, atlas-based, and bulk density methods. Int J Radiat Oncol Biol Phys 2019;103:479–90 .

[18] Kim J, Garbarino K, Schultz L, Levin K, Movsas B, Siddiqui MS, et al. Dosimetric evaluation of synthetic CT relative to bulk density assignment-based magnetic resonance-only approaches for prostate radiotherapy. Radiat Oncol 2015;10:239 .

[19] Farjam R, Tyagi N, Deasy JO, Hunt MA. Dosimetric evaluation of an atlas-based synthetic CT generation approach for MR-only radiotherapy of pelvis anatomy. J Appl Clin Med Phys 2019;20:101–9 .

[20] Maspero M, Tyyger MD, Tijssen RHN, Seevinck PR, Intven MPW, van den Berg CAT. Feasibility of magnetic resonance imaging-only rectum radiotherapy with a commercial synthetic computed tomography generation solution. Phys Imag Radiat Oncol 2018;7:58–64 .

[21] Wang H, Du K, Qu J, Chandarana H, Das IJ. Dosimetric evaluation of magnetic resonance-generated synthetic CT for radiation treatment of rectal cancer. PLoS ONE 2018;13:1–15 .

[22] Liu L, Jolly S, Cao Y, Vineberg K, Fessler JA, Balter JM. Female pelvic synthetic CT generation based on joint intensity and shape analysis. Phys Med Biol 2017;62:2935–49 .

[23] Katz LM, Wang H, Duckworth T, Kim D, Das IJ, Lymberis SC. Use of synthetic CT for magnetic resonance-only based external beam pelvic radiation therapy of cervical cancer. Int J Radiat Oncol 2017;99:E676–7 .

[24] Maspero M, Savenije MHF, Dinkla AM, Seevinck PR, Intven MPW, Jurgenliemk-Schulz IM, et al. Dose evaluation offast synthetic-CT generation using a generative adversarial network for general pelvis MR-only radiotherapy. Phys Med Biol 2018;63:1–14 .

[25] Köhler M, Vaara T, Van Grootel M, Hoogeveen R, Kemppainen R, Renisch S. White paper: MR-only simulation for radiotherapy planning. Philips 2015:1–16 .

[26] Kemppainen R, Vaara T, Joensuu T, Kiljunen T. Accuracy and precision of patient positioning for pelvic MR-only radiation therapy using digitally reconstructed radiographs. Phys Med Biol 2018;63. aaad21 .

[27] Klein S, Staring M, Murphy K, Viergever MA, Pluim JPW. Elastix: a toolbox for intensity-based medical image registration. IEEE Trans Med Imaging. 2010;29:196–205 .

[28] Maspero M, Seevinck PR, Schubert G, Hoesl MAU, van Asselen B, Viergever MA, et al. Quantification of confounding factors in MRI-based dose calculations as applied to prostate IMRT. Phys Med Biol 2017;62:010 .

[29] Andreasen D, Van Leemput K, Edmund JM. A patch-based pseudo-CT approach for MRI-only radiotherapy in the pelvis. Med Phys 2016;43:4742–52 .

[30] Persson E, Gustafsson C, Nordström F, Sohlin M, Gunnlaugsson A, Petruson K, et al. MR-OPERA: a multicenter/multivendor validation of magnetic resonance imaging-only prostate treatment planning using synthetic computed tomography images. Int J Radiat Oncol Biol Phys 2017;99:692–700 .

[31] Barney BM, Lee RJ, Handrahan D, Welsh KT, Cook JT, Sause WT. Image-guided radiotherapy (IGRT) for prostate cancer comparing kV imaging of fiducial markers with cone beam computed tomography (CBCT). Int J Radiat Oncol Biol Phys 2011;80:301–5 .

[32] O'neill AGM, Jain S, Hounsell AR, O'sullivan JM. Fiducial marker guided prostate radiotherapy: a review. Br J Radiol 2016;89:1–18 .

[33] Jonsson JH, Garpebring A, Karlsson MG, Nyholm T. Internal fiducial markers and susceptibility effects in MRI-simulation and measurement of spatial accuracy. Int J Radiat Oncol Biol Phys 2012;82:1612–8 .

[34] Maspero M, Seevinck PR, Willems NJW, Sikkes GG, de Kogel GJ, de Boer HCJ, et al. Evaluation of gold fiducial marker manual localisation for magnetic resonance-only prostate radiotherapy. Radiat Oncol 2018;13:1–12 .